Dissertation in Neurobiology

Histological and Morphological Analysis of Developing Neuronal Precursors Derived from Human iPS Cells

Daniela Catarina Gaspar Santos

Dissertation for the attribution of the Master's degree in Biomedical Research, in the speciality field of Neurobiology, under the supervision of Professor Doctor Cláudia Pereira, Professor Doctor Uwe Maskos and PhD student Célia Raïs, and presented to the Faculty of Medicine of the University of Coimbra.

Dissertação no âmbito do Mestrado em Investigação Biomédica, especialização em Neurobiologia, orientada pela Professora Doutora Cláudia Pereira, pelo Professor Doutor Uwe Maskos e pela aluna de doutoramento Célia Raïs, e apresentada à Faculdade de Medicina da Universidade de Coimbra.

July 2019

UNIVERSIDADE D
COIMBRA

“Science knows no country, because knowledge belongs to humanity, and is the torch which illuminates the world.”

- Louis Pasteur

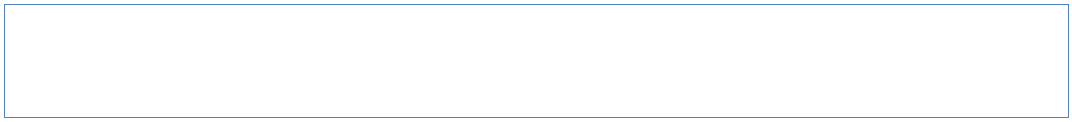

Acknowledgments

The work I developed throughout the past ten months would have never been possible without the presence and help of a group of people I would like to acknowledge.

I would like to begin by thanking Professor Henrique Girão, Coordinator of the Master's in Biomedical Research, for the scientific and life lessons taught during these last two years and for encouraging me in the application to a research project abroad. For her constant availability, I would like to thank Professor Cláudia Pereira, as well.

I would like to express my deep gratitude to the Integrative Neurobiology of Cholinergic Systems group that hosted me in the Pasteur Institute and, particularly, to the Head of the Unit, Doctor Uwe Maskos, for the availability and for being an academic example. A very special thanks to Célia Raïs, for being a great supervisor and friend, who trusted me, gave me time and space to learn and reassured me when my confidence was weakened.

I would like to acknowledge the rest of the people in the lab, who made me feel warmly welcomed since my first day, and specially the colleagues I shared the room with, Camille and Mihael, two friends that had the incredible ability to lift up my mood on a daily basis.

I would also like to leave a special thanks to the family living in Paris I had the opportunity to meet or reconnect with. To my cousins for the making me feel at home and, especially, to François for the precious advices and the continuous emotional support.

To my hometown friends and cousins for being always present and for bringing me back to my origins.

To the group of friends, we have created in the first year of Master. In particular, a huge thanks to Catarina Nascimento, Catarina Pelicano and Eduarda Gomes for sharing each other concerns, even when living and working all far apart, and for the tips that helped me overcoming the most challenging periods.

Lastly, I cannot go by without thanking profoundly to my family. To Tatiana, my childhood idol, who firstly introduced me to the reality of studies and who will forever be an example of leadership, persistence and hard work. To Joana, my first object of responsibility, for her sensible observations and impeccable values that inspire me to follow what she grew up to be. To my parents, for literally everything. For being the constant comfort figures in my life since my first memories, for funding my academic and leisure activities, and above all, for the unconditional support I can always find in every text message, call or face-to-face conversation.

Abstract

Schizophrenia and other human neurodevelopmental disorders are highly heterogenous conditions that encompass significant economic and social burdens. Their neurobiology is still elusive, and their study has been hampered by an inaccessibility to appropriate models. In *in vitro* studies the impact of the nervous system is difficult to assess, whereas in animal models, some hallmarks of neuropsychiatric conditions cannot be reliably replicated.

In this project we worked on a model of neurodevelopment in which Neuronal Progenitor Cells (NPCs) derived from human induced Pluripotent Stem Cells (hiPSCs) were injected into the cortex of immunodeficient mice and were characterized during a six-month period.

The grafting technique resulted in the successful migration and integration of the human NPCs in the most anterior brain areas, mainly in the motor and prelimbic cortex. There was no apparent rejection from the host, and the human cells started to develop neuronal processes as soon as 1 month after injection. To assess maturation, human neuronal filaments were traced and an increase in density was visible over time. These filaments were also projecting deeper into the mouse cortex and branching become more frequently.

Apart from the development of a complex network of projection, other key events of neurogenesis were reproduced inside the graft, including synaptogenesis and growth of dendritic spines. The expression of a mature marker increased over time, and it was possible to distinguish immature neurons. Nonetheless, a great number of human cells were still expressing a pluripotency marker. These experiments have demonstrated that the human graft is a very heterogenous environment, where some NPCs undergo development and differentiation, but others remain immature, which indicates that the graft had not reached a fully mature state at the end of the six months.

Additionally, different populations of glial cells were shown to respond to the human cells' presence. Astrocytes accumulated in the graft region and there was an increased GFAP infiltration. We could also detect the presence of radial glia in the first timepoint, suggesting that the mouse cells may be assisting the development and migration of the human NPCs. The number of oligodendrocytes was shown to increase, and myelin sheaths could be detected inside the graft after two months. These results confirmed that the host cells are interacting with the developing human neurons and this relationship is dynamic.

This study provides guidelines for the analysis of human NPCs developing in the mouse brain. In the long term, human iPSC could be genetically manipulated and the impact of specific variations in development could be assessed.

***KEYWORDS**: STEM CELLS; HUMAN GRAFT; NEURODEVELOPMENT; 3D TRACING; HOST -GRAFT INTERACTIONS*

Resumo

A esquizofrenia e outras perturbações do neurodesenvolvimento são condições muito heterogéneas que acarretam um grande fardo económico e social. A sua neurobiologia ainda não é totalmente compreendida, e o seu estudo tem sido dificultado devido à falta de modelos apropriados. Em estudos *in vitro* é difícil avaliar o impacto do sistema nervoso, enquanto que em modelos animais, não é possível reproduzir de forma fidedigna algumas características de doenças neuropsiquiátricas. Neste projeto, trabalhámos num modelo de neurodesenvolvimento no qual Células Neurais Progenitoras (NPCs), derivadas de Células Pluripotentes induzidas humanas (hiPSCs), foram injetadas no córtex de murganhos imunodeficientes e foram caracterizadas durante seis meses.

A técnica de enxerto resultou na migração e integração eficiente das NPCs humanas nas áreas mais anteriores do cérebro, principalmente no córtex motor e pré-límbico. Não pareceu existir rejeição por parte do hospedeiro, e as células humanas começaram a desenvolver processos neuronais a partir de um mês após a injeção. Para avaliar a maturação, os filamentos neuronais humanos foram traçados e verificou-se um aumento na sua densidade. Estes filamentos estavam também a projetar mais profundamente no córtex do murganho e a presença de ramificações tornou-se mais frequente. Para além do desenvolvimento de uma rede de projeções complexa, outros eventos marcantes da neurogénese foram reproduzidos no interior do enxerto, incluindo sinaptogénese e formação de espículas dendríticas. A expressão de um marcador neuronal maduro aumentou ao longo do tempo, e era possível distinguir neurónios imaturos. Ainda assim, um grande número de células humanas continuava a expressar um marcador de pluripotência. Estas experiências demonstraram que o enxerto humano é um ambiente altamente heterogéneo, onde algumas NPCs já se encontram em desenvolvimento e diferenciação, mas outras permanecem imaturas, o que indica que ao fim dos seis meses ainda não foi atingido um estado completamente maduro.

Para além disso, demonstrou-se que diferentes populações de células gliais estão a responder à presença das células humanas. Houve uma acumulação de astrócitos e infiltração de GFAP na região do enxerto. Também detetámos a presença de glia radial ao fim do primeiro mês, o que sugere que as células do hospedeiro poderão estar a auxiliar o desenvolvimento e migração das NPCs humanas. O número de oligodendrócitos aumentou, e a partir do segundo mês havia bainha de mielina no interior do enxerto. Estes resultados confirmaram que as células do hospedeiro estão a interagir com os neurónios humanos em desenvolvimento e que esta relação é dinâmica.

Este estudo sugere um método para a análise de NPCs humanas em desenvolvimento in cérebro de murganho. No futuro, hiPSCs poderão ser manipuladas geneticamente e o impacto que variações específicas têm no desenvolvimento poderá ser estudado.

PALAVRAS-CHAVE: CÉLULAS ESTAMINAIS; ENXERTO HUMANO; NEURODESENVOLVIMENTO; DETEÇÃO 3D; INTERAÇÕES HOSPEDEIRO-ENXERTO

List of Contents

List of Tables

List of Figures

List of Abbreviations

µL Microlitre

µm Micrometre

3D Three-dimensional

AMPA α-amino-3-hydroxy-5-methyl-4-isoxazolepropionic acid

bFGF basic Fibroblast Growth Factor

bHLH basic helix-loop-helix

BSA Bovine Serum Albumin

CASPR Contactin-associated protein 1

CD11b Cluster of differentiation 11b

CD31 Cluster of Differentiation 31

CD68 Cluster of Differentiation 68

CNS Central Nervous System

CNV Copy Number Variation

DAPI 6'-Diamidino-2-phenylindole

DCX Doublecortin

EBs Embryoid Bodies

ECs Endothelial Cells

EGF Epidermal Growth Factor

EPBs *en passant* boutons

EPSCs Excitatory Postsynaptic Currents

ESC Embryonic Stem Cell

FACS Fluorescence-Activated Cell-Sorting

FGF4 Fibroblast Growth Factor 4

GABA Gamma-aminobutyric acid

GFAP Glial Fibrillary Acid Protein

GFP Green Fluorescent Protein

hESCs human Embryonic Stem Cell

hiPSC Human induced Pluripotent Stem Cell

Iba1 Ionized calcium binding adaptor molecule 1

iPSC Induced Pluripotent Stem Cell

LCR Low Copy Repeats

MAGUK Membrane-associated guanylate kinase

MAP-2 Microtubule-associated Protein 2

MBP Myelin Basic Protein

mg Milligram

mM Millimolar

Mmp Matrix Metalloproteinase

mpi Month post injection

mRNA messenger Ribonucleic Acid

ms millisecond

NA Numerical Aperture

nAChR Nicotinic Acetylcholine Receptor

NeuN Neuronal Nuclei antigen

NG2 Nerve/glial antigen 2

NHS Normal Horse Serum

NMDA N-methyl-D-aspartate

NMDAR N-methyl-D-aspartate receptor

NOD Non-Obese Diabetic

NPC Neural Progenitor Cell

NSC Neural Stem Cell

ON Over night

PBS Phosphate-Buffered Saline

PCR Polymerase chain reaction

PECAM-1 Platelet/ Endothelial cell adhesion molecule 1

PFA Paraformaldehyde

PNNs Perineural Nets

PNS Peripheral Nervous System

PSD-95 Post Synaptic Density 95 protein

REX1 Reduced Expression 1

RT Room temperature

SCID Severe Combined Immunodeficiency

SD Standard Deviation

SEM Standard Error of the Mean

SNPs Single-Nucleotide Polymorphisms

SOPF Specific Opportunistic Pathogen-Free

SVZ Subventricular Zone

TBs *terminaux* boutons

WT Wild-type

1. Introduction

This chapter aims to provide the theoretical background necessary to support all the project. The long-term intention was to develop an appropriate model to study specifically schizophrenia and address the impact of genetic variations in nicotinic Acetylcholine Receptors (nAChRs) in neurodevelopment. Therefore, throughout the introduction, a special emphasis will be given to this mental health disorder.

However, only the initial step of this disease modelling experiments was performed and uniquely iPSCs derived from healthy donors' somatic cells were used. As a consequence, the model described in the present document can be adapted and later be applied to study any neurodevelopmental condition.

1.1. Schizophrenia and mental disorders

Neuropsychiatric disorders are a major cause of disability worldwide and are associated with significant economic and social costs (1,2). According to a 2017 report of the World Health Association, these conditions are highly prevalent, and more than 970 million people are affected across the globe. In the particular case of schizophrenia, around 19,8 million people are affected and the incidence is of more than 1 million new cases per year (3).

Schizophrenia is a chronic mental disorder characterized by disruptions in thought processes, perceptions, emotional responsiveness and social interactions. It comprises a range of cognitive, behavioural, and emotional symptoms that negatively impact social and occupational functioning (4).

Despite the relatively low prevalence, schizophrenia is the most disabling and socially disruptive of neurological conditions and is one of the top twenty leading causes of disability worldwide (1,3).

Even though the psychotic features of the disorder usually emerge between late teen years and early thirties, schizophrenia is often perceived from a developmental perspective. In fact, cognitive impairment and changes in social behaviours can appear in childhood and precede the actual diagnosis by years (5).

When compared to other chronic mental and physical health conditions, schizophrenia has a substantial financial impact and the annual costs, including direct medical costs and indirect costs, are estimated to range from US$94 million to US$102 billion (6).

Individuals diagnosed with schizophrenia have around 2.5 times the risk of premature mortality compared with the general population and this differential mortality gap has been growing during the past decades (7–9). On the one hand, more than half of the individuals with schizophrenia are estimated to have co-occurring mental or behavioural health conditions, including depression, anxiety or drug abuse disorder (10). Patients suffering from schizophrenia are also more likely to have suicidal thoughts and around 4.9% of patients die by suicide, mainly in the early stages of illness. This rate is far greater than the general population (around 0,3%) (11).

Even though, schizophrenia is a major contributor to disease burden, little progress has been made in the development of therapies and current treatments focus mainly on the mitigation of symptoms. As the etiology of this condition is still elusive, there is a lack of robust models that replicate its clinical characteristics (12).

1.2. Neurobiological alterations

Growing evidence has suggested that alterations in cortical connectivity, particularly in the hippocampus and prefrontal cortex (PFC), may underlie schizophrenia (17) and the most dominant hypothesis to explain this disorder has been for years based on abnormalities in the levels of dopamine and glutamate (13).

It has been hypothesized that the existence of a pattern of abnormal neurodevelopment during adolescence, that could trigger psychotic symptoms in genetically vulnerable people, may be in the origin of this condition (14).

The prefrontal cortex (PFC) plays an important role in cognitive processes such as attention control, verbal working memory, decision making and emotional processing (15–17) and deficits in prefrontal function have been noticed in schizophrenia (18), as well as in other neuropsychiatric disorders (19).

Both in humans and in mice, cognitive processes and neuronal activity are controlled by cholinergic transmission and, following elimination of PFC cholinergic innervation in mice, attention performance is reduced, whereas the opposite happens upon stimulation of cholinergic projections (20).

Many studies in both animal models and humans have shown that nicotinic acetylcholine receptors (nAChRs) are of particular importance for cognitive functions, reward, aging and schizophrenia, as well (21).

1.3. Cholinergic neurotransmission

Nicotinic acetylcholine receptors (nAChRs) are ligand-gated ion channels that can be expressed in certain neurons in the central nervous system (CNS) (22,23), but also in the neuromuscular junction (24). Upon activation through the binding of acetylcholine or nicotine, the ion channels open and there is an increased flux of cations, mainly Na^+ and K^+ that can induce cell depolarization (25). In mammals, eleven neuronal nAChRs subunits have been identified: α-2, α-7, α-9, α-10, β-2 and β-4 (26).

These pentameric homo- or heteromers are known to be involved in a number of physiological and behavioural processes, and have been implicated in several pathological conditions, including schizophrenia (27).

Neuronal nAChRs play an important regulatory role in neurotransmitter release and synaptic transmission of dopamine, glutamate, GABA and serotonin in several brain regions of the CNS (23,28).

Patients with schizophrenia often depict an abnormal response to environment and deficits in sensory processing. These could be linked to a defect in inhibitory gating, which can be caused by an activation of nicotinic receptors in the hippocampus. *Post-mortem* analyses have identified decreased levels of nAChRs in many specimens of hippocampal brains of schizophrenic patients (29).

Nicotine is known to upregulate the expression of nAChRs in the brain, however, in schizophrenic patients that effect is not as evidenced (30). This could explain the increased rates of tobacco smoking among people with schizophrenia, as nicotine may be used to self-medicate symptoms (31).

Studies with twins and adopted people have shown that schizophrenia is highly genetically influenced and the risk results from a combination of diverse genetic variants and environmental factors (32).

More recently, several genomic studies also support these findings, demonstrating that the genetic components linked to schizophrenia are extremely heterogeneous and may involve a wide spectrum of risk factors. These factors include *de novo* variants, copy-number variations (CNV), Single Nucleotide Polymorphisms (SNPs) and Single Nucleotide Variant with different frequencies and effect sizes (33,34).

The expression of α7 nAChRs is decreased in multiple regions of *post-mortem* brain in schizophrenic subjects, including the hippocampus, cortex, and the reticular thalamic nucleus (35,36). Polymorphisms in the core promoter regions of CHRNA7, that encodes α7 subunit, result in lower transcription levels of these receptors, which may justify the reduced expression of this subunit linked to schizophrenia (37).

Another link between this disease and nAChRs is the chimeric gene CHRFAM7A, formed from the partial duplication of CHRNA7 and resulting in a truncated α7. This is a mutation exclusively seen in humans, and a deletion polymorphism in this duplicated gene has also been linked to schizophrenia (35).

Many studies demonstrated that nAChRs containing the α7 subunit facilitate glutamate release, and this mechanism has been implicated in the pathophysiology of several neuropsychiatric disorders (38).

The presence of Low Copy Repeat (LCR) in chromosome 15q13.3, where the CHRNA7 gene is located, make this region a hotspot for CNVs that are implicated in neurophsyciatric disorders. Similar common and rare deletions and duplications in this same region have been reported in intellectual disability, autism, bipolar disorder and attention deficit hyperactivity disorder (36).

Incorporation of α5 subunit into α4β2 nAChRs increases nicotinic signalling and is required for normal attention performance in adult mice (39). Moreover, nAChRs containing this subunit appear to mediate dendrite retraction in layer VI neurons of the prefrontal cortex, a characteristic process of normal development. In wild-type (WT) mice, long apical dendrites extend from cortical layer VI into layer I and decrease abruptly in length, afterwards, whereas in knockout mice for α5 subunit this shift is not detected (40).

A recent Genome Wide Association Study (GWAS) found a strong association between schizophrenia and the CHRNA5-CHRNA3-CHRNB4 gene cluster (41). This cluster located in human chromosome 15 encodes three nAChR subunits: α-5, α-3 and β-4. Seven single-nucleotide polymorphisms (SNPs) located within this cluster were associated with nicotine dependence, which is highly prevalent amongst schizophrenic subjects (42). One of these polymorphisms, the non-synonymous SNP rs16969968, that causes a change from aspartic acid to asparagine in the CHRNA5 gene sequence, is the most consistent potential causal variant in nicotine dependence. In addition, its presence has also been associated with schizophrenia in non-smokers and with negative symptoms of schizophrenia (43). Interestingly, the frequency of this genetic variant is distinct across different ethnic populations. In African, Asian and American populations it is almost non-existent, while

around 40% of the European and Middle Eastern population have this allele (44). Additionally, it has been suggested that these gene cluster may underlie the formation and functionality of brain networks and could have a regulatory role during development (45).

1.4. Modelling neuropsychiatric disorders

Due to the complexity of the human nervous system, studying neurodevelopment and modelling its associated diseases has been a challenge. For the majority of conditions described in DSMV, the pathophysiology is poorly understood, and targeted diagnostic and therapeutic strategies have not been efficiently developed (12).

A disease model should be derived from plausible risk factors or causative agents and should be able to replicate neural or behavioural features that can be credibly linked to a human disease (12).

Animal models

In an attempt to tackle the environmental impact, different animal models of neurological disorders have been generated through selective breeding, genetic engineering, brain lesions, and environmental manipulations (12). Some etiological processes that cause the disease in human are recreated in the animal model and hence the neural and behavioural features of the disorder are replicated *in vivo*.

The 22q11 Deletion Syndrome is a hemizygous deletion that appears to be the strongest genetic risk factor for schizophrenia. Around 25% of patients with this syndrome are estimated to develop schizophrenia (46,47). This condition was reproduced in mice and, after *in vivo* analyses of circuitry function, dysfunctions in working memory were found. These abnormalities are a major deficit area in patients with schizophrenia (46).

However, chromosome 22q11.2 microdeletions are rare and a question is raised on whether studying the hereditary forms of illness caused by rare mutation is useful to shed light on common forms of the disorder (12).

Another drawback of this system is the lack of specificity, as many patients containing the deletion are diagnosed with bipolar disorder and it can be associated with autism spectrum disorders, intellectual disability, attention deficit hyperactivity disorder, anxiety, and depression (48).

Apart from this, other models to study schizophrenia have been developed, namely transgenic mice lacking cyclin D2, pencyclidine (PCP)-induced deficit model, the toxicity

model MAM (prenatal methylazoxymethanol acetate), the model of ventral hippocampal hyperactivity and a model containing a Disruptive translocation in Disc-1. These models have helped in understanding the roles of identified mutated genes in diseases and some features reminiscent of schizophrenia, such as behavioural abnormalities and cognitive decline, can be reproduced (49).

However, the mutations on which these models are based have been associated with other disorders and, for most mental illnesses, the disease-causing genes have not been undoubtedly established (50).

As a consequence, there has not been much success in translating preclinical work into novel therapeutic agents to treat neurological disorders, mainly because of species differences in brain complexity and disease-specific phenotypes (12).

In vitro models have enabled the study of molecular mechanisms underlying neurological pathologies and explore possible pharmacological targets (51). The role of isolated cells of one particular type and the role of specific molecules and compounds can be investigated in a more controlled environment. Secondly, screening for potential actions of drugs is also facilitated in these models (51).

Human ESC

Embryonic stem cells (ESCs) allow the directed differentiation of specific neural cell types and their use hold great potential in neurobiology. ESCs differentiation replicates the most important hallmarks of corticogenesis, including the generation of multipotent cortical progenitors that give rise to layer-specific cortical pyramidal neurons (52).

The *in vitro* differentiation system of embryonic stem cells and genetic manipulation promising tool to define the function of genes in early development.

The maturation of human ESCs (hESCs) into functional neurons and glia through a process analogous to *in vivo* development has been reported (53,54).

Cortical pyramidal neurons, in particular, have been generated from mouse ESCs cultured without any morphogen, but in the presence of a sonic hedgehog inhibitor. After engraftment in the mouse cerebral cortex, these ESCs have been proven to integrate in the host circuitry and gradually acquire similar characteristics to the native cortical neurons, such as development of axonal projections (52,55).

Apart from their role in modelling human disorders and drug screening, embryonic stem (ES) cells have been an interesting target because of their ability to generate all cell types

in culture and provide a ready supply of transplantable cells for human therapy of genetic and degenerative diseases (56).

Despite the potential of human embryonic stem cells (hESC) and the remarkable advances that they have prompted in the last decade, the debate on the moral status of the embryo from which hESCs are derived still prevails (57). In addition, with the development of new techniques like gene editing and mitochondrial replacement, new ethical, social and policy concerns have been raised, and the popularity of these cells has been decreasing (58).

Neurons differentiated from human induced pluripotent stem cells (iPSCs) have hence appeared as a powerful alternative tool to the use of hESC.

Human iPSC

For the past two decades, it has been possible to reprogram somatic cells to an embryonic-like state by transfer of nuclear content into enucleated oocytes (59) or fusion with human embryonic cells (60). These hybrid cells show morphology, growth rate, and antigen expression patterns characteristic of hESCs, suggesting the existence of factors that can induce pluripotency.

In 2006, Takahashi *et al.* firstly obtained induced pluripotent stem cells (iPSCs) from adult mouse somatic cells and, since then, this promising method has been explored to create genetically tailored patient-specific models for the study and treatment of human diseases. These researchers transduced mouse embryonic and adult fibroblasts with a retroviral vector encoding four transcription factors, OCT3/4, SOX2, C-MYC, and KLF4 and cultured them under ES cell culture conditions. The reprogrammed cells exhibited proliferative properties typical of ESCs, including the ability to grow indefinitely, the maintenance of pluripotency and the potential to generate cells of endo-, meso- and ectoderm. Morphologically, these cells also resembled ESCs. Moreover, iPSCs had a gene expression signature similar to that of human ES cells and several marker genes such as NANOG, ERas, fibroblast growth factor 4 (FGF4), reduced expression 1 (REX1), Dax1 or Zfp296 were expressed at high levels (61).

One year later, the group reported the generation of human iPSCs (hiPSCs) from human skin fibroblasts, similar to human ESCs (hESCs) in morphology, expression of surface antigens and other marker genes, and epigenetic status of pluripotent cell-specific genes.

Furthermore, these cells could differentiate into cell types representative of each of the three embryonic germ layers, both *in vitro* and in teratomas. They were also able to differentiate hiPSCs into neural and cardiac cells (62).

Since their discovery, many others have shown that it is possible to generate hiPSCs from other human adult somatic cell types, including peripheral blood cells (63), pancreatic cells (64), amniotic cells (65) or adipose cells (66).

Apart from allowing the study of human cortical development and pathogenesis, iPSC-base experiments also represent a powerful tool to test drug development with higher predictability of their effects in humans (67). iPSCs reprogrammed from patient somatic cells also allow temporal analyses of neurodevelopmental deficits and longitudinal studies that tackle the disease processes *in vitro* (68).

Human iPSCs generated from somatic cells have been efficiently differentiated into neurons or neural progenitor cells (NPCs), upon specific culture conditions and growth factors administration (69–71).

Besides the ability to recapitulate the cellular and molecular phenotypes of different diseases, systems based on these cells have also been shown to allow drug screening, in a model of motor neurons generated from amyotrophic lateral sclerosis patients' iPSC (72). Using a iPSC-derived hematopoietic cells in a humanized mouse model of sickle cell anaemia, these iPSCs have been used to restore physiological function of diseased tissues (73). These studies establish that iPSCs have a vast potential to generate a variety of functional cell types and can be used to modify the course of disease in rodents (74).

Neuronal defects characteristic of neurodegenerative disease have also been modelled using patient-derived induced pluripotent stem cells (75). These data suggest that hiPSC-derived neuronal precursors offer new possibilities for the *in vivo* modelling and study of human cortical development. Furthermore, the advent of hiPSCs makes it possible to study various psychiatric and neurological syndromes, including autism spectrum disorders and schizophrenia, which are complex genetic disorders of human neurodevelopment (76).

Functional properties of NPC-derived neurons and glia and neuron-glia interactions can be studied using hiPSCs-based *in vitro* model, nonetheless, neural circuits and their disruptions can uniquely be measured *in vivo*. To overcome that limitation iPSCs can be transplanted in living animals and their development followed *in vivo*. Recently, an example of modelling early events in transplanted iPSC from Down syndrome patients has confirmed the power of this approach (77).

For these studies it is important to consider some differences in neurodevelopment between the mouse and the human species. Apart from differences in size, surface area and folding, there are other key distinctions in neocortical development. In primates there is an

increased proliferation of cells in the subventricular zone (SVZ) and inner and outer regions can be distinguished. These two sub-layers are not visible in mice (78).

This zone persists into adulthood, as a main neurogenic area, where both neurons and glia can be generated. In neonatal and adult mice, it remains mitotically active throughout life in rodents (79).

Neocortical development also differs between rodent and human in the columnar organisation and characteristics of glial cells. The complexity of the astrocyte population is significantly different in the mouse and human brains. Four different classes of human cortical astrocytes have been identified and characterized while in rodents only protoplasmic and fibrous astrocytes exist. Human astrocytes also display an enlarged morphology and complexity, projecting longer and stronger processes than the rodent counterpart (80).

These differences have to be considered in transplantation-based experiments of human cells in animal models, so that species-specific features are taken into account and results can be extrapolated.

2. Aims of the project

There is an urgent need for an *in vivo* model capable of replicating the physiological human brain environment. The model presented here is a promising alternative, because it takes into account the human background and makes possible the study of specific genetic variations. It is based on the transplantation of human iPSC-derived neuronal precursors into the mouse cortex, and provides a means to replicate the physiological context and more closely assess the interaction between the developing neuron and the rest of the brain environment.

The work developed during the past ten months concerned the maturation and integration of these neuronal precursors expressing the wild-type form of nAChR subunits.

The first objective of the project was to characterize the model in terms of morphological changes and expression of specific cell markers characteristic of distinct differentiation states, over time.

We also intended to evaluate how the human graft is integrated, which kind of interaction is being established with the mouse glial cells and, overall, if the host environment can provide basic support for the survival and development of the human cells.

Later, neuronal precursors containing the polymorphic form of this receptor subunit gene will also be characterized and the maturation and activity patterns of both will then be compared. The long-term goal of the project is, therefore, to delineate the importance of genetic variations in nicotinic receptors on human neuronal development and address the participation of these receptors, in the context of schizophrenia.

3. Materials and Methods

In order to evaluate the differentiation and maturation of the human Neural Progenitor Cells (NPCs) in the mouse cortex of immunodeficient mice, these cells were cultured *in vitro* and transplanted in the mouse brain one day after birth. In total 56 mice divided in 6 groups, corresponding to the 6 timepoints, were used for the transplantation assays. The morphology of the cells and the host-graft interactions were evaluated for each timepoint, resorting to immunofluorescence labelling in fixed brain slices. Images were acquired using epifluorescence and confocal/spinning disk microscopy and analysed qualitatively on Fiji. A three-dimensional tracing software was used to trace neuronal projections of the human cells into the mouse cortex.

I was mostly involved in the *post-mortem* morphological characterization; however, this project also includes functional analyses using two-photon microscopy in awake mice, through which calcium transients are measured and neuronal activity of the human neurons is evaluated.

3.1. iPSC-derived Neural Precursor Cells expressing GCaMP6f

Previously, induced Pluripotent Stem Cells (iPSCs) were reprogrammed from human fibroblasts of healthy donors and were differentiated into neuronal precursors (Fig. 1).

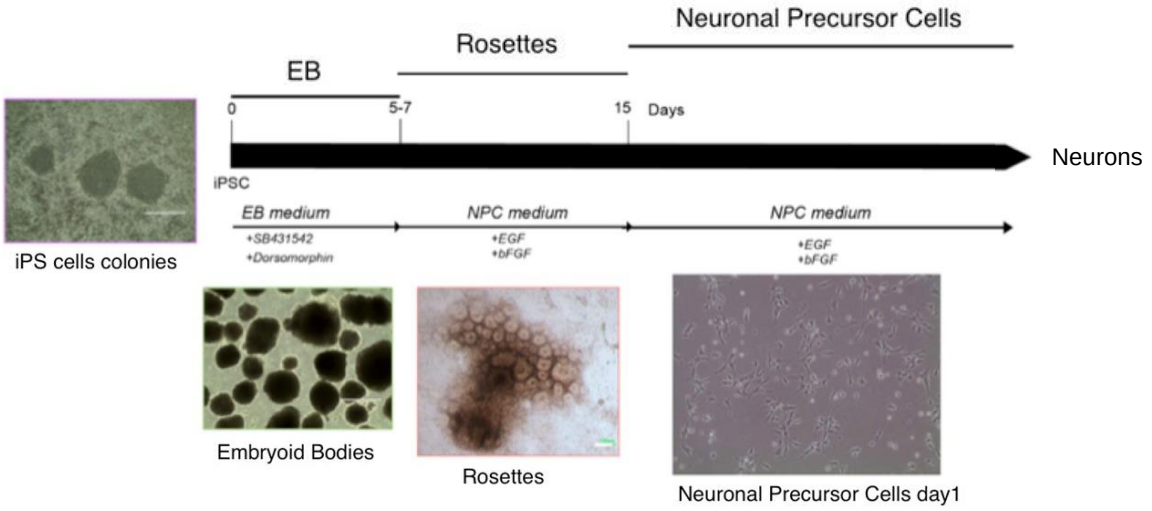

(Stéphane Blanchard)

Figure 1 – Schematic timeline of the differentiation of induced Pluripotent Stem Cells in Neural Progenitor Cells. After 15 days in culture under appropriate conditions, iPSC have gone through Embryoid Bodies and Neural Rosettes stages and have been differentiat

For the differentiation, human iPSCs (hiPSCs) were cultured in the presence of dorsomorphin and SB-431542, two factors that allow rapid and highly efficient neural conversion (81,82). After a few days, they became free-floating aggregates with a shape characteristic of Embryoid Bodies (EBs). EBs were plated and cultured in a Neuronal Progenitor Cell (NPC) medium containing Epidermal growth factor (EGF) and basic Fibroblast Growth Factor (bFGF) until they acquired the morphology of Neural Rosettes.
The human NPC line was then transduced with a lentiviral vector in order to express GCamp6f, a calcium probe that combines calmodulin with a circularly permutated green fluorescent protein (GFP) molecule. GCamp6f is characterized by a fast rise and decay kinetics and allows sensitive measurements of Ca^{2+} dynamics in living cells, making it a very useful tool to study neuronal activity (83). Even though GCamp6f already benefits from intrinsic fluorescent properties, for the immunofluorescence experiments it was necessary to amplify the signal using an antibody against GFP.
After their characterization for pluripotency(75), the iPSC clones were kept in NPC medium until passage 7/8, frozen in a CryoStor cryopreservation solution at –80ºC and, after 24 hours, in liquid nitrogen. I did not take part in this part of the project and only the frozen stocks of NPCs, already expressing GCamp6f, were used.

3.2. Culture of Neural Precursor Cells

NPCs were thawed and cultured for approximately three weeks. Cells were plated on 6 cm-dishes coated with Geltrex (ref.: 12063569, Gibco, 1/100 in cold DMEMF12, 1-hour incubation) in an appropriate medium. The NPC medium includes Neurobasal A medium (ref.: 21103049, Thermo Fisher), 2% of vitamin B27 without vitamin A (ref.: 12587010, Thermo fisher), 1% antibiotics solutions of penicillin and streptomycin (Pen-Strep 10,000 U/mL, ref.: 15140122, Thermo Fisher) and 1% of Glutamax supplement (ref.: 35050061, Thermo Fisher). After filtering through a 0,22 µm pore-vacuum system, 20 ng/mL of EGF (human EGF, ref.: 130-093-825, Miltenyi Biotec) and bFGF (human FGF-2, ref.: 130-093-842, Miltenyi Biotec) are added. Apart from their role in adult neurogenesis *in vivo*, these two factors promote proliferation, survival and self-renewal of the NPCs *in vitro* (84,85).
Once every week, the NPCs were trypsinized, centrifuged and counted in KOVA Glasstic Slides (ref.: 22-270141, KOVA), and 2×10^6 cells were split in each freshly coated dish. The culture medium was changed every other day. The cell cultures were incubated at 37ºC, in a 5% CO_2 atmosphere and kept until passage 15/16, to prevent the differentiation into

populations of non-neuronal cells that are formed later in development, such as astrocytes. Immediately prior to transplantation, cells were rinsed in Phosphate-Buffered Saline (PBS), trypsinized, centrifuged and counted. Suspensions of 200.000 cells/μL were prepared in PBS, making up a total volume of n × 1μL (n= number of animals to be injected).

3.3. Animals

NOD.CB17-Prkdc^{scid}/NCrCrI mice were used throughout the whole experiment to avoid transplant rejection. Rejection of xenogeneic NPCs engrafted in the cortex and striatum of murine brains has been documented, demonstrating the necessity of using an immunosuppressed host or perform an immunosuppressive treatment (86). This mouse strain is homozygous for the Severe Combined Immunodeficiency (SCID) spontaneous mutation Prkdc^{scid} and is characterized by an absence of T and B lymphocytes, lymphopenia, hypogammaglobulinemia, but a normal hematopoietic microenvironment. These animals also lack functional natural killer cells due to the non-obese diabetic (NOD) background. Therefore, they are very useful for xenograft research. Animals were raised in Charles River and purchased at 3 weeks of age. They were bred and their offspring, the pups used for this project, were born in the Pasteur Institute Animal Facility. Animals had unlimited access to food and water and were maintained in a specific pathogen-free (SOPF) animal facility, where strict barrier practices and aseptic techniques are implemented. All food, water and cages entering the room were autoclaved or sterilized, wearing personal protective equipment was mandatory and all manipulations were performed under a laminar flow hood. The number of adult animals per cage was limited to seven and housing conditions were appropriate, as evidenced by a high breeding rate and the delivery of large litters (ten pups per litter, on average).

Nine animals were assigned to each of the six timepoint groups, corresponding to 1-, 2-, 3-, 4-, 5- and 6-month post injection (mpi) and, in total, 54 mice were used for the transplantation assays. Both male and female mice were analysed.

All experiments were approved by the ethical committee of Pasteur Institute and the French Ministry for Superior Education and Research.

3.4. NPC injections

200.000 human iPSC-derived neuronal precursors in 1 µL, were transplanted into the right side of the cortex of new-born NOD/SCID mice, aged postnatal day 1 (P1). The mice were manipulated under a laminar flow biological safety cabinet, where they were manually immobilized. The injection site was located approximately 1mm laterally and 1mm caudally from Bregma (Fig. 2). The NPCs were injected 1 mm deep, using a Hamilton syringe containing a blocking system that prevented deeper perforation.

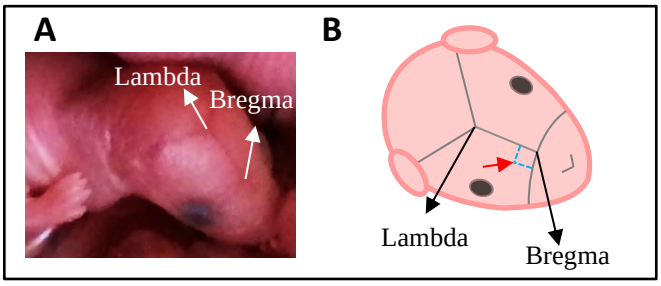

Adapted from D'Alessio et al.

Figure 2 – Intracranial injection of hiPSCs derived neuronal precursors into the cortex of neonatal mice. (A) Picture of a NOD/SCID newborn pup, where lamda and bregma landmaks used to target the motor cortex for injection are easly perceptible throught the skin (B) Schematic view of the mouse head and the injection coordinate, indicated by the red arrow. The target site is located approximately 1mm from bregma and 1mm lateral to the sagittal suture, with 1mm of depth (88).

3.5. Perfusion and fixation

For the neuron histological and morphological analyses, the transplanted mice corresponding to each timepoint were sacrificed, once every month, until the final timepoint of 6 months. Mice were deeply anesthetized with 12,5µL/mg of bodyweight of ketamine (Imalgen 1000, 15% in PBS; Rhone Mérieux) and Xylazine (Rompun, 2.5% in PBS; Bayer AG) until the paw retraction reflex was no longer visible. Mice were transcardially perfused with saline solution, followed by a paraformaldehyde solution 4% in PBS (PFA, Santa Cruz). The dissected brains were kept in the same fixating agent at 4°C for at least 24 hours before cutting.

3.6. Slicing and immunofluorescence

The fixed brains were sliced in 50 µm-thick coronal sections using a Leica Vibrating blade microtome. After removing the olfactory bulbs and cerebellum, the brains were glued with the dorsal part facing the razor blade and were cut immersed in PBS at RT. For storage, slices were immersed in PBS Azide 0,2% to prevent microbial contamination and maintained at 4ºC.

For the immunofluorescence labelling, slices across the whole brain were initially stained against GFP to localize the human graft. Posterior stainings were undertaken to evaluate neuronal maturation and host-graft interactions. Anti-STEM101 antibody was used to stain human nuclei and anti-Tuj1 to detect neurons. As markers of level of differentiation, Sox2 and NeuN were used. Synapses were localized with anti-PSD-95 and anti-synapsin1.

Primary antibodies	Dilution	Source	Reference
Rabbit anti-GFP	1/750	Invitrogen	A6455
Chicken anti-GFP	1/1000	Abcam	Ab13970
Mouse anti-STEM101	1/100	Takara Bio	Y40400
Mouse anti- Tuj1	1/100	Biolegend	MMS-435P
Rat anti-Sox2	1/200	eBioscience	14-9811-82
Mouse anti-NeuN	1/200	Milipore	MAB377
Rabbit anti-PSD95	1/800	Abcam	Ab18258
Rabbit anti-synapsin	1/500	Milipore	AB1543P
Rabbit anti- CD31	1/800	Abcam	Ab 124432
Rabbit anti-GFAP	1/400	Abcam	Ab7260
Chicken anti- MBP	1/100	Milipore	AB9348
Rabbit anti-Olig2	1/1000	Abcam	Ab109186

Table 1 - List of the primary antibodies used, their dilution, the supplier and the respective reference

For the vascular staining, CD31 antibody was used. GFAP was targeted to label astrocytes and oligodendrocytes were identified with antibodies against MBP and Olig2. The primary and secondary antibodies used are listed Tables 1 and 2.

Secondary antibodies	Dilution	Source	Reference
Goat anti-rabbit AF 488	1/400	Invitrogen	110008
Goat anti-chicken AF 488	1/1000	Invitrogen	11039
Goat anti-mouse AF 488	1/200	Life Technologies	A11029
Goat anti-rabbit AF 594	1/400	Invitrogen	A11012
Goat anti-mouse AF 594	1/400	Invitrogen	A11005
Donkey anti-rat AF 594	1/400	Jackson ImmunoResearch	712-585-150
Donkey anti-chicken Cy3	1/200	Sigma-Aldrich	AP194C
Donkey anti-rabbit AF 647	1/200	Jackson ImmunoResearch	711-605-152
Donkey anti-mouse AF 647	1/200	Jackson ImmunoResearch	715-605-150
Donkey anti-rabbit DL 405	1/200	Jackson ImmunoResearch	711-475-152

Table 2 - List of the secondary antibodies used, their dilution, the supplier and the respective reference; AF – AlexaFluor®; DL – DyLight®

Most of the immunostainings were performed following the same protocol. After two short washings in PBS, the brain slices were incubated for thirty minutes in a solution of PBS containing 10% of Normal Horse Serum (NHS) and 0,5% of triton at RT, to block unspecific sites and permeabilize the cells. Slices were then rinsed in PBS with 2% of NHS and 0,2% of triton and incubated with the primary antibodies of interest in the same solution overnight (ON), at 4ºC, over a plate shaker. The primary antibodies solution was discarded, the slices were washed in PBS three times and the secondary antibodies were incubated in the same solution of PBS 2% NHS and 0,2% triton, for two hours, at RT, also over a shaker. Lastly, DAPI was added and incubated for 10 minutes, followed by two additional washings in PBS. The labelled brain slices were finally mounted over Superfrost Plus microscopic Slides (Thermo Scientific) with Prolong Gold Antifade Reagent (Invitrogen, Ref P36930) and a glass coverslip (~0.15mm of thickness). For the particular case of the MBP labelling an initial incubation in absolute ethanol is required to facilitate denaturation. For the CD31 antibody the protocol was slightly altered. Firstly, slices were heated in citrate buffer (10mM Sodium citrate, 0,05% of Tween 20, pH 6.0) in a water bath at 95ºC,

for 20 minutes. After the container cools down, the samples were rinsed twice in PBS with 0,05% Tween 20 and were then saturated in PBS, 10% NHS and 1% Bovine Serum Albumin (BSA) for 30 minutes, at RT. PBS Tween 20 was used for the washings and the primary and secondary antibodies were incubated in PBS with 2% NHS 0,05% Tween 20 and 1% BSA.

3.7. Epifluorescence and Spinning disk Confocal microscopy

In the beginning all samples were imaged in a Zeiss AxioVert epifluorescence microscope equipped with Apotome and AxioCam camera controlled by the AxioVision Software. For the localization of the GFP stained graft, mosaic multi-channel images of whole slices were obtained using a 5x 0.16 NA objective.

To evaluate the cell-cell interactions between the host and the human graft with greater spatial resolution and contrast, the stained samples were imaged in Opterra II, a confocal spinning disk microscope, and acquired with Prairie View software. This swept-field confocal microscope allies the resolution advantage conferred by confocal microscopy with the speed of spinning disk technologies. Apart from the speed and resolution flexibility, the point illumination eliminates out-of-focus signal enabling a decrease in phototoxicity and bleaching during the acquisition.

Depending on the level of detail needed and the trade-off between resolution and speed that could differ from one experiment to another, images were taken using either a 20x dry objective, a 40x oil objective or a 60x oil objective. The power of the three lasers (405nm, 488nm and 561nm) was differently adjusted to each channel and staining. The GFP staining was typically very bright and relatively low powers sufficed, whereas the DAPI signal was dim and harder to detect, requiring a constantly higher power of the 405nm laser. The exposition time varied between 100 and 150ms.

Multichannel mosaic and/or Z-stack images were captured, according to the goal of each assay and were subsequently stitched using the Fiji Plugin. Brightness and contrast adjustments, filters application and additional image processing was performed in Fiji, as well.

3.8. 3D Neuron tracing in Imaris

For a more accurate analysis of cell morphology over time, Imaris (Imaris v 9.3, Bitplane AG) was used to trace the human neurites and measure a set of relevant parameters, including filament length, straightness, density and branching level. The Imaris Filament Tracer software allows the reconstruction of three-dimensional structures from two-dimensional images and is ideal for fluorescently labelled confocal images, because the very specific staining facilitates the Filament segmentation step.

To make sure that most of the human graft was captured and that the highest number of neurons possible was included, samples were imaged in mosaics and Z-stacks of around 20µm of depth and a step size of 0,8µm.

Before the tracing, images are pre-processed in Fiji, to enhance the contrast between signal and background and guarantee that the filaments edges were as sharp as possible.

Pre-processing in Fiji

To begin with, images were opened through the Grid/Collection stitching plug-in and the tiles were fused using the "Linear Blending" method. The fused image was, then, duplicated and a Gaussian Blur filter was applied to this copy image.

This plug-in filter uses convolution with a Gaussian Function to calculate the transformation that each pixel needs to suffer in order to smooth the image. By setting a high sigma factor, the standard deviation of the gaussian function, we attenuate high frequency signals and the signal is not visible anymore. We used a sigma of 50, that results in highly blurred images and creates, thus, a background estimation. Afterwards, we used the Image Calculator operation to subtract the blurred image from the original fused one, creating a new image in which the edges of the cell structures are more defined (Fig. 3).

After adjustment of brightness and contrast in each of the three channels, images are converted to 8-bit, saved as tiff files and converted to .ims format.

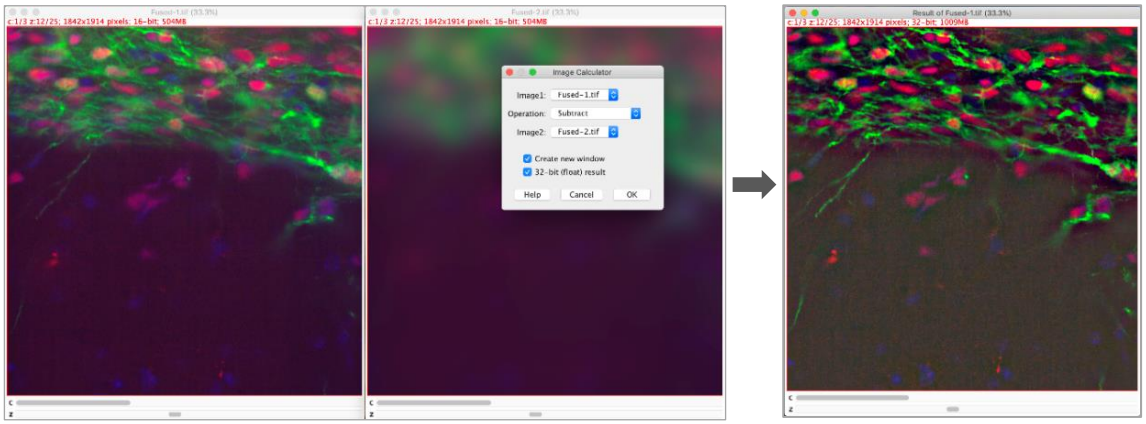

Figure 3 - Pre-processing on Fiji. Effect of the application of the Gaussian Blur and Image Subtraction in creating more defined borders. Human cells expressing GCaMP6f are presented in green and the respective human nuclei are in red, DAPI is labelling all nuclei.

Nuclei detection and masking in Imaris

The .ims images were opened in Imaris and the Voxel Size was adjusted in the Image Properties to correct the scaling. Even though the input images could be multi-channel, the Filament Tracer could only process one channel at a time. Firstly, we had to create a mask of the human nuclei on the green channel. We asked the software to detect automatically the spots in the red channel, STEM101 staining, based on an estimated XY diameter value that we provided as a reference. The threshold could be changed, and the user could also manually include or exclude some spots. The mask would then be imprinted in the green channel, corresponding to the GFP staining, and a duplicated green channel containing the nuclear imprint was created for each image (Fig.4).

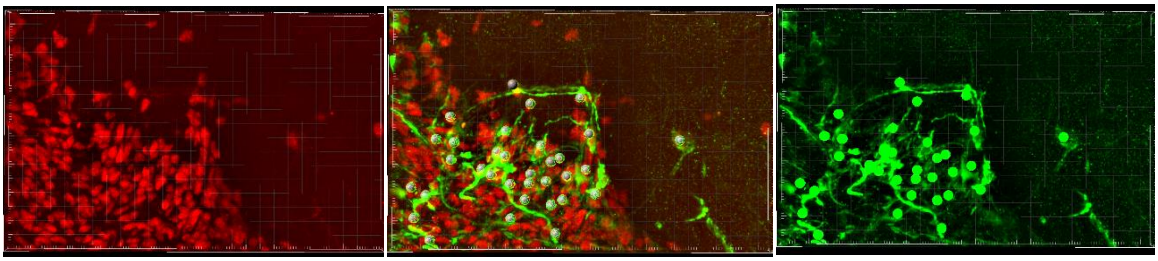

Figure 4 - Application of the human nuclei mask on the green channel, the initial step in Imaris neuron tracing. GCaMP6f is stained with GFP, in green, and the human nuclei, stained with STEM101 are in red.

Neuron tracing in Imaris

The filaments tracing was carried out in the masked green channel, using a semi-automated strategy that could be applied in all samples and that would allow a more reliable comparison of the interaction of the human cells with the mouse cortex between the different timepoints. We traced the neurites that emerged out of the graft and projected into the mouse cortex using the Autopath mode with the automated centre and automated diameter functions activated. In most cases, it was not always possible to identify the filaments origin, so by default we selected the border of the graft as the starting points.

Lastly, once all the tracings were done the desired parameters were chosen in the Statistics Tab and exported in the form of an .xml file.

The main parameters analysed were neurite straightness, length and number of branches.

3.9. Nuclear counting in Fiji

To count the number and density of oligodendrocytes and neural stem inside cells the human graft and in the mouse cortex, a cell counting task was performed on Fiji.

Similarly to the pre-processing that preceded the Imaris tracing, the Gaussian Blur (sigma of 10) and Image Calculator tools were used to increase the definition of the cell borders. Each channel was thresholded (for each sample the value was the same across all channels) and converted to 8-bit mask. The graft area was delineated using the polygon selection, according to the STEM101 staining, the area was measured, and the Analyze Particles function was used to detect the number of nuclei inside the areas of interest (Fig. 5).

When applying the threshold, the nuclei inside the graft appeared frequently fused. In these cases, watershed segmentation was employed to avoid undercounting.

These data were transferred to an Excel sheet, the density of oligodendrocytes was calculating dividing the number of $Olig2^+$cells per area. The percentage of pluripotent cells was calculated dividing the number of $Sox2^+$ cells by the total number of nuclei (stained with DAPI).

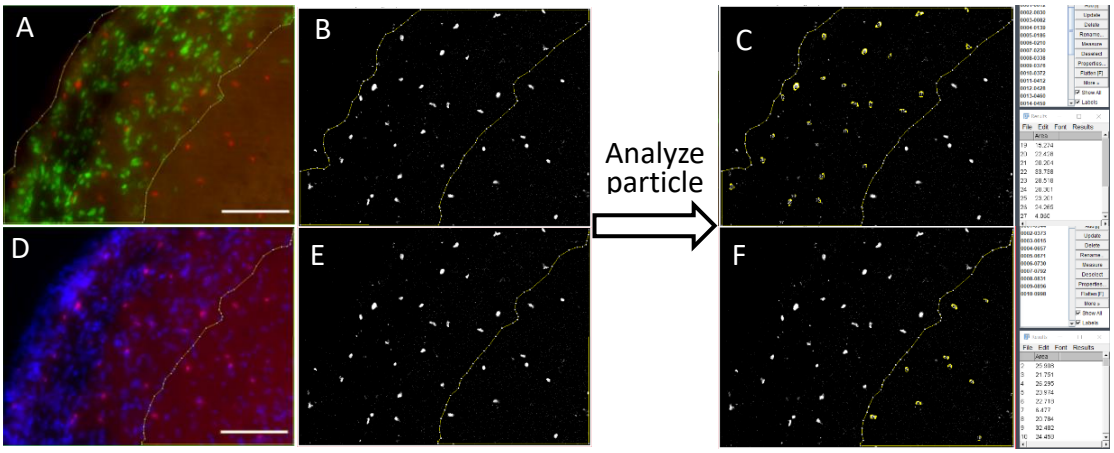

Figure 5 - Nuclear counting of oligodendrocytes in Fiji. In the first column, representative initial images preceding the application of the gaussian blur and threshold are presented; the human nuclear staining, in green, is used as a reference to define the graft boundaries (A) and the mouse cortex (D) areas. Thresholded images of the Olig2 staining are obtained and the Analyze Particle function is run both inside the graft (B) and in the mouse cortex (E). The detected particles appear in the image and a listing of the number of particles and the respective areas inside (C) and outside (F) the human graft is generated. Olig2 is in red, STEM101 in green and DAPI in blue. Scale bars: 100µm

3.10. Statistical Analysis

Statistical analysis was performed using GraphPad Prism Software. For the neuron morphological analysis, the data were tested by Kruskal-Wallis test followed by a Dunn multiple comparison analysis. Differences were considered statistically significant at $p<0.05$. Data are presented as means ± SEM.

4. Results

The grafting technique and the parameters such as day of injection, spatial coordinates and the volume and number of cells injected were adapted from previous grafting studies (52,87) and optimized in the group (88). The neuronal development and integration into the mouse brain were followed up to 6 months post-injection (mpi). Efficient transplantation of hiPSC-derived neuronal precursors into the cortex of new-born mice was achieved and there were no signs of rejection of the transplanted cells.

Several immunostainings against markers of cell identity and synaptic proteins were carried out in order to assess the maturation status at the different timepoints. Quantitative morphological analyses were performed and double labellings of the human GCamp6f-expressing cells and two populations of mouse glial cells, astrocytes and oligodendrocytes, were done to explore how the graft and the host circuitry interact (Fig. 6).

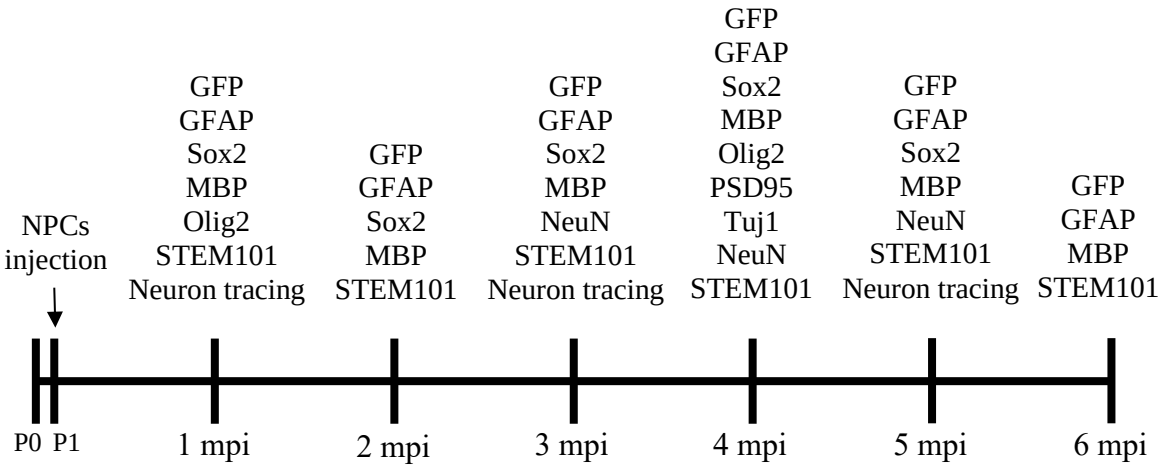

Figure 6 - Schematic overview of the immunofluorescence experiments performed over the 6-months period. The injections were done one day after birth (P1) and once a month a set of animals were perfused, and the brains were collected for the indicated immunostaining assays

4.1. Human iPSC-derived neuronal precursors migrate and integrate efficiently into the mouse cortex

Initially, we performed an immunolabelling against GFP to localize the GCamp6f-expressing human cells. Despite the injection of the same number and volume of NPCs, the appearance of the graft was heterogenous. Most samples displayed a graft with a minimum thickness of around 30 µm, that allowed further characterization. In a few brains the injected cells were released in the ventricles and did not succeed in migrating towards the cerebral cortex, and in others we could not detect any GFP staining at all. There were still some brains where the cells migrated but were present in such a reduced number that they were excluded from the following staining assays.

We injected the NPCs in a total of 52 animals, but during the course of the experiment, 5 mice died due to natural causes. We were able to detect grafts that enabled further characterization in 29 of these 47 brains, making the success rate of the injection protocol of approximately 62%.

When analysing the successfully injected brains at different timepoints, we detected the presence of grafts of variable sizes, localized mainly in the most rostral brain region. The human cells migrated from the injection site to the most dorsal part of the brain, where they were accommodated on the top of the mouse cortex (Fig. 7).

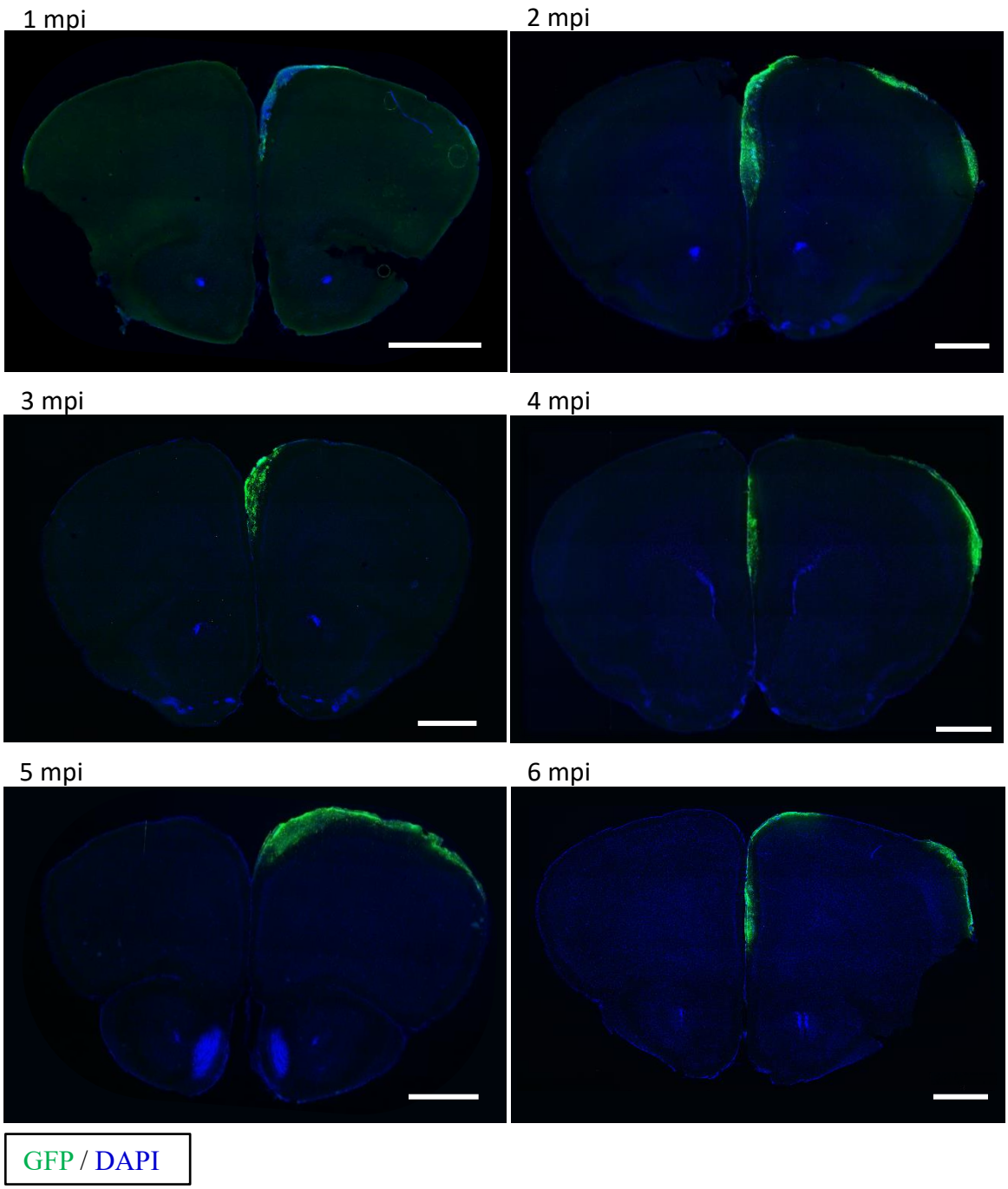

Figure 7 - Representative images of the GFP staining of the human graft in each of the 6 timepoints. Human cells migrate from the injection site and are accommodated on the top of the mouse cortex since 1mpi. Nuclei are counterstained with DAPI. Scale bar: 1000µm

Apart from the differences in size, there was also a variation in the graft location across the samples. They were typically present in pre-limbic, cingulate and motor cortex, but a few also extended to somatosensory cortex (Fig. 8). The highest concentration of human cells was generally between +2.3mm and +0.8mm AP (anteroposterior axis, from bregma) and tended to be closer to the medial axis.

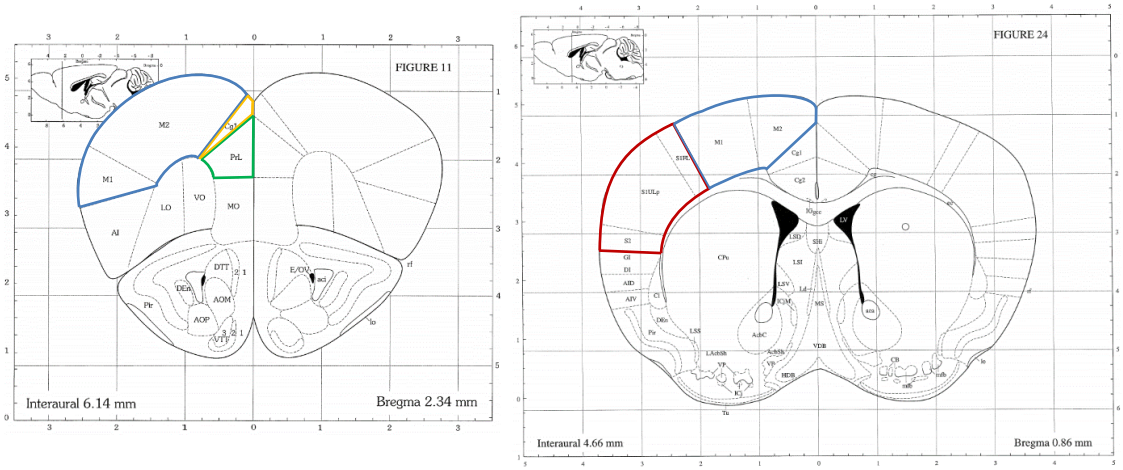

Figure 8 – Identification of the human graft placement in relation to reference images of a Mouse Brain Atlas. The graft is localized in the prelimbic cortex (highlighted in green), cingulate cortex (in yellow), motor cortex (in blue) and somatosensory cortex (in red). The grafts extended from around 2,3 to 0,8 mm AP. Atlas images were adapted from Paxinos and Franklin, 2004.

In spite of the differences, certain features are shared between all samples, such as the higher density of nuclei inside the graft, highlighted with the DAPI staining (Fig. 9)

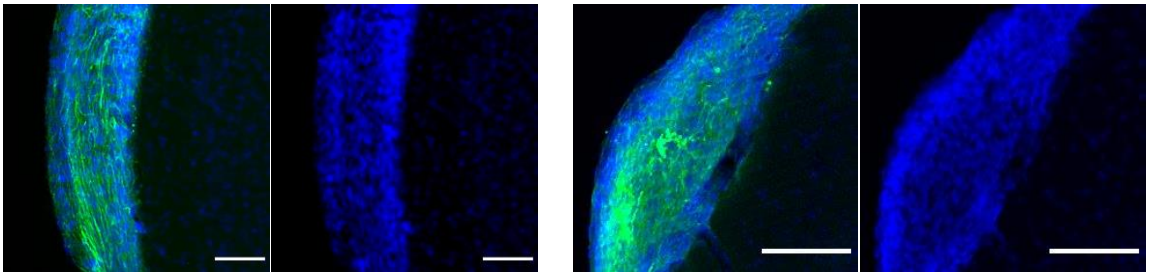

Figure 9 – Detailed images of the GFP staining at 1mpi. The density of nuclei, counterstained with DAPI, is significantly higher in the human region in comparison with the mouse cortex. Scale bars: 100 µm

Another consistent observation was the tendency for a medial distribution. Even in grafts of considerable size where the neuronal cells extend for longer distances, the distribution of human cells was not totally homogenous. The density was higher in the medial and lateral regions of the brain and slightly lower in the most dorsal parts (Fig. 7, especially the right column).

In some samples the presence of green traces in more ventral locations, underneath the cortex, made the localization of the injection site possible. In other samples, human cell migration was not fully attained and a GFP^+ cluster could be found inside the ventricles (Fig. 10).

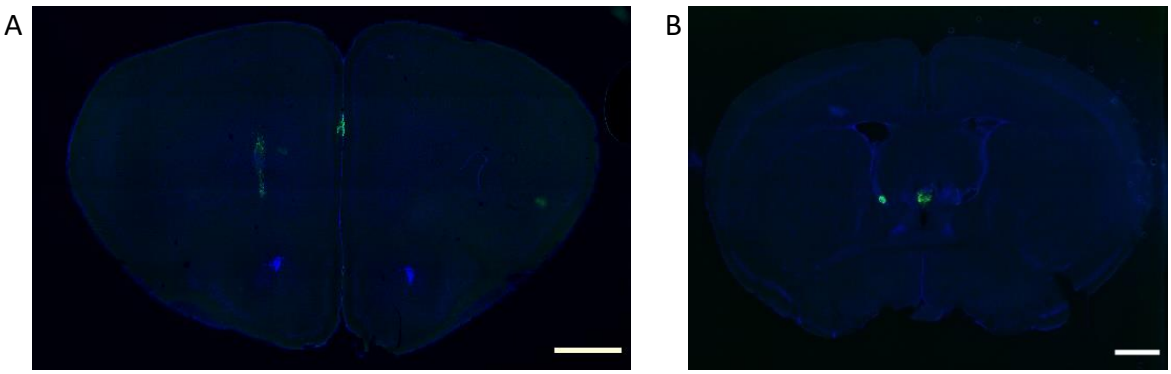

Figure 10 - Examples of human grafts that did not migrate to the mouse cortex (A) Human cells cluster in the middle of the left hemisphere is localized in the site where the NPCs were released (B) Some human cells are confined to the ventricle. Human cells are stained with GFP and nuclei are counterstained with DAPI. Scale bars: 1000µm

Taking into account the dense configuration of the cortical human grafts and the clear dissimilarity between them and the mouse cortex, we proceeded with further investigations to directly assess complexification, differentiation and interaction with the surrounding environment.

4.2. Human iPSC-derived neuronal precursors become more complex and project deeper into the mouse cortex over time

Looking into the GFP staining samples with bigger detail it was possible to detect the presence of green filaments coming out of the human graft and projecting into the mouse cortex, especially in the later timepoint (Fig. 11). This observation gave us a hint that differentiation processes were occurring over this 6-month period. Interestingly enough, these neuronal projections were even visible emerging from the green cell clusters accumulated around the injection site.

In the first two timepoints, but mainly in 1mpi, very few projections are visible outside the graft and the ones that extend are short, frequently bent and disorganized, i.e. the angle they

establish with the border of the graft is very variable (Fig. 10A and 10B). In 3mpi, it is already possible to detect slightly longer and straighter projections and there is a tendency for a perpendicular distribution in relation to the graft (and mouse cortex) edge (Fig.10C, second image). In 4 mpi, the number of projections rises even more, as well as their length. Nonetheless, in these two intermediate timepoints the neurites distribution is still unsystematic, and regions of longer straight perpendicular projections alternate with regions of short misguided ones (primarily in Fig.10 D). The uneven level of organization is suggestive of a not totally mature state. In the latter timepoints, 5 mpi and 6 mpi, neurites are clearly more developed, more organized and longer. Some appear to reach up to 500µm of length (more evident in Fig.10E, second image, and 10F, first image). The number of curved filaments is practically inexistent and even in some thinner grafts a considerable sum of GFP^+ fibres could be observable.

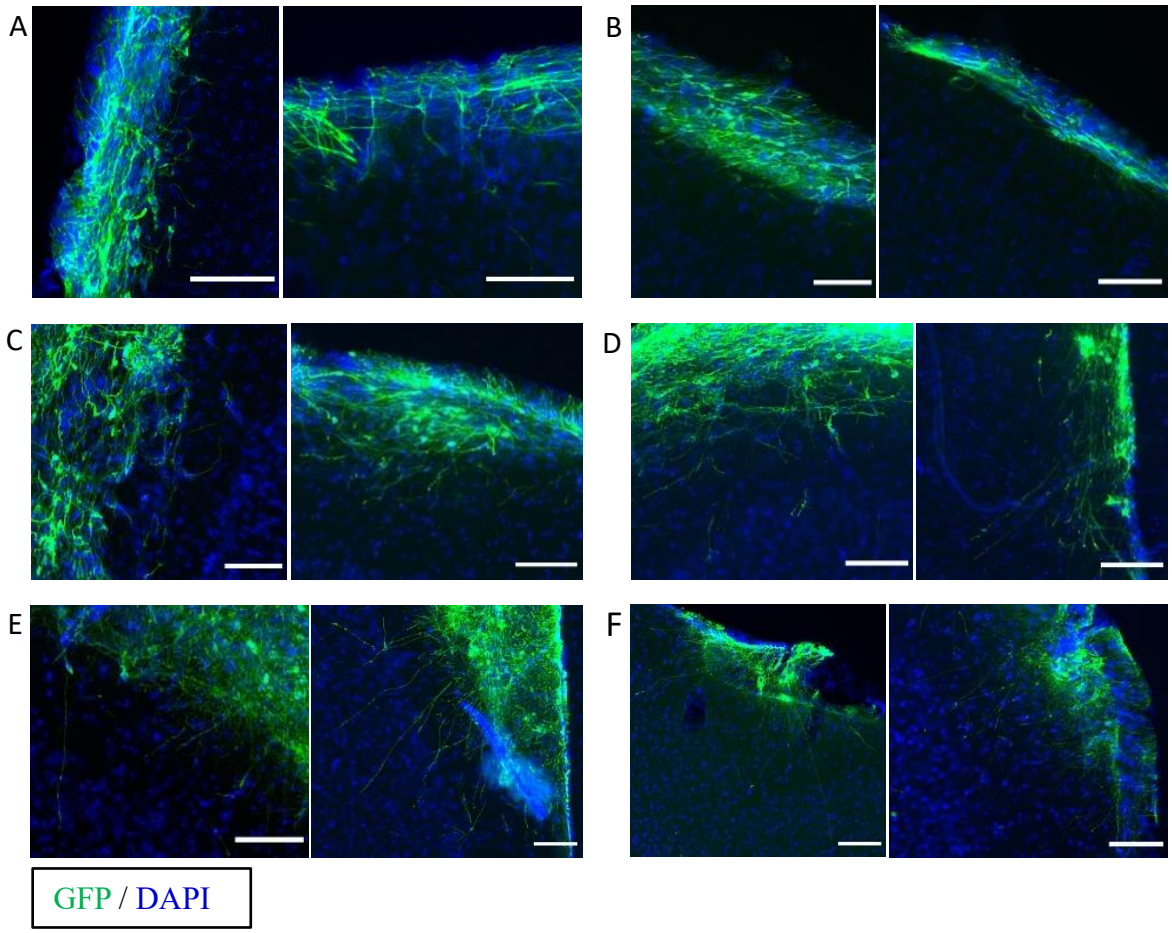

Figure 11 – Amplified images of immunofluorescent GFP labelling of brain sections at 1 mpi (A), 2 mpi (B), 3mpi (C), 4mpi (D), 5 mpi (E) and 6 mpi (F) timepoints. DAPI was used as counterstain. Scale bar: 100 µm

Considering the morphological differences between the brains imaged in the two last timepoints were not substantial, and also due to time limitation, most of the further analysis was carried out only until 5mpi.

The GFP staining indicated the overall disposition of the human cells and, even though there is some variability in the size and localization of the graft across the different brains, we distinguished a pattern of increasing complexity. The projections that were coming out of the graft were becoming denser, longer and straighter over time. This progressive organization was the first evidence that the human cells develop in the host brain and acquire some degree of differentiation over time. We realised that further analysis of differentiation could be a great advantage to understand which parameters are changing and at which rate. For that purpose, we proceeded to a quantitative examination using Imaris, a tracing software that enables the three-dimensional outlining of neurons. This software was designed for the 3D visualization and neuronal tracing of confocal data like the one we had.

In our preliminary approach we were using uniquely the GFP and DAPI signal, and later we introduced a new staining, against human nuclei, in order to better localize the starting points and the limits of the graft, and to improve the detection globally. Therefore, for the human nuclear labelling the antibody STEM101 was used alongside the anti-GFP antibody. This human nuclear antibody reacts specifically with the human nuclear protein Ku80, a helicase involved in non-homologous end joining that is required to repair double-strand breaks.

Once again, this staining confirmed the development and maturation of the projections in the injected cells. It demonstrated that all the densely packed nuclei within the graft that were previously detected with DAPI, are truly of human origin. In addition, as there were no human nuclei outside the relatively well-defined areas of the graft, this experiment also showed that all human filaments have their origin inside the graft and become indeed longer over time (Fig. 12).

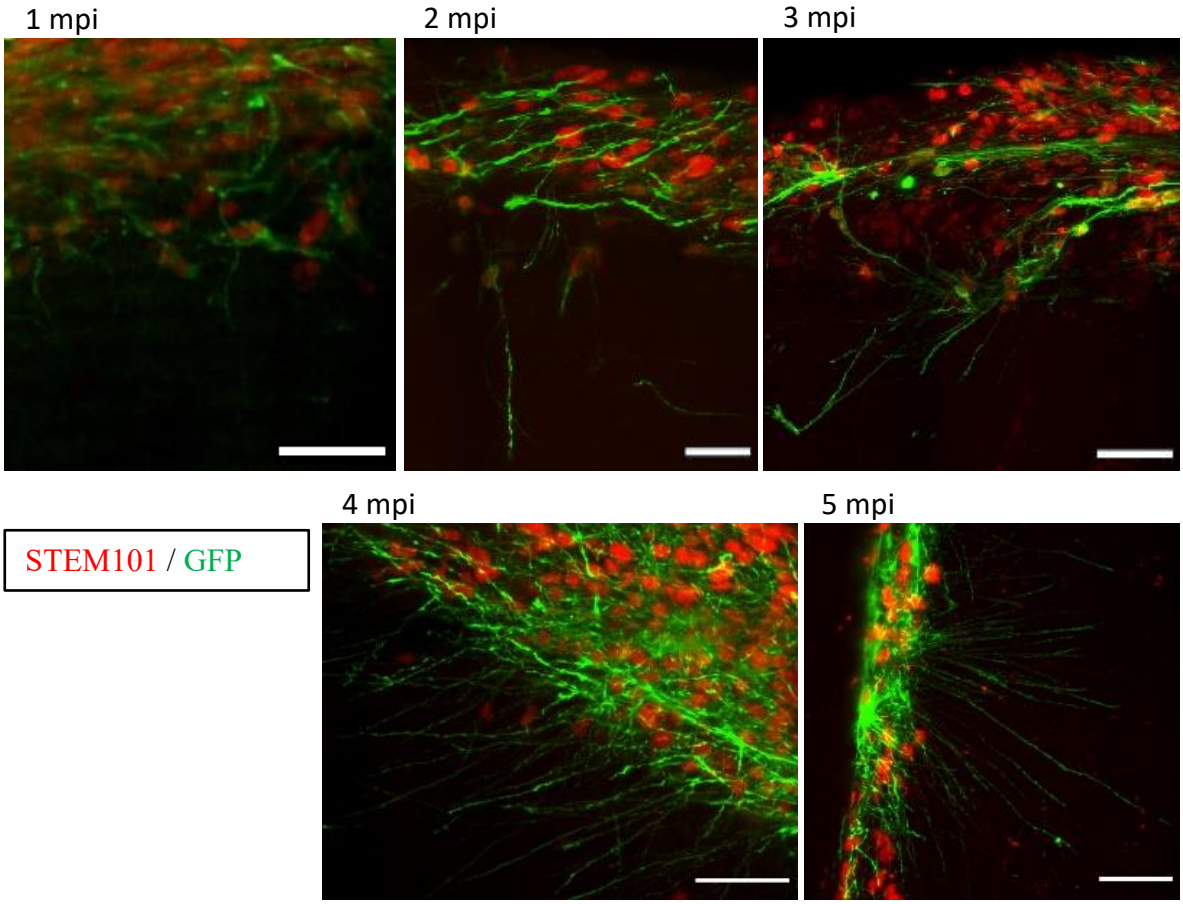

Figure 12 - Representative images of the human grafts of the first 5 timepoints, double-stained with the STEM101 (red) and the GFP (green) antibodies. Scale bars: 40 µm

After the stained brain slices were imaged in the confocal/spinning-disk microscope, pre-processed on Fiji and converted to the correct format, the 1, 3 and 5 mpi images were traced in the tracing software (Fig. 13A and 13B) and the relevant statistics were exported (Fig.13C-E). In total, 31 filaments from four 1 mpi samples, 42 filaments from two 3 mpi samples and 121 filaments from three 5 mpi samples were traced.

As it was evidenced by the GFP initial staining, the human projections become more complex over time. The filaments become increasingly longer, being the most substantial difference from the third to the fifth timepoints (Fig. 13C). From the first to the third month, the neurite length increases but the difference is not statistically significant. In both timepoints the mean is around 40 µm, while at 5mpi neurites are, on average, 80 µm long. Regarding straightness, the difference is not striking between timepoints. Imaris defines filament straightness as the distance between the starting and ending points divided by the length of the filament (displacement/length). It is always smaller or equal to 1 (an index of

1 corresponds to a totally straight neurite). The change in the mean straightness is slightly bigger from 1 mpi to 3 mpi, while from 3 mpi to 5 mpi there is hardly any fluctuation (Fig. 12D). In the first month, the dispersion is higher evidencing the existence of more heterogenous neurites than in the following timepoints.

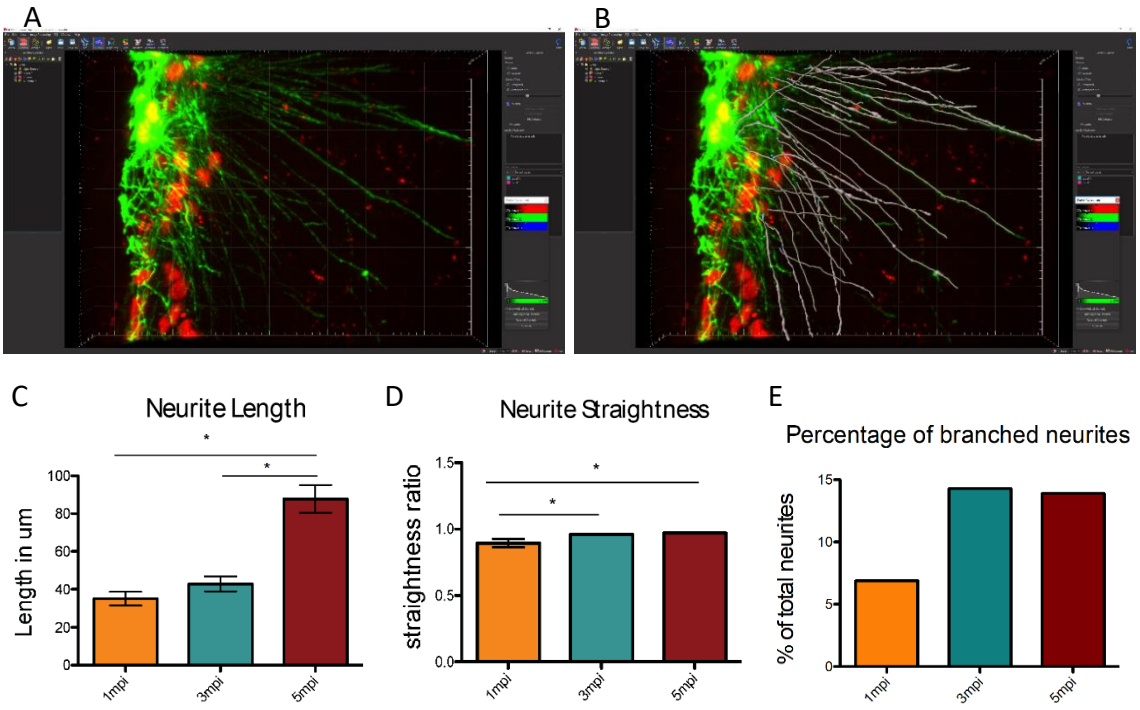

Figure 13 – Imaris filament tracing and quantification of three parameters in the 1 mpi, 3 mpi and 5 mpi samples. Representative image of a section of a 5 mpi brain slice before (A) and after (B) the three-dimensional tracing, in grey. The human projections are represented in green and the human nuclei in red. (C) Bar chart of the mean projection length, in µm, for each timepoint, with the respective standard error (SEM) (D) Bar chart of the mean projection straightness index for each timepoint, with the respective SEM (E) Percentage of branched projections in each timepoint.

Regarding the branching level, the percentage of filaments that have bifurcations doubles from 1 to 3 month and is basically identical between the 3rd and the 5th months. Around 7% of 1 mpi filaments display branches while the percentage of branched filaments in 3 and 5 mpi is of almost 15%.

We can infer that the network becomes more complex and the human cells interact more with the mouse cortex over the 5-month period.

Apart from these evident changes in filaments morphology, we could also detect the presence of dendritic spines. We firstly observed these structures in 2 months brains (Fig. 14), but they were still not abundant in the 3- and 4-months samples. These specialized post synaptic compartments that are present on the surface of dendrites receive input from excitatory synapses and exhibit diverse morphologies and functions within the cortex. They are thought to be important for synaptogenesis, synaptic regulation and cognition, and their appearance is perceived as a hallmark of neuronal differentiation and specialization (89).

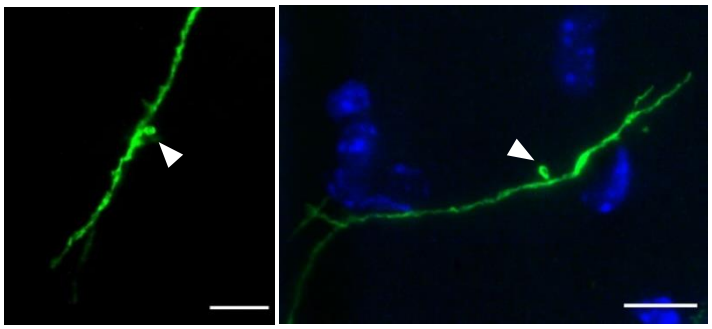

Figure 14 - Representative images of dendritic spines detected at 2 mpi, indicated by the white arrowheads. These images are Maximum Intensity Projections of 2µm-thick Z-stacks. Human dendrites are represented in green and nuclei are in blue. Scale bars: 10 µm

These experiments revealed that the human progenitor cells acquire distinctive neuronal traits over the 6-month period, including dendritic spines, neurite outgrowth and an increasingly intricate network of projections into the mouse cortex.

4.3. Some human iPSC-derived neuronal precursors mature and differentiate in the mouse cortex

To further study the maturation of the human cells, we stained 4-month samples with an antibody against the postsynaptic density protein 95 (PSD-95), to spot the presence of synapses (Fig. 15).

PSD-95 is a membrane-associated guanylate kinase (MAGUK) that interacts with NMDAR and is recruited at postsynaptic sites for the clustering of receptors, ion channels, and signalling proteins. It is required for synaptic plasticity and it prevents synaptic depression (90,91).

Labelling this protein allowed us to distinguish a region on the top of the brain slice, corresponding to the human graft, where the synaptic density was superior (Fig.15A). These data imply that the human neuronal precursors develop mature synapses over a 4-month period *in vivo*. However, despite the evident brighter red band, the background noise

in all the samples appeared to be very pronounced and the microscopic resolution we could afford was not enough to assure us of the specificity of the staining.

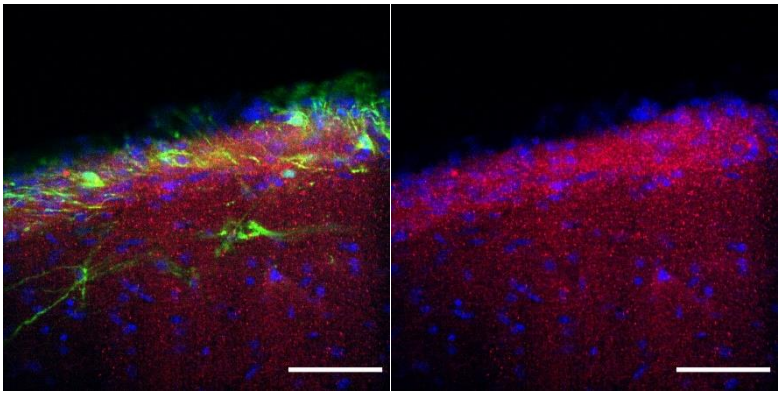

Figure 15 - Representative image of synapse density in the human graft region, at 4mpi. PSD-95, in red, is staining the post-synaptic compartments and GFP, in green, is staining the human graft. DAPI is used as counterstain.
Scale bars: 100 µm

An immunostaining for synapsin1 (syn1), a presynaptic marker, was also done, in an attempt to corroborate the PSD95 results and clarify on the synaptic maturation of the human graft. The pattern of syn1 distribution was similar to the one of the postsynaptic marker, but the labelling seemed even less specific. For that reason, and on account for the limited number of viable grafted samples, we did not proceed with this staining in the grafted brains.

Apart from the synaptic markers, we also performed an immunolabelling of the Neuronal Nuclei Antigen (NeuN) in 3 mpi, 4 mpi and 5mpi brain slices, to help establishing the evolution of the neuronal phenotype (Fig. 16A-C). NeuN is a neuronal specific nuclear

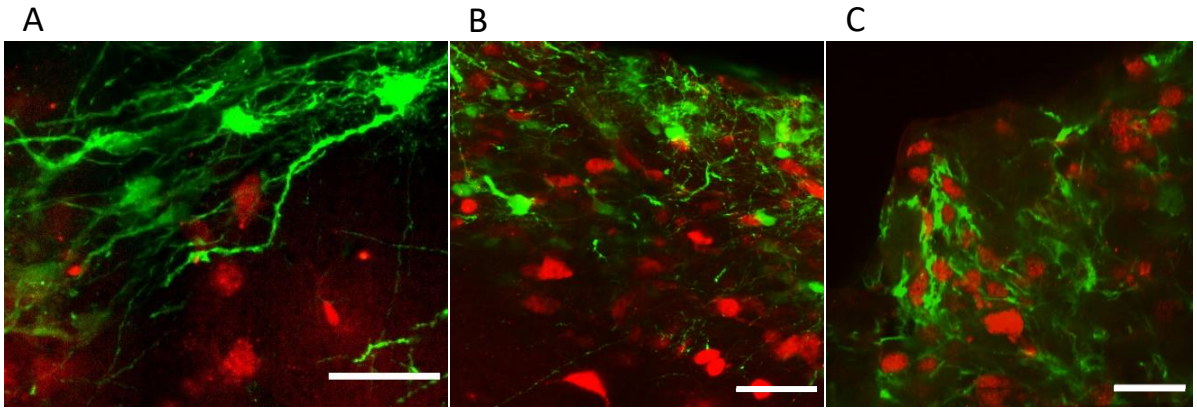

Figure 16 - Representative images of Neuronal Nuclei Antigen staining in the human graft area of 3 mpi (A), 4 mpi (B) and 5 mpi (C) samples. NeuN is represented in red and GFP in green.
Scale bars: 40 µm

protein present in postmitotic cells that appears at the point of differentiation into mature cells. It can be used to detect almost all neuronal cell types (92,93).

There is an increase in the amount of $NeuN^+$ cells inside the graft, suggesting that the injected cells become gradually more mature and there are more neurons entering the terminal differentiation. Nevertheless, in comparison to the NeuN expression detected in the mouse cortex, and considering the total number of human cells, this quantity is still modest. In addition, in the graft these cells are more disorganised than in the mouse cortex (Appendix, Fig. 26).

These two stainings reflect that a part of the engrafted neurons are undergoing differentiation and replicating two key steps of neurodevelopment – synapse formation and arrival to a postmitotic stage.

4.4. Human iPSC-derived neuronal precursors exhibit an immature neuronal phenotype at 4 months post-injection

Brain sections of 4 mpi were also stained for Tuj-1, neuron-specific class-III β-tubulin (Fig. 17). Tuj-1 is a lineage marker that is present in cell bodies, dendrites, axons and axonal terminations of immature neurons in PNS and CNS. It participates in axonal transport and assists in microtubule stability in neuronal cell bodies and axons (92,94).

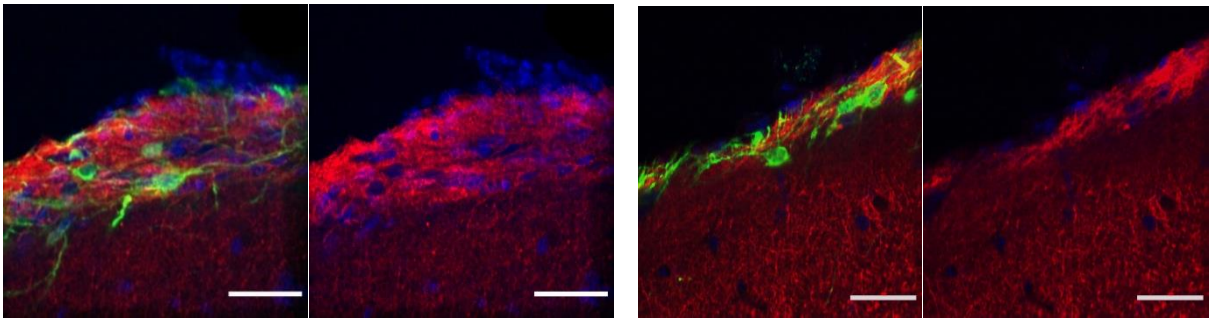

Figure 17 - Representative images of the labelling of immature neurons in the human graft region, at 4 mpi. Tuj1, in red, is staining β-tubulin III in neurons, GFP is staining the human cells and DAPI is counterstaining the nuclei. Scale bars: 40 µm

The density of β-III tubulin is more prominent in the graft than in the mouse cells area at this stage, as it was expected. This result suggests that the human cells have started differentiation but are still immature.

4.5. Some human NPCs retain markers or pluripotent cell state

Another marker of cell identity used to assess the maturation state of the human cells was Sox2, a transcription factor that participates in the regulation of stem cell fate in both early embryos and embryonic stem cells. It has been shown to be capable of inducing pluripotency in human somatic cells(61,62) and its expression levels have to be tightly regulated to ensure normal neuronal development(95). Apart from its role during embryonic development, Sox2 is present in adult neurogenic regions and is essential for the homeostasis of different adult tissues, especially in the CNS. It is expressed in multipotent neural stem cells at all stages of mouse ontogeny and helps in the identification of precursor cells that display self-renewal and an ability to multipotential differentiation properties. It is thus perceived as a universal neural stem cell (NSC) marker (96).

In order to assess the differentiation state of the human cells, in comparison to the rest of the mouse cortex, we firstly did a double-staining of Sox2 and GFP (Fig. 18).

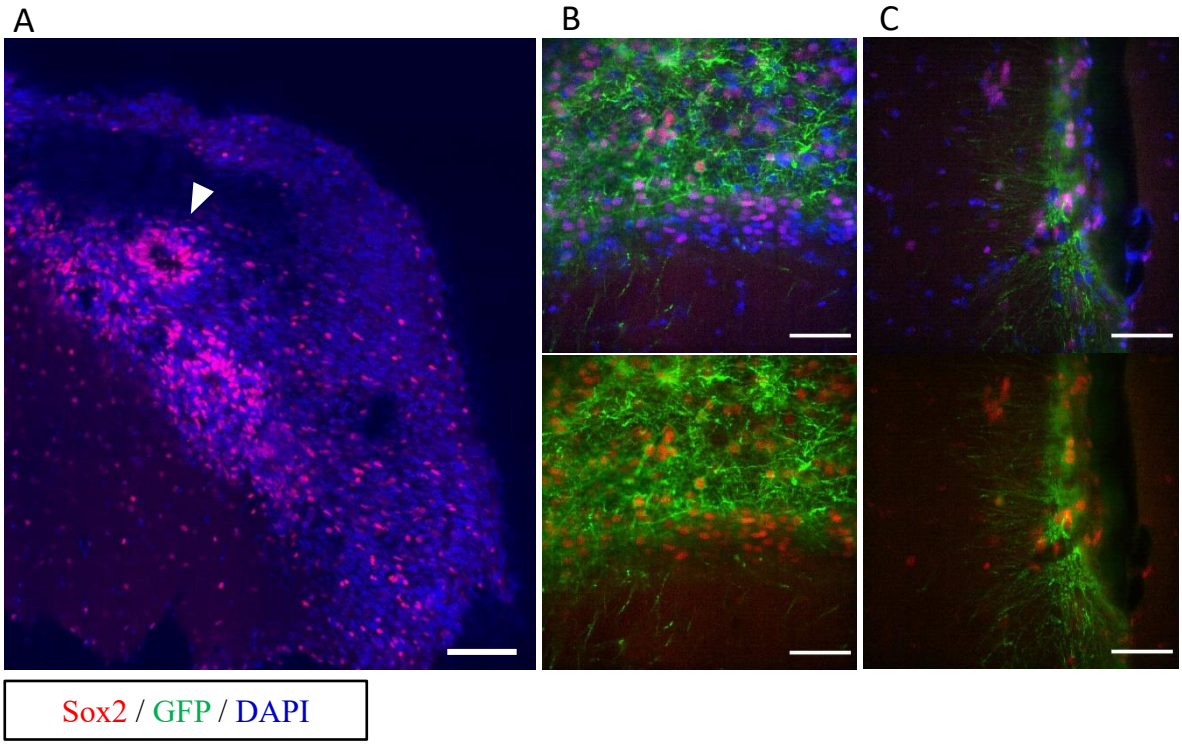

Figure 18 - Representative images of Sox2 (red) and GFP (green) immunostaining. (A) Large overview of a frontal slice at 1mpi, where the colocalization of Sox2 and DAPI is evident. A rosette-like structure is indicated with the arrowhead. Scale bar: 100 µm. (B) and (C) Detailed images of 6 mpi samples, where the $Sox2^{+}$ cells appear to be more concentrated around the graft neighbourhood. Scale bars: 40 µm

In Fig. 18A we recognise the higher concentration of Sox2 inside the graft, the area that correspond to the denser DAPI labelling on the right of the slice. In particular, Sox2 is more expressed in the region closest to the mouse cortex, where a rosette-like structure expressing high levels of Sox2 is visible (evidenced with the white arrowhead). Neural rosettes are radial arrangements visible during ESCs development *in vitro*. Cultures of neuronal progenitors undergo this stage in their differentiation and their presence in the graft may indicate the level of immaturity of the human NPCs. These assemblies were detectable uniquely in some of the 1 mpi brains (Appendix, Fig. 27).

The presence of rosette structures and the apparent segmentation could be reflecting different levels of neuronal differentiation within the graft.

In the detailed images at 6 mpi (Fig. 18B and 18C), the concentration of $Sox2^{+}$ cells continues to be more pronounced near the GFP filaments. The separation perceived in Fig.18A is also visible at this timepoint, especially in Fig. 18B.

The observation that Sox2 perfectly colocalized with DAPI suggested that evaluating how the number of neural stem cells varies over time could be a straightforward task.

As the human nuclei had been successfully labelled with STEM101 antibody before, we proceeded to a Sox2 and STEM101 double-staining to quantify the number of cells that still exhibited stem cell characteristics, inside and outside the human transplant (Fig. 19).

The nuclear antibodies used as references for these experiments were STEM101 (for the human graft area) and DAPI (for the mouse cortex area).

In total eighteen samples were analysed: three of 1 mpi, four of 2 mpi, four of 3 mpi, five of 4 mpi and 2 of 5 mpi. After delimiting both the human and the mouse cortical areas, the number of cells labelled with each of the three antibodies was counted. The percentage of Sox2+ cells was calculated in relation to the total amount of DAPI or STEM101 nuclei, according to the condition.

As a control for the quantification, images of the contralateral side, i.e. the counterpart region of the brain where the cortex was constituted uniquely of mouse cells, were taken.

The accumulation of Sox2-expressing cells appears to be higher in the graft than in the rest of the cortex and this value seems to lower in 4 mpi and 5 mpi (Fig. 19A).

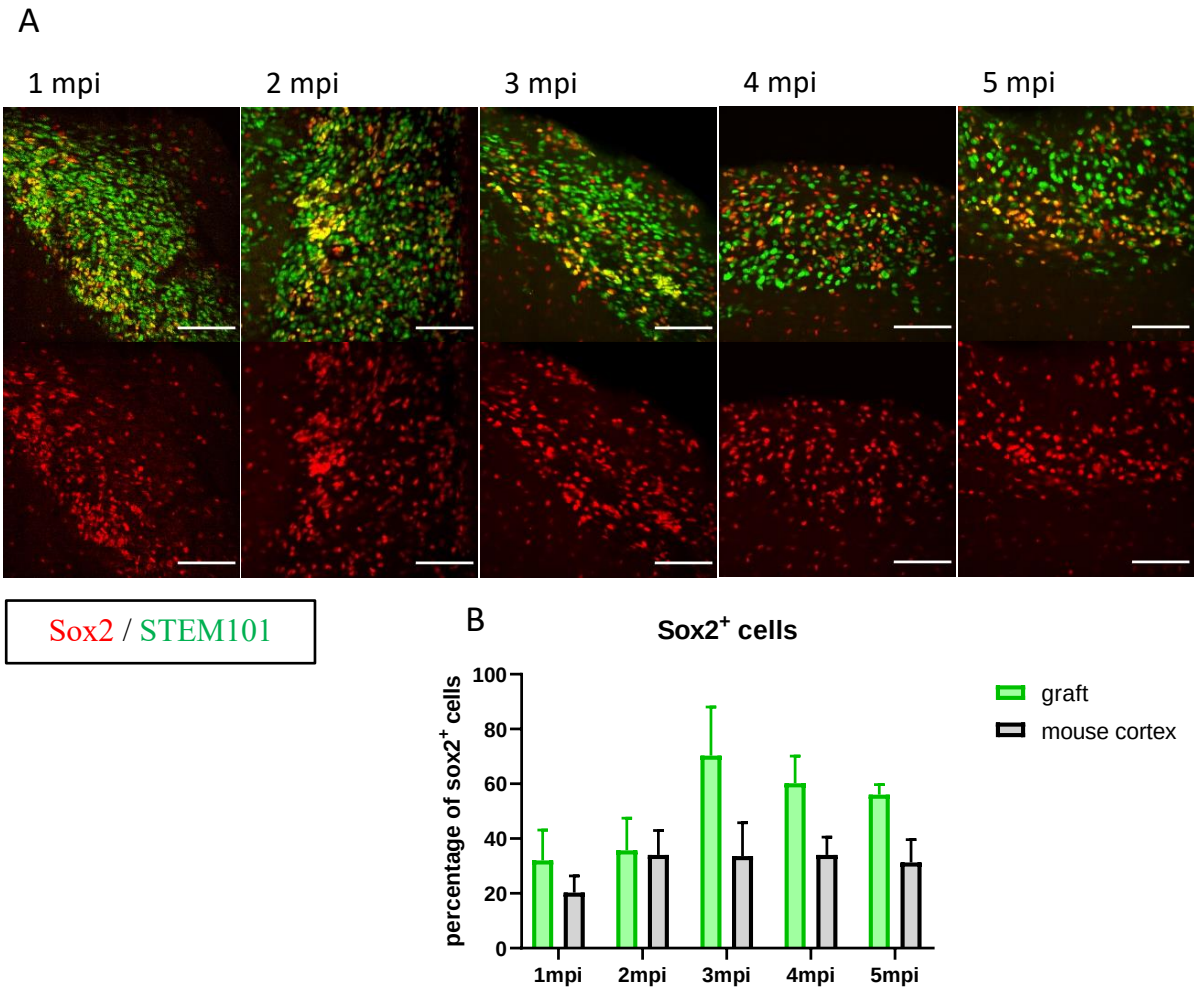

Figure 19 – Variation of the percentage of Sox2+ cells inside and outside the graft (A) Representative images of the Sox2 and STEM 101 double stainings at each timepoint, until 5 mpi, taken in the confocal microscope, Scale bars: 100 µm (B) Bar chart and respective standard deviation (SD) of the percentage of cells expressing Sox2 in both regions, in each of the five timepoints.

As expected, the mean percentage of $Sox2^+$ cells within the graft is higher than in the mouse cortex in all timepoints and there is just one 2 mpi sample where the counterpart percentage of sox2 is higher (Fig. 19B).

However, this percentage is not reduced in a linear fashion over time, unlike what we predicted. There is a tendency for increase from 1 to 3 mpi and then it declines until 5 mpi. In the mouse cortex, the number of immature cells does not suffer as much variation as in the human graft and remains relatively unaltered over time.

These data indicate the predominance of pluripotent cells in the human graft, compared with the mouse cortex. As Sox2 expression is usually restricted to undifferentiated neural stem cells, these labelled nuclei correspond most likely to human NSC that have not begun to differentiate.

4.6. Astrocytes are present in the human graft

Following the differentiation analysis, we sought to tackle the question of neuron-glia interactions between the human cells and the mouse brain environment.

The paramount importance of glial cells in the correct neuronal development and functionality has long been recognised. Their ability to respond to intra- and extracellular clues and change remains to be fully understood and, thus, these cells continue to be an object of investigation.

For the host-graft interaction, we started with the detection of astrocytes, which are key players in the regulation of synaptic plasticity and in adult neurogenesis. The main roles ascribed to these glial cells are those of neurotransmitters recycling and nutrients delivery to neurons (97).

To detect astrocytes we performed a double immunofluorescence labelling of GFP and Glial Fibrillary Acid Protein (GFAP), a protein expressed in astrocytes that is involved in controlling its shape, movement and function (Fig. 20).

A higher concentration of GFAP-positive cells was visible in the region of the human graft, in all timepoints, with no evident change over time. There was no colocalization suggesting that these astrocytes were of mouse origin and could have migrated to the graft.

The morphology of the astrocytes was very heterogenous. On the edge of the graft, externally, there was an accumulation of star-shaped astrocytes. Despite resembling the rest of the mouse cortical astrocytes in shape, these cells were more abundantly present, suggesting a host response to the presence of heterologous cells (all images in Fig. 20).

Similarly, to the rest of the ipsilateral mouse cortex, we did not remark any significance change in the astrocytic configuration of the contralateral side, across the distinct samples.

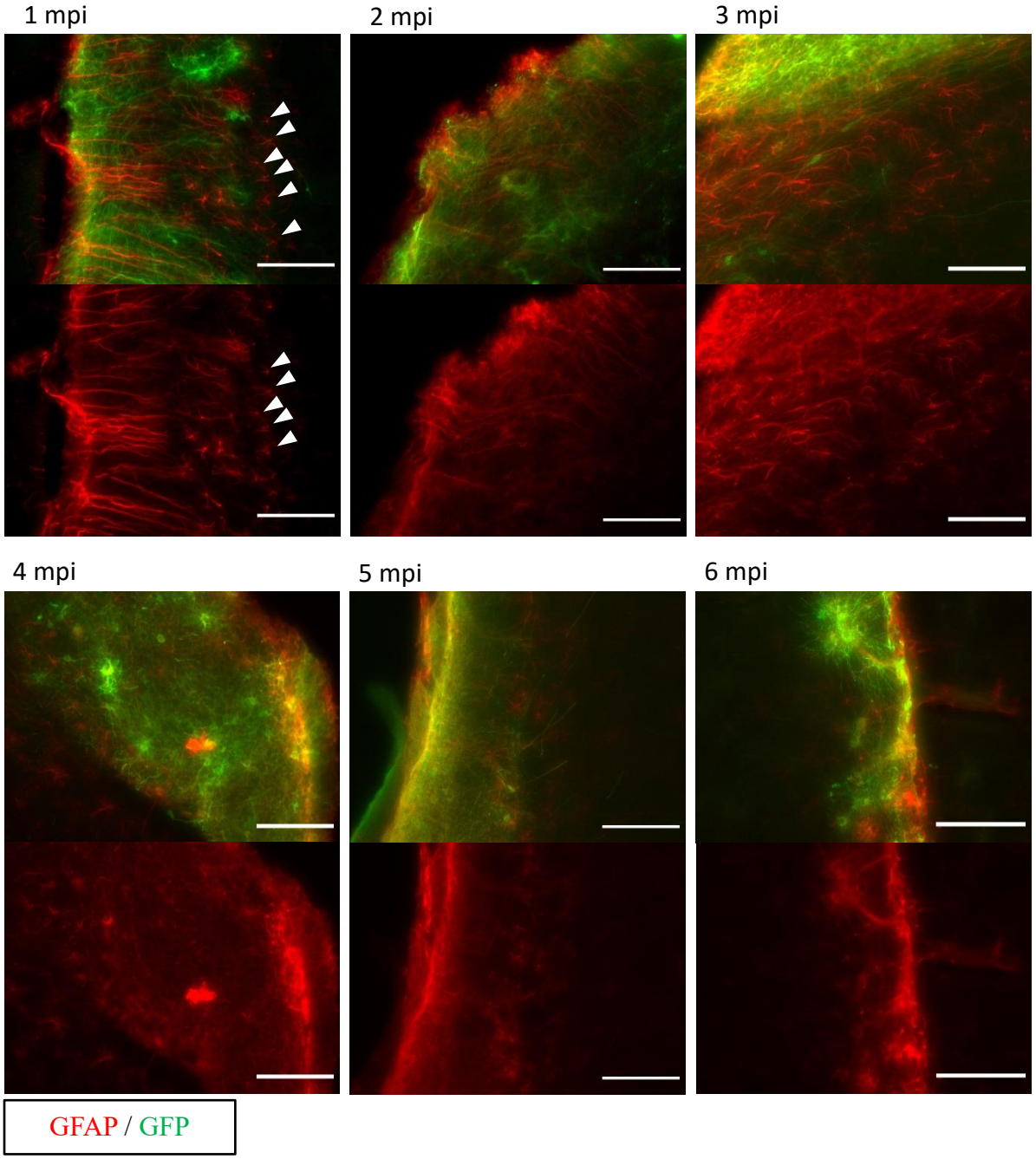

Figure 20 - Detailed view of the GFAP and GFP staining in each of the 6 timepoints. In all timepoints there is a clear stronger signal inside the graft. Arrowheads in 1 mpi images some star-shape astrocytes. Scale bars: 100 µm

Within the graft, the GFAP staining revealed a very disorganized distribution of astrocytes. The signal was very strong and highly diverse, contrasting with the mouse astrocytes that were disposed in a predicted way all over the brain slices (Appendix, Fig. 28).

This significant density of astrocytes and the variability from sample to sample, even within the same timepoint group, made the quantification impractical.

In the first timepoints, mainly in the 1-month brains, we noticed that the mouse astrocytes were atypically organized. It was possible to discern the presence of thick $GFAP^+$ filaments arranged perpendicularly to the brain surface (first image in Fig. 20 and Fig.21). Surrounding the edges of these 1 mpi grafts, the star-shaped astrocytes were also more defined (indicated with the arrowheads in Fig. 20).

These 1-month filaments were disposed parallelly, and resembled the processes of radial glial progenitor cells, present in the intermediate zone of the fetal cortex (Fig.21). Considering this distribution was only possible in the first timepoint, we theorised they could indeed be representing radial glia that was providing the physical support required for the migration of the immature human neuronal cells.

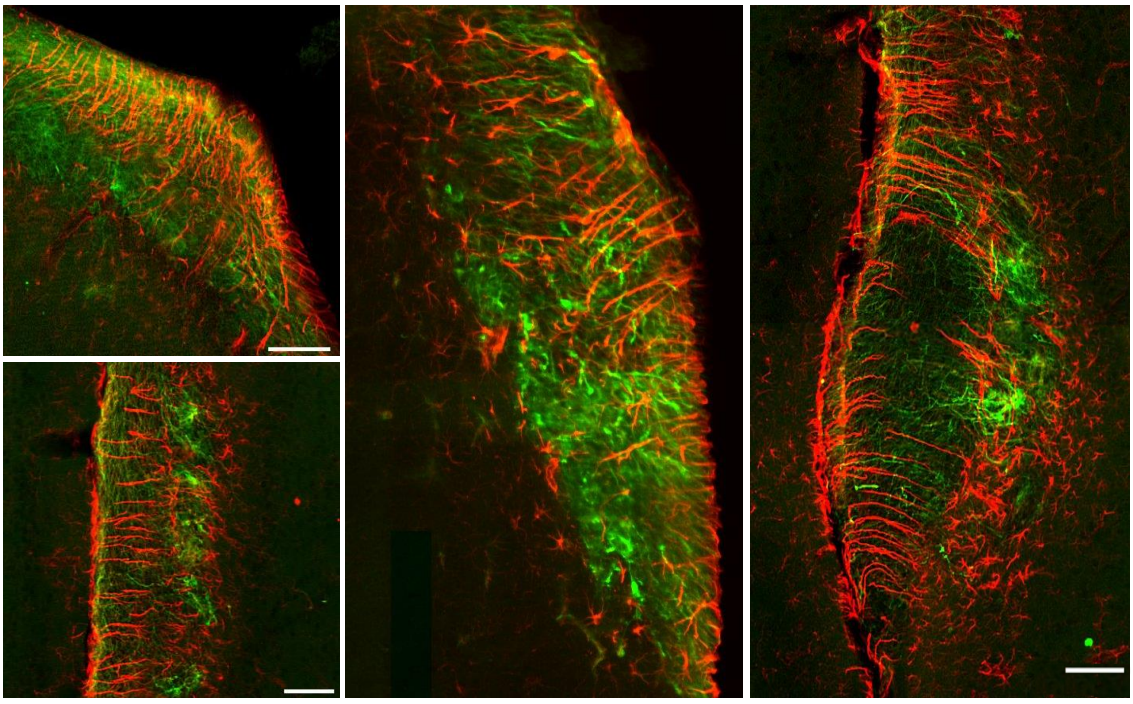

Figure 21 – Other examples of GFAP and GFP double-staining at 1 mpi. Radial fibres that are around 100 µm long localize in a more external position, both medial and laterally. They are visible in almost all 1-month brains. Scale bars: 100 µm

As the GFP signal was very dense and it did not accompany the radial pattern of the GFAP staining, it was difficult to evaluate the nature of the interaction between the human cells and the mouse glial cells using these images.

This assay provided the first demonstration that the host is sensing the foreign presence and responding to it differently over time. It disclosed not only that astrocytes are migrating to the human graft, but also that there is a reaction, an increase in GFAP synthesis.

4.7. The GFAP-positive fibres inside the graft express Sox2 in their nuclei

To test our hypothesis of whether these fibres corresponded to radial glia or had a different cell identity, we proceeded to a Sox2, GFP and GFAP triple-staining. Radial glia is a type of neuroprogenitors expressed in the early stages of neuronal development that supports the migration of developing neurons in the cerebral cortex. Apart from being precursors of neuronal cells, they can also give rise to certain lineages of astrocytes and oligodendrocytes, both in the rodent and human brain (98,99).

We took advantage of the stem cell marker Sox2 because it is also expressed in embryonic radial glial cells and is maintained in GFAP-positive radial glia in the adult nervous system (96,99).

This immunostaining exposed the distribution of Sox2 expression inside and outside the graft and confirmed the association of $GFAP^+$ fibres with the $Sox2^+$ nuclei (Fig. 22).

In Fig. 22A, we can see the clear distribution and the tendency for segmentation in Sox2 expression inside the graft. There is a cluster of Sox2 in the most internal region, closer to the mouse cortex, that seems to colocalize with GFP (precise colocalization cannot be assessed because of the expression pattern of GCamp6f). On the other hand, the more externally located Sox2 nuclei belong to mouse $GFAP^+$ cells and do not seem to interact with the GFP-labelled human cells (Fig. 22C and D).

Even though most GFAP filaments that are linked to Sox2 expression exhibit a unipolar shape, and their cell body is in the most outer region (Fig. 22C), a few bipolar cells were detected as well.

Regarding the mouse cortex, this triple-staining showed that a great part of the Sox2-positive cells are actually astrocytes and not adult stem cells (Fig. 22B). The arrowheads pinpoint a few cells where the astrocytic processes are stained with GFAP.

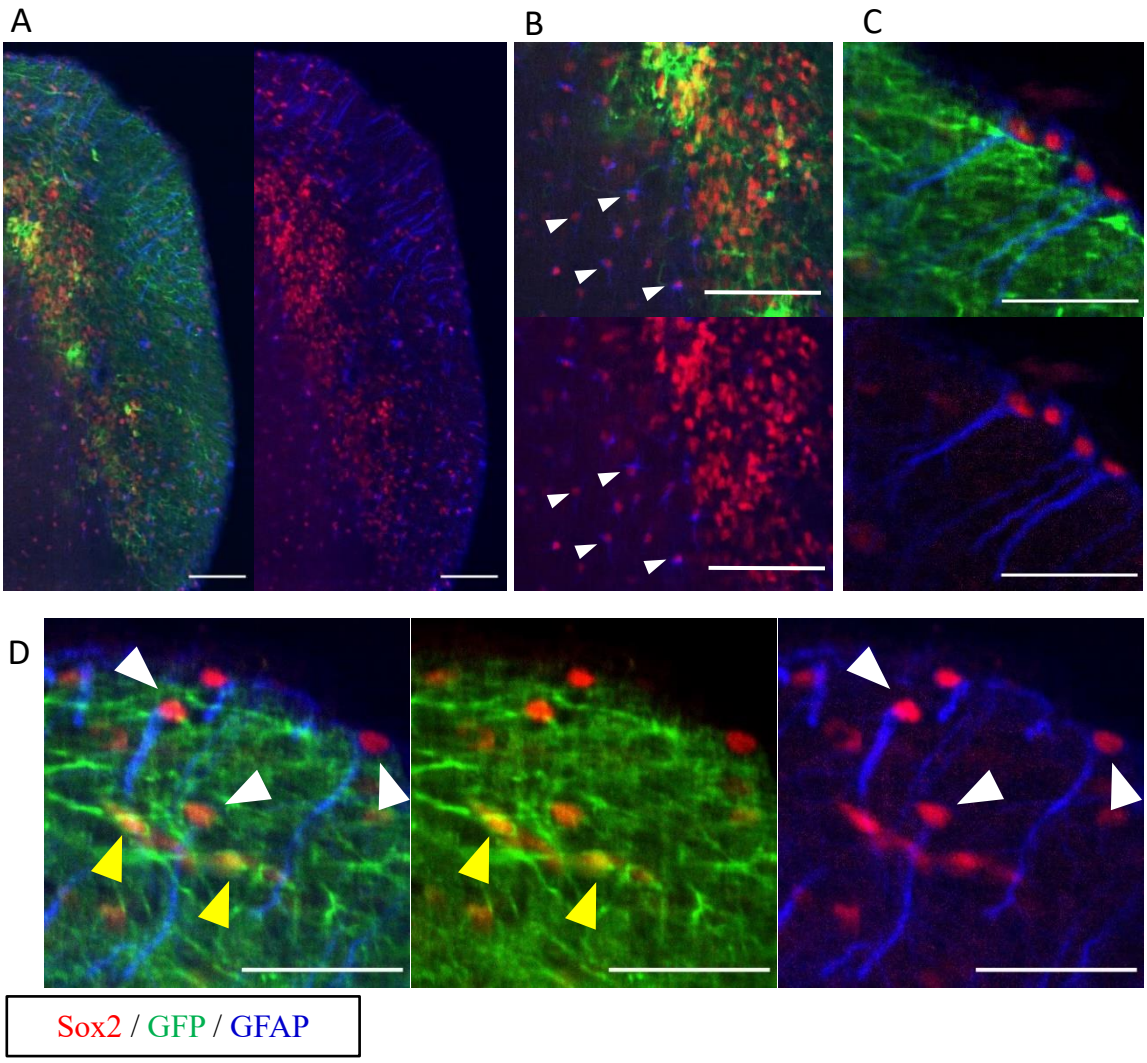

Figure 22 - Images of the GFAP, GFP and Sox 2 triple-staining in the 1 mpi samples, acquired in the confocal microscope. (A) Large overview of the human graft, where Sox2 is more concentrated closer to the mouse cortex surface and the GFAP fibres on the other side of the graft. Scale bar: 100 µm (B) Detailed image of the graft border, where some mouse astrocytes expressing Sox2 are pointed out by the arrowheads. Scale bar: 100 µm (C) Detailed image of the brain surface in the graft region, where the nuclei of three GFAP filaments directing towards the inner part of the brain are expressing Sox2. Scale bar: 40 µm (D) Detailed image of a section of the graft where some Sox2 nuclei are human, GFP^+ (yellow arrowheads), and others are associated with the radial fibres, $GFAP^+$ (white arrowheads). Scale bar: 40 µm

In Fig. 22 D the yellow arrowheads indicate nuclei of immature human cells (GFP and Sox2 colocalize), while the white arrowheads indicate the $Sox2^+$ nuclei that correspond to the mouse filamentous cells expressing GFAP. This result illustrates that not all of the $Sox2^+$ cells inside the graft are human.

This staining confirmed that the GFAP fibres are associated with Sox2 nuclei, reinforcing the idea that the host and the graft cells interact and that the mouse radial glia may be assisting the development of the human NPCs.

4.8. Oligodendrocytes are present in the human graft

We then analysed the disposition of oligodendrocytes, the CNS glial cells whose main function is the production of the myelin sheath that insulate neuronal axons. Myelin is very abundant membrane protein in the vertebrate nervous system. Its enrichment in fatty acids and the segmental arrangement confer electrical insulation and support rapid propagation of nerve impulses (100). Myelination is, consequently, crucial for neuronal function and is an essential maturation process in development.

In order to investigate whether the mouse oligodendrocytes could be interacting with the human neuronal precursors and myelinating them, we performed a double staining against GFP and Myelin Basic Protein (MBP), a major constituent of the myelin sheath of oligodendrocytes (Fig. 23).

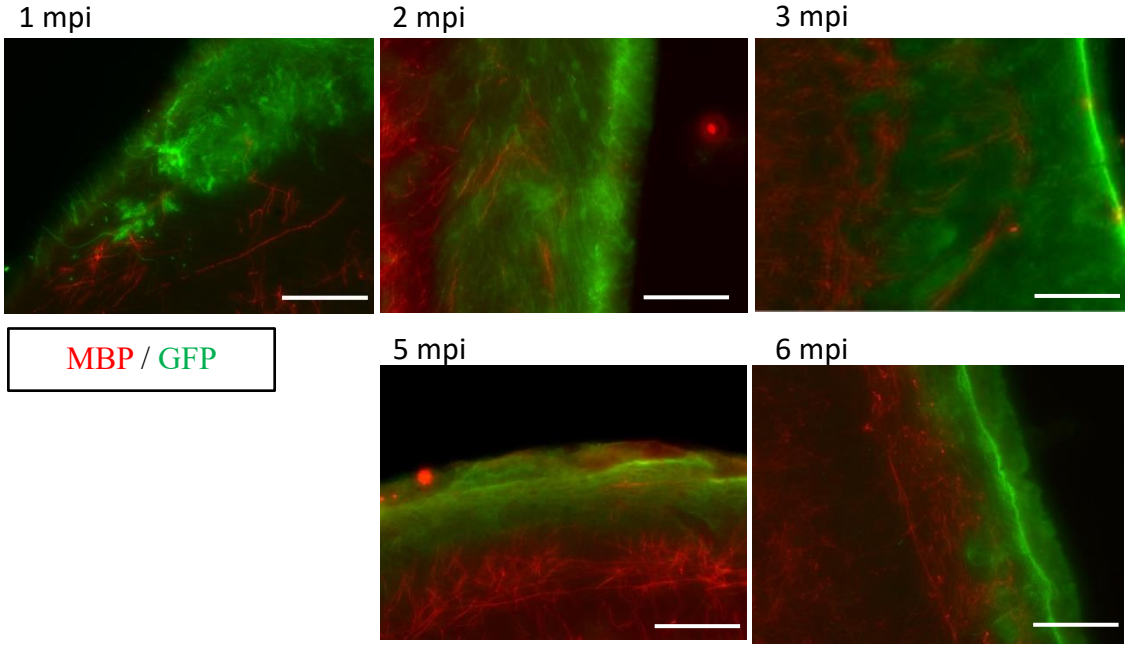

Figure 23 - Representative images of MBP-stained brains at 1, 2, 3, 5 and 6 mpi. Over time there is some colonization of this protein in the human graft. MBP is indicated in red and the human cells in green. Scale bars: 100 µm

In the first month, there were no oligodendrocytes in the region where the human NPCs were developing. Contrasting with the astrocyte distribution, there was an absence of MBP signal in the graft, and despite being more obvious at 1 mpi, this darker region was common between all samples analysed of all timepoints.

Nonetheless, from 2 months, mouse oligodendrocytes started to migrate and, until the last timepoint, some MBP-positive cells were present among the human neuronal cells, specially near the border regions. The MBP presence became more evident, but it was not possible to detect an unequivocal organization or recognise a consistent pattern of interaction. The oligodendrocytes found within the human graft displayed an atypical morphology and their irregular arrangement contrasted with the very organized disposition of MBP across the rest of the brain slices (Appendix, Fig. 29).

After imaging these samples in the confocal microscope, we could confirm the absence of colocalization, indicating that all MBP fibres present in graft were from the host.

As expected, there was MBP expression in the graft at different timepoints, but this protein was disorderly arranged. Bearing in mind that the MBP staining may not correspond to the full extent of oligodendrocytes, and in order to gain a more comprehensive view of the their distribution, we were prompted to search for alternative markers of this cellular population.

We performed an immunostaining against oligodendrocyte transcription factor 2 (Olig2), also known as basic helix-loop-helix (bHLH) transcription factor (Fig. 24). This protein promotes oligodendrocyte differentiation and is required for motor neuron specification in the spinal cord, and for the development of somatic motor neurons in the hindbrain. It also participates in neural cell fate acquisition (101).

For this assay four 1 mpi and six 4 mpi samples examined, quantified and compared. The Olig2 transcription factor was co-stained with STEM101, so that the quantification process would be facilitated.

Olig2-expressing nuclei inside the human graft were visible in both timepoints, and the number of these oligodendrocytes increased in an evident manner from 1 to 4 mpi (Fig. 24A). This pattern was confirmed with the nuclear counting and quantification (Fig. 24B). There is a considerable increase in the oligodendrocyte density in the graft from 1 mpi (~14 oligodendrocytes / 9000 µm2) to 4 mpi (~29 oligodendrocytes / 9000 µm2). On the other hand, in the mouse cortex the mean density of oligodendrocytes is practically the same at

the end of the first and the fourth months (~30 and ~28 oligodendrocytes / 9000 µm2, respectively).

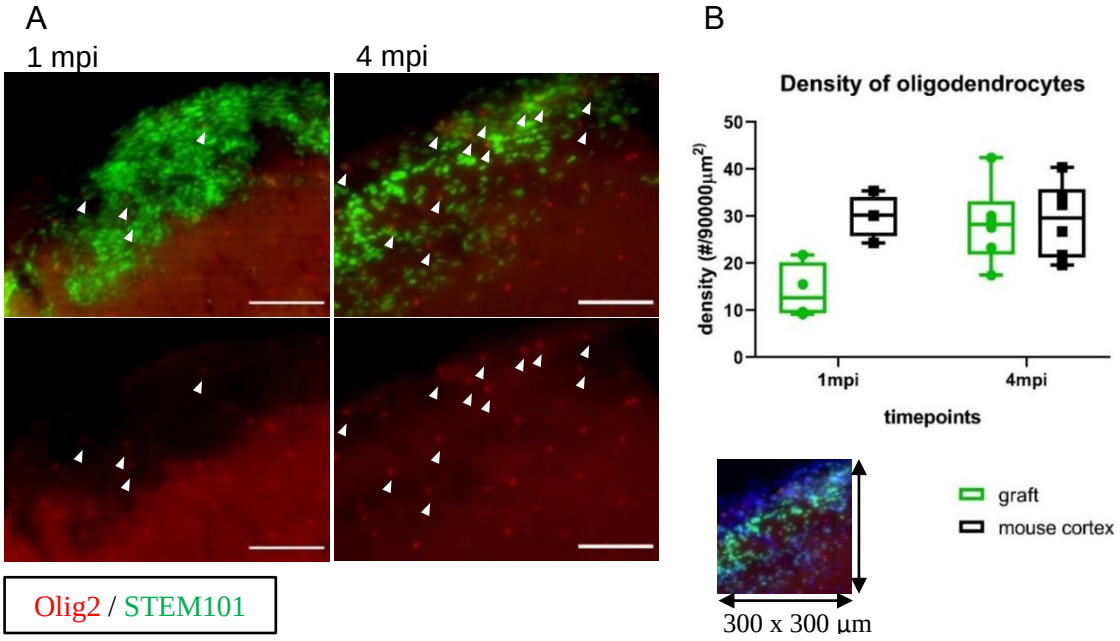

Figure 24 – Quantification of the number of mature oligodendrocytes inside and outside the human graft. (A) Representative fluorescent images of the Olig2 (in red) and STEM101 (in green) double staining at 1 mpi and 4 mpi. The olig2 nuclei that are adjacent to the human nuclei are identified with the white arrowheads. Scale bars: 100 µm (B) Box plot of the mean density of olig2-positive cells inside the human graft at each of the timepoints and respective standard deviation bars. The density is indicated as the number of cells per 9.000µm^2.

In both conditions of 4 mpi the standard deviation is higher which may be explained by the higher number of stained slices analysed at this timepoint. These results confirm the increased colonization of the graft with oligodendrocytes over a 3-month period.

Altogether, these data show that, despite the lack of organization, myelin sheaths are visible inside the human cells' region and the number of mouse oligodendrocytes increases, suggesting the dynamic interaction of this glial cell population with the developing human neurons.

4.9. Blood vessels develop inside the human graft

To detect the presence of blood vessels inside the graft we performed a double staining of GFP and the endothelial cell marker cluster of differentiation 31 (CD31) (Fig. 25). CD31, also known as Platelet/ Endothelial cell adhesion molecule 1 (PECAM-1), is a single-chain transmembranar glycoprotein highly expressed on the surface of endothelial cells (ECs).

Despite being primarily concentrated in the intercellular junctions of ECs in several human and murine tissues, CD31 is also expressed in lower density in a variety of hematopoietic cells (102).

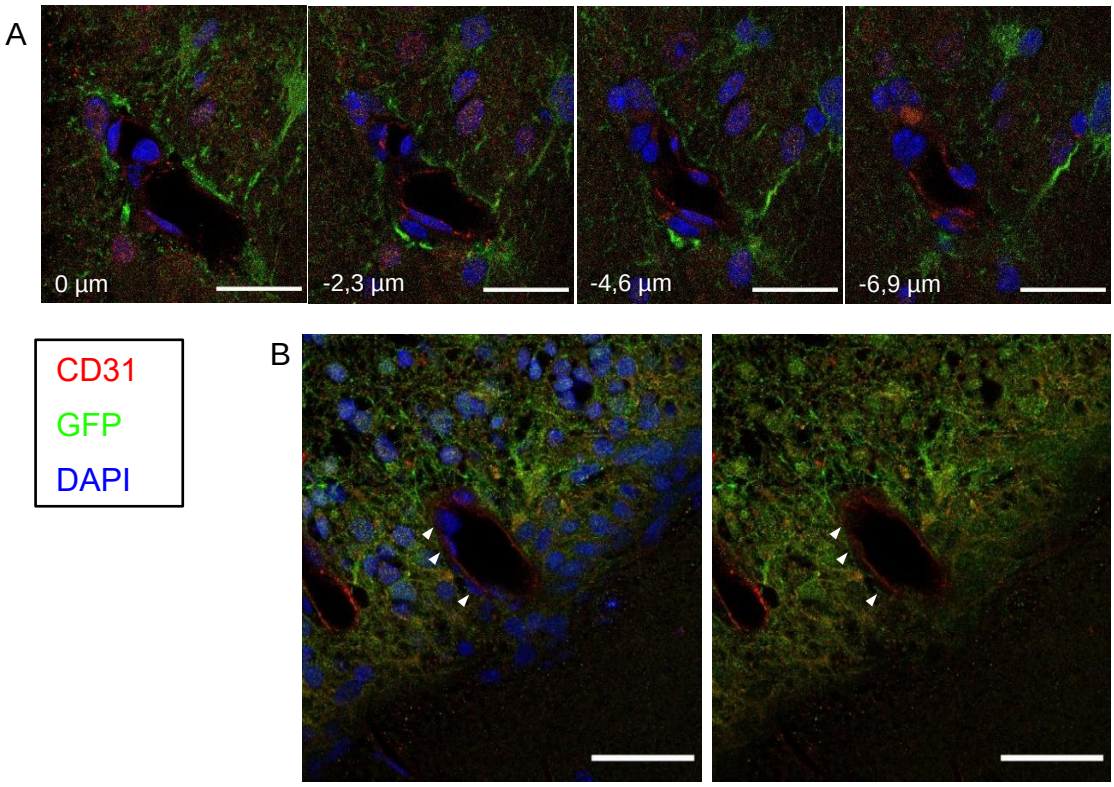

Figure 25 - Representative immunostaining of endothelial marker CD31 (in red) inside the human graft at 6 mpi; GFP is staining the human cells (in green) and DAPI is staining all the nuclei. (A) Z-stack of a blood vessel imaged across a 6.9 µm-thick region. Scale bar: 20 µm (B) Detailed picture where three nuclei of endothelial cells are indicated by the white arrowheads. Scale bar: 40 µm

Even though the labelling of CD31 was not very specific, we could distinguish the brighter red signal around the blood vessels. There was no GFP signal in these border areas, reinforcing the exclusive mouse origin of the stained ECs. Likewise, GFP did not colocalize with DAPI in these regions either, contrarily to what is seen in the rest of the images, making the host ECs nuclei easily perceptible (Fig. 25B).

This assay demonstrated that the human graft is vascularized, and the mouse brain environment has the potential to support the development and maturation of the human NPCs.

5. Discussion

There are a number of key findings emanating from the present work.

- The human neuronal progenitor cells (NPCs) survive and differentiate in the mouse brain, without any apparent sign of rejection.
- They migrated from the injection site and were efficiently integrated in the upper part of the mouse cortex.
- They do exhibit protracted neuronal development innate to human neurons.

There were a number of phenotypes observed inherent to the experimental approach chosen, a transplantation into neonates, without stereotaxic procedures. Despite the injection of the same number and volume of NPCs, the size of the graft varied significantly between samples. The existence of several brains where just a small number or no human cells were present may be explained by some technical errors in the homogenisation of NPCs solution or miscounting. Despite the use of a syringe that has a blocking system, the existence of NPCs in the ventricles highlights that the coordinates used should be more precise. Apart from the differences in size, the variation in the graft location could also be justified by the use of approximate coordinates. All animals underwent the injections at P1, and the NPCs used to inject all litters were in an identical passage number, however not all the litters were injected at the same time and the conditions might have been different between the different days of injection. Another issue that could be introducing variability was the performance of the injections by two different researchers that had distinct previous experience. Additionally, there is always some intrinsic variability inherent to each litter and each animal.

Human cells were localized in relatively confined areas and very few human nuclei (labelled with STEM101) were found outside these areas and inside the more radial zone of the mouse cortex. Nonetheless, different grafts displayed distinct overall configurations and the type of limits differed. In some grafts, especially bigger ones, the boundary between the human cells and the mouse cortex was very well-defined and the cells appeared to be contained in a strict environment. In other grafts, the human precursors were confined to a specific area, but parts of this interface were “disrupted” allowing a better interaction between the host and graft cells. The majority of the samples, however, exhibited human grafts that blended with the mouse cortical cells and a sharp boundary was lacking. A timepoint-specific variation in the type of limit did not appear to exist. However, in the first

timepoints, the only projections coming out of the graft were found in the areas where the graft and the mouse cortex fuse more smoothly, indicating that this configuration could be facilitating the mouse-graft interaction.

We remarked that the proportion between human nuclei and GFP+ cells was unequal, revealing that a part of the human cells do not seem to express GCaMP6f in their cell body and, hence, the totality of the graft cannot be identified through this method.

This preliminary staining showed the overall disposition of the human cells but taking into account their variability and the uncertainty regarding the GFP staining, inferring any conclusions uniquely from these immunofluorescence results would not be appropriate.

As we were seeking to reliably reproduce the neurite outgrowth and complexification that was perceptible in the microscope, we proceeded to the 3D tracing and quantitative analysis of the neuronal projections.

Developing this quantitative method to study morphology was a major challenge, not only due to the dense nature of the human graft but also because we could not distinguish dendrites from axons in the earliest timepoints. These difficulties resulted in the tracing and joint quantification of both types of projections.

Initially, we attempted to use the automatic filament generation of Imaris, providing the values of the largest diameter (corresponding to the starting points, the soma) and the thinnest diameter (corresponding to the seed points, the average thickness of the filaments) as inputs. Even though the starting and seed points were usually placed correctly, and it was possible to adjust the thresholds and stringency parameters, the automatic approach had major obstacles we could not surpass. Due to its intensity-based nature, the software often connected unrelated filaments whenever there was a gap in the signal and the filament being traced was interrupted. Crossing points were also a problem since Imaris could not discriminate the right path, even when it was evident to the naked eye. In addition, as a consequence of the image resolution and the filaments density, the tracing in the centre of the graft was nearly impossible in almost all our samples as we could not precisely define the limits of each neuron, and neither could the software. We noticed that it was still easier for the human eye to define the limits of the filaments, however, the option of tracing the neurons completely manually was discarded because of the bias that would be introduced and the lack of reproducibility. Consequently, we ended up adopting a semi-automated strategy where we traced each filament individually, but the centre and diameter were automatically detected. This strategy could, therefore, be applied in all timepoints and

would give us a more unbiased understanding of the interaction between the human and mouse neurons.

Axon length, straightness and level of branching were followed, and compared over time and they helped us elucidate the development of the human neuronal projections. Axon length increases considerably, primarily from 3 to 5 mpi; the number of branched axons increases from 1 to 3 mpi and the straightness augmented mildly but did not suffer a substantial global difference. The Imaris analysis mirrored the human precursors' variability, as well. A small number of samples were analysed, but the standard errors were elevated, especially in the length at 5 mpi and the straightness at 1 mpi. In the 5-month brains, understandably, a broad span of projections length exists, and the persistence of shorter ones does not necessarily translate an immature state. On the other hand, the dispersion in straightness values of 1 mpi projections may be linked to immaturity, as this was the only timepoint were some filaments described curvatures superior to 90º. The lack of organisation of the human cortex at this stage was more emphasised.

In spite of being three crucial factors to comprehend neurodevelopment, a more complete assessment could be achieved if additional variables were measured. In this case, we could still take advantage of Imaris as it qualifies for a great deal of quantifications, including filament density, number of dendritic spines, mean diameter of dendrites and spines, or orientation angle that neurites establish with the edge of graft. Density, in particular, was changing visibly and most 5-months samples had a few dozens of filaments emanating from at least one focal point. The orientation of the neurites was also changing over time and we could perceive a clear tendency for perpendicularity in relation to the graft surface from 4 mpi forward. Unfortunately, because the grafts were always disposed in a different orientation and Imaris only measures the angle that a filament establishes with the X-axis, it was not possible to quantify it. Other parameters, like the diameter, could not be analysed because of image quality limitations that precluded the software detection.

For these supplementary analyses, a more extensive optimization process would be required. We observed that when the immunolabeling protocols were not as successful and, more importantly, when the brains were imaged in low resolution, the tracing was much harder. Other imaging techniques that offer better resolution, such as multi-photon laser-scanning microscopy could, consequently, be of great benefit. Apart from image acquisition, processing could also be enhanced, and some computational treatment could be applied. Another solution could be an approach using machine-learning algorithms that

would incorporate new information about neuronal shape and development and could result in a more a consistent automatic detection.

We tried to trace our samples using a virtual reality software, SyGlass, and it did help, but the resolution limitation and the thin Z-stacks (of approximately 10-15 µm) were imposing problems.

In order to complement the analysis, including the maximum values of certain parameters such as the maximum length, could also be useful.

It is difficult to draw further conclusions and, in the future, more cells of each of the three already analysed timepoints should be traced, as well as cells of the remaining timepoints (2 mpi, 4 mpi, 6 mpi).

Apart from the cortical ones, there were projections stemming from the engrafted cells clusters that were trapped in ventricles at the moment of the injection. These were not quantified, but they resembled the cortical filaments, in shape and length. Further analysis and characterization could help understanding the identity of these cells and the similarities with the human precursors that develop on the top of the mouse cortex. Comparing the development of these cells to the ones on top of the cortex, could give us an indication on the existence of intrinsic properties or a fate commitment that leads to neuronal specification and neurite outgrowth, as well as the importance of host environmental factors.

Mouse cortical layers start to form in the first days after birth and, shortly after, synapses begin to mature and then prune. The cortex undergoes axon and dendrite outgrowth throughout the whole first month and only near the end of this period synapses start exhibiting mature morphology (97). This reorganization of neural circuits does not depend uniquely on large-scale axonal and dendritic changes, but also on alterations in synaptic structure. Thus, characterizing synaptic development is also a major part of developmental studies.

Dendritic spines are key players in excitatory synaptic transmission in the central nervous system and their appearance is recognised as a hallmark in neuronal differentiation and specialization. The dynamics of these structures is known to underlie neural circuit refinement, and following the formation period, they undergo a characteristic pruning phase. In our samples, spines were detected in the confocal microscope as early as 2 mpi, and their presence was also evident at 3 and 4 mpi. However, as our images did not have enough resolution, the detection and tracing of these structures in Imaris were unfeasible.

Further analysis could shed light on this subject and help us understand at which stage reorganization and stabilization are taking place. The use of super-resolution imaging could be very advantageous in the measurement of size, density, and pattern of distribution and *in vivo* imaging would allow the quantification of spine formation and elimination, turnover ratio and surviving rate.

A recent study following the same dendritic spines over time detected a remarkable plasticity in their sizes (77), and will need to be followed up further under different experimental conditions. Apart from dendritic spines, axonal boutons could also be detected. In the neocortex, synapses of excitatory neurons can be associated with either *en passant* boutons (EPBs) or *terminaux* boutons (TBs) (103). These two specialized structures take part in synaptic development, intracellular signalling and circuit connectivity, and an analysis of their stability could hint on circuit plasticity.

Synaptogenesis is vital for the correct functioning of the nervous system and we wanted to go beyond the detection of synaptic structures based on morphology. We hoped to evaluate the expression of synaptic proteins and, for that purpose, the post-synaptic protein PSD-95 was labelled. PSD-95 has been shown to play a role in excitatory synapse stabilization and plasticity, namely plasticity associated with NMDA receptor signalling (104). Its overexpression promotes maturation of glutamatergic synapses in hippocampal neurons and it also enhances maturation of the presynaptic terminal and increases the number and size of dendritic spines (90,91).

The higher concentration of PSD-95 found inside the graft may be suggestive of excitatory neuron maturation and the targeting of NMDA or AMPA receptors subunits could be very useful to further analyse neuronal cell identity.

Despite the evident brighter red zone, we could not be sure about the specificity of the staining and better resolution images should be acquired. In addition, it is difficult to draw a conclusion about the volume of synapses inside the human cells' region in relation to the mouse cortex, considering the density of the graft. An analysis of the other timepoints would also be a great advantage to evaluate how PSD-95 expression may be changing over time.

An antibody to target synapsin 1, a neuronal phosphoprotein that is connected to synaptic vesicles, was also tested but we did not continue with its analysis. This protein can be localized not only in the synapse but also in the Golgi apparatus, cytosol and nucleus, which may justify the lack of specificity in its staining.

The protocol for the labelling of PSD-95 could also be subjected to optimization. Considering that this is a membrane-associated protein, the permeabilization step may have to be performed with a gentler detergent, or different buffers may have to be used for the incubations.

Additional immunostaining of synaptophysin, a glycoprotein that exists in neuronal presynaptic vesicles, could also be used to detect synapses.

In the long-term, the dynamics of synaptogenesis could be characterized using *in vivo* electrophysiological tests or live imaging techniques.

The neurotransmission speed upon stimulation could be examined in the later timepoints. As the prefrontal cortex maturation corresponds to the last stage of neurodevelopment, for this experiment an axonal population that projects from the corpus callosum to the cingulate cortex could be stimulated, similarly to previous studies (105).

To study the behaviour of ion channels and the fluctuations in ionic currents in the human neuronal cells, Excitatory Postsynaptic Currents (EPSCs) could be recorded at a fixed voltage and compared over time. Whole-cell current-clamp recordings could also be performed to detect transmembranar potential in response to a precise current injection. This would inform on the generation of action potentials in the developing human neurons.

Finally, the content of intracellular Ca^{2+} could be measured through live imaging (and a calcium indicator) and the measurement of spontaneous activity would indicate active neurons.

Alternatively, c-Fos expression could be used as a functional marker of activity.

Subsequently, an antibody against Neuronal Nuclei (NeuN) was used to localize mature neurons. NeuN was identified as Fox-3, a protein involved in mRNA splicing, and it functions in regulating neural cell differentiation (106). The appearance of the NeuN corresponds to the withdrawal from the cell cycle. It is present in the human forebrain after 20 weeks of gestation and is detectable in both embryonic and adult neurons. In comparison to other neuron-specific proteins, such as microtubule-associated protein 2 (MAP-2), NeuN is more specific can also be present epithelial cells and reactive astrocytes (107). Parallelly, NeuN allows nuclear recognition, opening the way for quicker quantification and resulting in a more straightforward analysis.

An increase in the number of mature neurons was seen inside the graft but, even at 5 mpi, this number was reduced compared to the mouse cortex.

To quantify the evolution in the number of $NeuN^+$ cells and in the ratio $NeuN^+$/human cells, this protein could be co-stained with STEM101 (or a different human nuclear protein). Due to a timing limitation, there was no opportunity to perform this staining and quantify it in all samples.

Tubulins are a major constituent of microtubules and, as cytoskeletal elements, they participate in cell structure maintenance, mitosis, meiosis, and intracellular transport. β-III tubulin, also recognised as Tuj1, is thought to be specifically involved in neuronal cell differentiation. *In vitro* studies have verified that human embryonic stem cells start expressing Tuj1 during differentiation, but remain functionally immature (108) and, in immunohistochemistry assays, TuJ1 has been found in the cell bodies, dendrites, axons, and axonal terminations of immature neurons. It can also be expressed in differentiated neurons and some mitotically active neuronal precursors (109).
Hence, we targeted Tuj-1 in our samples to identify early committed neurons, and we noticed a higher density inside the graft, implying that some neural progenitors have started differentiation.
It would be interesting to compare the expression of this protein over time and assess how long it is observed.

Despite the presence of mature and immature human neurons, a great part of the cells remained to be characterized. Taking into consideration the prolonged neurogenesis in our species, we hypothesized that some cells in the graft were still in an undifferentiated neural stem cell state. The expression of Sox2 allowed us to recognise the pluripotent identity of a number of cells in all samples and timepoints analysed. Sox2 plays a central role during embryonic development, promoting the differentiation of ESCs to neuroectoderm and inhibiting regulators of other lineage fates. It is an indicator of embryonic radial glial cells (96) but continues to be expressed in the mouse adult brain, particularly in regions where neurogenesis occurs, like the subventricular zone (SVZ). This could explain the reason why some non-human cells are labelled with Sox2, they maintain a capacity to proliferate.
Still with this antibody, we distinguished the presence of rosette-like structures in the earliest timepoint brains, coincident with a concentration of Sox2-expressing cells. A grafting strategy analogous to ours has previously led to the detection of similar structures (77).

The arrangement of these round-shape assemblies could be studied using Paired box protein 6 (Pax6), a marker of neuronal progenitors, and Nestin, a marker for radial glia, to understand if processes are extending radially outwardly and parallelly.
A more extensive analysis during the first month could be achieved through the staining of Ki67 nuclear protein. This cell proliferation marker would be expected to be positioned in the centre of the rosettes and decreasing over time.
Additionally, throughout the 1st month post-injection, human progenitors' migration could be measured using doublecortin (DCX). This marker contributes to microtubule assembly and is widely expressed in migrating neuroblasts. Similarly to βIII-tubulin, its expression is downregulated with maturation and it is no longer expected to be present in newly generated neurons in the neocortex.
The expression matrix and cell adhesion proteins, such as perineural nets (PNNs), could still be addressed to help in understanding how migration might be proceeding. PNNs ensheath certain neurons in the CNS and underlie synaptic regulation. As they are altered during aging, memory and learning, and drug abuse, it would be valuable to assess them in the grafting model of WT iPSC for later comparison with the model containing the polymorphic nAChR subunits.

Apart from evaluating maturation, we were seeking to deepen our knowledge about the interaction that the human engrafted cells establish with the host glia. Glial cells are known to underlie correct development and govern functions in mature neurons. They can sense environmental changes and adapt, which is crucial for nervous system homeostasis. We started with the labelling of astrocytes, a glial cell population that expresses glial fibrillary acidic protein (GFAP). Astrocytes assist in neuronal development and, particularly, in synapse formation and functionality. Even though mouse neurogenesis finishes at birth, neuronal synapses and branching only occur when astrocytes have been generated. Axons and dendrites only achieve a mature morphology at the end of the first month, which matches the astrocytic timing for process outgrowth and elaboration (97).
The fact that mouse astrocytes are still maturating throughout the first month may justify the distinct configuration that the GFAP signal displays at 1 mpi, in comparison to the following timepoints.
In the mouse brain approximately one-third of the cells are astrocytes, while in the human case, they are more abundant and make up virtually half of the brain cells (110). Differences in this ratio might suggest that human cells demand greater astrocytic support, and some

recruitment could be happening, resulting in higher GFAP concentration inside the graft. Nevertheless, because of the atypical shape and organization of this protein, the nature of the interaction appears to be more complex.

In cases of neurotrauma, ischemia, or a neurodegenerative disease, astrocytes have been shown to undergo molecular, cellular and functional modifications, in a process called astrogliosis, characterized by an upregulation of GFAP expression (111). In fact, the mRNA level of this protein is very sensitive to pathological conditions and extracellular signals and it is typically used to stain naïve astrocytes. Therefore, the more significant concentration of GFAP-positive cells in the graft is more likely to be a sign of astrogliosis. Changes associated with astrogliosis are regulated in a context-specific manner by different signalling processes (111) and further tests could be applied to evaluate how astrocyte activities are being altered around the graft.

The presence of Vimentin and Nestin could be easily assessed, as their re-expression is also a biochemical hallmark of gliosis and matrix metalloproteinases could be used to label reactive astrocytes.

Several *in vivo* grafting experiments have proven that glial cells tend to respond manifestly to different syngeneic or xenogeneic cells transplanted into either the striatum, the hippocampus, the cortex or underneath the external capsule. These studies have detected reactive astrocytes and astrogliosis, as well as microgliosis (denounced by the presence of M1, $Iba1^+$ and $CD11b^+$ microglia) in the region of the grafted cells (112). Although the rejection and glial response vary according to the region of injection (86), the increase in the number of activated microglia appears to be the most common feature across these experiments. Assessing the microglia recruitment to the graft is, thus, essential in a transplantation assay of this kind.

The research group has detected the presence of ionized calcium-binding adapter molecule 1 (Iba1), a microglia-specific calcium-binding protein, in animals that underwent an analogous grafting procedure. High infiltration of $Iba1^+$ cells would have been a sign of reactivity and graft rejection. Nonetheless, those tests revealed no significant changes between this protein expression in graft and the mouse cortex.

Other markers could also be used to check for an immune response, like the myeloid cell marker CD68. The tight regulation of CD68 expression during human neurodevelopment and the fact that it follows a spatiotemporal pattern, make this protein a promising target for this grafting experiment. Apart from it, the altered expression of this transmembranar protein has been reported in several neurological disorders.

Afterwards, radial glial cells were detected with the antibodies against Sox2, GFAP and GFP. Radial glia are known as the precursors of astrocytes that provide a scaffold for neuron migration. They persist through the neurogenetic period and extend long processes that span the cortex (97,98). It was possible to detect the presence of $GFAP^+$ radial glia that expressed the multipotent stem cell marker Sox2 in their nuclei. These fibres were only present in the human graft and in the earliest timepoint, 1 mpi, suggesting that their prolonged stay (they were not visible in the contralateral hemisphere) was caused by the presence of the human cells.

Experiments in different animal models have shown that radial glia may determine neuronal specification, and its ability to produce diverse types of projection neurons becomes progressively restricted during development. When radial glia neurogenesis is extended in mice, an overproduction of upper cortical layer neurons can be noticed. In addition, the shift from continuous to discontinuous radial glia corresponds to the well-established transition from generating deep to generating upper layer neurons, which constitutes another evidence that radial glia is playing a role in neurogenesis. Altogether this suggests that the mouse radial glia may be contributing to the neuronal differentiation of the human NPCs (113).

Proceeding with the host-graft interactions, oligodendrocytes were then targeted. We were firstly interested in evaluating the myelination state of the human cells.

Myelination is an essential maturation process that allows rapid nerve conduction and assists in neuronal electrical communication. In the mouse brain this process starts at birth and finishes around the end of the first month. In the human, it typically begins around the second trimester of pregnancy and proceeds into late adolescence, when the last association pathways in the cerebral cortex finish maturation. Henceforth, considering its role during development, it is of the utmost importance to understand whether the host oligodendrocytes are providing this type of support to the engrafted cells.

The staining for Myelin Basic protein (MBP) revealed the existence of some myelin sheaths inside and in the vicinity of the human cells. We could notice an increase, mostly from the first to the second timepoints, but the progressive colonization was not striking. Moreover, a clear organization, similar to the one found in the mouse tissue, was missing. This could be due to the differences in timing between human and mouse development. Myelination undergoes a set of sequential steps starting with migration of oligodendrocytes towards the

axons, followed by the adhesion of the oligodendrocyte process; and ending with the process wrapping around the axon. In this process the oligodendrocytes have to be capable of recognising certain areas that should not be myelinated (nodes of Ranvier) and establishing the right number of myelin sheaths (100).

Mouse oligodendrocytes migrate to the graft, meaning they appear to be sensing the human cells, and myelination has started. However, as this is supposed to be a rather lengthy process in the human brain, we may not be able to see the mouse oligodendrocytes completing this task in the human neurons, in the period of six months.

To better visualize MBP and study the myelination status, electron microscopic immuno-histochemical assays could be performed with this antibody. Electron microscopy would not only allow the detection of oligodendrocyte features that are uniquely visible at this scale, such as axon diameter, but also the characterization of myelin molecular organization and ultrastructural alterations (100).

Staining against contactin-associated protein 1 (CASPR), a membrane protein found in the paranodal section, could also be a strategy to complement the myelination analysis. This protein is interposed between sodium channels at the nodes of Ranvier and potassium channels in the juxtaparanodal regions and performing a co-labelling of CASPR and Kv1.2, a potassium channel protein, would give insights on the presence of these axonal structures.

Regarding the oligodendrocyte distribution and density inside the graft, the Olig2 labelling showed that there were fewer oligodendrocytes at the first timepoint, which was consistent with the MBP results. Nonetheless, unlike the MBP staining whose configuration was more heterogenous and harder to interpret, Olig2 is a transcription factor and gave rise to a very specific nuclear staining.

It revealed that the number of oligodendrocytes in the mouse cortex did not change significantly from 1 to 4 mpi and was in accordance with previous calculations (114).

Inside the graft this number was lower but increased from the first to the second timepoint analysed. As the $Olig2^{+}$ nuclei did not colocalize with STEM101, these corresponded to mature oligodendrocytes from the host, that had migrated there. One of the roles that Olig2 plays during neurodevelopment is the determination of neuronal versus glial cell fate (101), so these mouse oligodendrocytes could have migrated to the graft to assist in this processes. We did not assess in more detail the nature of interaction, but this quantification already reinforced the idea that the mouse glia is interacting with the human cells.

Taking advantage of a neuron-specific antibody, it would also be interesting to compare the ratio of oligodendrocytes and neurons inside and outside the human region and try to understand how it changes over time.
The expression of Nerve/glial antigen 2 (NG2) could also be addressed. NG2-glia, also known as oligodendrocyte progenitors cells, is an additional class of glial cells that can differentiate into astrocytes (115). It is involved in embryonic and early postnatal events of neurodevelopment, and its functions in the brain also include vessel network formation. Even though they are thought to disappear from the mouse cortex shortly after birth (at around P10), the introduction of human cells that require, among other things, new vessel formation could be a trigger for a more prolonged expression of this marker (116).

Another decisive finding was the detection of blood vessels inside the xenograft. There was some CD31 signal across the whole slice, probably because PECAM-1 is also expressed in microglial and other central nervous system cells (102). Nonetheless, the limit of the vessels was clear, demonstrating that there is vascularization of the human graft. The mouse brain microenvironment can adapt to the xenograft, grow blood vessels and, hence, support the development of a multicellular transplant, as previously reported (77).

In the past few years, the laboratory has developed and optimized the grafting technique until it was possible obtain a success rate of injection superior to 50%.
Some variability in the grafts location and size still prevails, but it is difficult to eliminate it completely, considering the number of variables that an *in vivo* study encompasses.
The NPCs culture and injection, the animal perfusions and the brain fixation, sectioning and storage, had been set up, and only minor adjustments in the immunostaining protocol were required, depending on the antibody. Continuous adaptation was required, as the set of antibodies used was very broad, ranging from transcription factors to transmembranar and cytoskeletal proteins, that were often targeted in the same assay.

An adjustment that could further improve the outcome concerns the cell characterization before injection. It has been shown that NPCs derived from human iPSC reflect very early human development and express Nestin, Pax6, and Sox2 (117). It would have been helpful to detect the expression of these progenitor/stem cell markers, and make sure these cells

were not differentiating yet. For example, fluorescence-activated cell-sorting (FACS) analysis or immunofluorescence could be used for this purpose.

Regarding imaging, higher resolution techniques, such as electron microscopy or *in vivo* multiphoton microscopy could be used as a complement to better assess interactions between the labelled proteins.

When it comes to image processing and analysis of non-nuclear labellings, fluorescence quantification (through measurement of mean grey value) could be performed in Fiji, after optimizing the stainings and acquisition of images. Some 2D and 3D image deconvolution could also be explored.

Supplementary characterization could be also undertaken. GABA could be used to detect GABAergic interneurons, tyrosine hydroxylase to detect dopaminergic neurons and specific cortical layers could be labelled. Tbr1 and Ctip2 could be used for deep, V and VI layers and Satb2 or Cux1 for upper, supragranular layers. Neurons that populate the distinct cortical layers are produced sequentially (113) and it would be enlightening to see which kind of segmentation (if any) is developing inside the graft. In previous experiments with this grafting model, researchers in the lab have detected the expression of Cux1 in human cells and the expression of Ctip2 inside the graft area, but not colocalizing with GFP. It remains to be investigated whether these proteins levels remain stable throughout the six-month period or experience variations.

The transcriptional activity in the graft could additionally be analysed through quantitative real-time PCR to detect, for example, glutamatergic and GABAergic neurons, or somatostatin and parvalbumin interneurons.

6. Conclusion

As a response to the urging necessity of an *in vivo* model capable of replicating human neurodevelopment and neuropathology, we have developed and characterized a grafting technique that results in the successful integration of human neuronal progenitor cells in the cortex of immunodeficient mice. We have shown that most of these iPSC-derived cells concentrate anteriorly and tend to accommodate in the motor or prelimbic cortex regions, where they project progressively longer neurites into the mouse cortex.

One of the most important aspects in neuronal maturation analysis is the neurite outgrowth and differentiation. We were able to optimize a tracing protocol that can be explored in the future to quantify axonal and dendritic characteristics among different conditions.

Regarding their development, it was possible to observe that human cells gradually acquire features characteristic of mature neurons, including formation of dendritic spines, complexification of the projections network and establishment of synapses. The number of cells expressing postmitotic proteins grew, while the number of pluripotent stem cells tended to decrease. Neurons that have started differentiation but are still in an immature state were also detected.

Altogether these experiments have revealed the highly heterogenous nature of the human graft, where cells at distinct stages coexist. Further investigations on the cortical identity of the developing human cells should be carried out.

In addition, we were able to confirm the dynamic interaction between host glial cell populations and the developing human neurons. Both astrocytes and oligodendrocytes are found in the graft and are reacting to its presence, exhibiting an unorganized distribution. Astrocytes are very concentrated in the graft in all timepoints, while the number of oligodendrocytes is low in the beginning and increases over time. Another important finding was the localization of radial glia fibres in the initial timepoint, which suggested that mouse glia could be assisting in the development and migration of the human NPCs.

As a last result, we noticed the existence of blood vessels inside the human graft, an essential requirement for cell survival.

The high variability between samples poses a challenge to the interpretation of results, consequently the following step would be to increase the number of sampled brains per timepoint. Some supplementary immunofluorescent or immunohistochemical assays to

target other proteins could also be performed to corroborate these results and finalise the characterization of the graft development.

In addition, functional analysis should be completed to better assess the maturation and differentiation of these neurons. Information about the spontaneous activity, the conduction velocity and latency upon stimulation, the changes in membrane potential or the frequency of excitatory and inhibitory events could be measured.

In the future, the influence of a human specific polymorphism in the gene of a nAChR subunit can be assessed following a similar protocol. Human reprogrammed iPSCs can be manipulated with a gene-editing technique, then differentiated into NPCs and injected, and, lastly, their development can be inspected along the lines of this project.

Changes in morphology, interaction with the host cell populations and activity could also be assessed when other polymorphisms and mutations are introduced, or specific proteins are deleted, silenced or overexpressed. Henceforth, this system could be adapted to model other human specific neurological disorders.

7. Bibliography

1. Eaton WW, Martins SS, Nestadt G, Bienvenu OJ, Clarke D, Alexandre P. The burden of mental disorders. Vol. 30, Epidemiologic Reviews. Oxford University Press; 2008. p. 1–14.

2. Buka SL. Psychiatric epidemiology: Reducing the global burden of mental illness. Vol. 168, American Journal of Epidemiology. 2008. p. 977–9.

3. James SL, Abate D, Abate KH, Abay SM, Abbafati C, Abbasi N, et al. Global, regional, and national incidence, prevalence, and years lived with disability for 354 diseases and injuries for 195 countries and territories, 1990–2017: a systematic analysis for the Global Burden of Disease Study 2017. Lancet [Internet]. 2018 Nov 10 [cited 2019 Jun 9];392(10159):1789–858. Available from: http://www.ncbi.nlm.nih.gov/pubmed/30496104

4. American Psychiatric Association. Diagnostic and Statistical Manual of Mental Disorders. Fifth. 2013. 947 p.

5. Saha S, Chant D, Welham J, McGrath J. A systematic review of the prevalence of schizophrenia. PLoS Med [Internet]. 2005 May;2(5):e141. Available from: http://www.ncbi.nlm.nih.gov/pubmed/15916472

6. Chaiyakunapruk N, Chong HY, Teoh SL, Wu DB-C, Kotirum S, Chiou C-F. Global economic burden of schizophrenia: a systematic review. Neuropsychiatr Dis Treat [Internet]. 2016 Nov [cited 2019 Jun 10];12(7):357. Available from: https://linkinghub.elsevier.com/retrieve/pii/S1098301514022232

7. Saha S, Chant D, Mcgrath J. A Systematic Review of Mortality in Schizophrenia Is the Differential Mortality Gap Worsening Over Time? Population-based studies that re-ported primary data on deaths in people with schizo-phrenia [Internet]. Vol. 64, Arch Gen Psychiatry. 2007 [cited 2019 Jun 10]. Available from: www.archgenpsychiatry.com

8. Parks J, Svendsen D, Singer P, Foti ME. Mortality and Morbidity Final Report 8.18.08 [Internet]. 2006 [cited 2019 Jun 10]. Available from: www.nasmhpd.org

9. Piotrowski P, Gondek TM, Królicka-Deręgowska A, Misiak B, Adamowski T, Kiejna A. Causes of mortality in schizophrenia: An updated review of European studies. Vol. 29, Psychiatria Danubina. 2017. p. 108–20.

10. Tsai J, Rosenheck RA. Psychiatric comorbidity among adults with schizophrenia: A latent class analysis. Psychiatry Res [Internet]. 2013 Nov [cited 2019 Jun 10];210(1):16–20. Available from: https://linkinghub.elsevier.com/retrieve/pii/S0165178113002722

11. Palmer BA, Pankratz VS, Bostwick JM. The Lifetime Risk of Suicide in Schizophrenia. Arch Gen Psychiatry. 2005 Mar 7;62(3):247.

12. Nestler EJ, Hyman SE. Animal models of neuropsychiatric disorders. Nat Neurosci [Internet]. 2010 Oct [cited 2019 Jun 9];13(10):1161–9. Available from: http://www.ncbi.nlm.nih.gov/pubmed/20877280

13. Howes O, McCutcheon R, Stone J. Glutamate and dopamine in schizophrenia: an update for the 21st century. J Psychopharmacol [Internet]. 2015 Feb [cited 2019 Jul 19];29(2):97–115. Available from: http://www.ncbi.nlm.nih.gov/pubmed/25586400

14. Kirkpatrick B, Messias E, Harvey PD, Fernandez-Egea E, Bowie CR. Is schizophrenia a syndrome of accelerated aging? Vol. 34, Schizophrenia Bulletin. 2008. p. 1024–32.

15. Coutlee CG, Huettel SA. The Functional Neuroanatomy of Decision Making: Prefrontal Control of Thought and Action. Brain Res [Internet]. 2012 Jan 5 [cited 2019 Jul 19];1428C:3. Available from: http://www.ncbi.nlm.nih.gov/pubmed/21676379

16. Kaya S, McCabe C, Kaya S, McCabe C. What Role Does the Prefrontal Cortex Play in the Processing of Negative and Positive Stimuli in Adolescent Depression? Brain Sci [Internet]. 2019 May 7 [cited 2019 Jul 19];9(5):104. Available from: https://www.mdpi.com/2076-3425/9/5/104

17. Lumer ED, Rees G. Covariation of activity in visual and prefrontal cortex associated with subjective visual perception. Proc Natl Acad Sci U S A [Internet]. 1999 Feb 16 [cited 2019 Jul 19];96(4):1669–73. Available from: http://www.ncbi.nlm.nih.gov/pubmed/9990082

18. Ochoa ELM, Lasalde-Dominicci J. Cognitive deficits in schizophrenia: Focus on neuronal nicotinic acetylcholine receptors and smoking [Internet]. Vol. 27, Cellular and Molecular Neurobiology. 2007 [cited 2019 Jun 10]. p. 609–39. Available from: https://www.ncbi.nlm.nih.gov/pmc/articles/PMC4676572/pdf/nihms733485.pdf

19. Hauer L, Sellner J, Brigo F, Trinka E, Sebastianelli L, Saltuari L, et al. Effects of Repetitive Transcranial Magnetic Stimulation over Prefrontal Cortex on Attention in Psychiatric Disorders: A Systematic Review. J Clin Med [Internet]. 2019 Mar 27 [cited 2019 Jul 19];8(4). Available from: http://www.ncbi.nlm.nih.gov/pubmed/30934685

20. Granon S, Changeux J-P. Deciding between conflicting motivations: What mice make of their prefrontal cortex. Behav Brain Res [Internet]. 2012 Apr 15 [cited 2019 Jul 19];229(2):419–26. Available from: http://www.ncbi.nlm.nih.gov/pubmed/22108342

21. Parikh V, Kutlu G, Gould TJ. nAChR dysfunction as a common substrate for schizophrenia and comorbid nicotine addiction: current trends and perspectives HHS Public Access.

Schizophr Res [Internet]. 2016 [cited 2019 Jun 10];171(0):1–15. Available from: https://www.ncbi.nlm.nih.gov/pmc/articles/PMC4762752/pdf/nihms753711.pdf

22. Changeux J-P, Bertrand D, Corringer P-J, Dehaene S, Edelstein S, Léna C, et al. Brain nicotinic receptors: structure and regulation, role in learning and reinforcement. Brain Res Rev [Internet]. 1998 May 1 [cited 2019 Jul 19];26(2–3):198–216. Available from: https://www.sciencedirect.com/science/article/pii/S0165017397000404?via%3Dihub

23. Picciotto MR, Higley MJ, Mineur YS. Acetylcholine as a neuromodulator: cholinergic signaling shapes nervous system function and behavior. Neuron [Internet]. 2012 Oct 4 [cited 2019 Jul 19];76(1):116–29. Available from: http://www.ncbi.nlm.nih.gov/pubmed/23040810

24. Changeux J-P. Allosteric Receptors: From Electric Organ to Cognition. Annu Rev Pharmacol Toxicol [Internet]. 2010 Feb 6 [cited 2019 Jul 19];50(1):1–38. Available from: http://www.annualreviews.org/doi/10.1146/annurev.pharmtox.010909.105741

25. McCorry LK. Physiology of the autonomic nervous system. Am J Pharm Educ [Internet]. 2007 Aug 15;71(4):78. Available from: http://www.ncbi.nlm.nih.gov/pubmed/17786266

26. Albuquerque EX, Pereira EFR, Alkondon M, Rogers SW. Mammalian Nicotinic Acetylcholine Receptors: From Structure to Function. 2009 [cited 2019 Jul 18]; Available from: https://www.ncbi.nlm.nih.gov/pmc/articles/PMC2713585/pdf/nihms106860.pdf

27. Adler LE, Olincy A, Waldo M, Harris JG, Griffith J, Stevens K, et al. Schizophrenia, Sensory Gating, and Nicotinic Receptors. Schizophr Bull [Internet]. 1998 Jan 1 [cited 2019 Jun 10];24(2):189–202. Available from: https://academic.oup.com/schizophreniabulletin/article-lookup/doi/10.1093/oxfordjournals.schbul.a033320

28. Berman JA, Talmage DA, Role LW. Cholinergic circuits and signaling in the pathophysiology of schizophrenia. Int Rev Neurobiol [Internet]. 2007 [cited 2019 Jul 19];78:193–223. Available from: http://www.ncbi.nlm.nih.gov/pubmed/17349862

29. Javitt DC, Freedman R. Sensory processing dysfunction in the personal experience and neuronal machinery of schizophrenia. Am J Psychiatry [Internet]. 2015 Jan [cited 2019 Jul 19];172(1):17–31. Available from: http://www.ncbi.nlm.nih.gov/pubmed/25553496

30. D'Souza DC, Esterlis I, Carbuto M, Krasenics M, Seibyl J, Bois F, et al. Lower β2*-nicotinic acetylcholine receptor availability in smokers with schizophrenia. Am J Psychiatry [Internet]. 2012 [cited 2019 Jun 10];169(3):326–34. Available from: https://www.ncbi.nlm.nih.gov/pmc/articles/PMC3881431/pdf/nihms-521771.pdf

31. D'Souza MS, Markou A. Schizophrenia and tobacco smoking comorbidity: NAChR agonists in the treatment of schizophrenia-associated cognitive deficits [Internet]. Vol. 62, Neuropharmacology. 2012 [cited 2019 Jun 10]. p. 1564–73. Available from: https://www.ncbi.nlm.nih.gov/pmc/articles/PMC3116036/pdf/nihms276442.pdf

32. Shih RA, Belmonte PL, Zandi PP. A review of the evidence from family, twin and adoption studies for a genetic contribution to adult psychiatric disorders. Int Rev Psychiatry [Internet]. 2004 Nov 11 [cited 2019 Jul 18];16(4):260–83. Available from: http://www.tandfonline.com/doi/full/10.1080/09540260400014401

33. Jia P, Chen X, Fanous AH, Zhao Z. Convergent roles of de novo mutations and common variants in schizophrenia in tissue-specific and spatiotemporal co-expression network. Transl Psychiatry [Internet]. 2018 Dec 24 [cited 2019 Jul 17];8(1):105. Available from: http://www.ncbi.nlm.nih.gov/pubmed/29799522

34. Sanders AR. Genetics of schizophrenia. In: Schizophrenia: Recent Advances in Diagnosis and Treatment. 2014.

35. Sinkus ML, Graw S, Freedman R, Ross RG, Lester HA, Leonard S. The human CHRNA7 and CHRFAM7A genes: A review of the genetics, regulation, and function [Internet]. Vol. 96, Neuropharmacology. NIH Public Access; 2015 [cited 2019 Jun 11]. p. 274–88. Available from: http://www.ncbi.nlm.nih.gov/pubmed/25701707

36. Gillentine MA, Schaaf CP. The human clinical phenotypes of altered CHRNA7 copy number. Biochem Pharmacol [Internet]. 2015 Oct 15 [cited 2019 Jul 18];97(4):352–62. Available from: http://www.ncbi.nlm.nih.gov/pubmed/26095975

37. Leonard S, Gault J, Hopkins J, Logel J, Vianzon R, Short M, et al. Association of Promoter Variants in the α7 Nicotinic Acetylcholine Receptor Subunit Gene With an Inhibitory Deficit Found in Schizophrenia. Arch Gen Psychiatry [Internet]. 2002 Dec 1 [cited 2019 Jul 17];59(12):1085. Available from: http://archpsyc.jamanetwork.com/article.aspx?doi=10.1001/archpsyc.59.12.1085

38. Koukouli F, Maskos U. The multiple roles of the α7 nicotinic acetylcholine receptor in modulating glutamatergic systems in the normal and diseased nervous system. Biochem Pharmacol [Internet]. 2015 Oct 15 [cited 2019 Jul 19];97(4):378–87. Available from: https://www.sciencedirect.com/science/article/abs/pii/S0006295215003883

39. Proulx E, Piva M, Tian MK, Bailey CDC, Lambe EK. Nicotinic acetylcholine receptors in attention circuitry: the role of layer VI neurons of prefrontal cortex. Cell Mol Life Sci [Internet]. 2014 Apr [cited 2019 Jul 19];71(7):1225–44. Available from:

http://www.ncbi.nlm.nih.gov/pubmed/24122021

40. Bailey CDC, Alves NC, Nashmi R, De Biasi M, Lambe EK. Nicotinic α5 Subunits Drive Developmental Changes in the Activation and Morphology of Prefrontal Cortex Layer VI Neurons. Biol Psychiatry [Internet]. 2012 Jan 15 [cited 2019 Jun 11];71(2):120–8. Available from: http://www.ncbi.nlm.nih.gov/pubmed/22030359

41. Consortium SWG of the PG, Ripke S, Neale BM, Corvin A, Walters JTR, Farh K-H, et al. Biological insights from 108 schizophrenia-associated genetic loci. Nature [Internet]. 2014 Jul 22 [cited 2019 Jun 11];511(7510):421–7. Available from: http://www.nature.com/articles/nature13595

42. Winterer G, Mittelstrass K, Giegling I, Lamina C, Fehr C, Brenner H, et al. Risk gene variants for nicotine dependence in the CHRNA5-CHRNA3-CHRNB4 cluster are associated with cognitive performance. Am J Med Genet Part B Neuropsychiatr Genet [Internet]. 2010 Dec 5 [cited 2019 Jul 17];153B(8):1448–58. Available from: http://www.ncbi.nlm.nih.gov/pubmed/20886544

43. Jackson KJ, Fanous AH, Chen J, Kendler KS, Chen X. Variants in the 15q25 gene cluster are associated with risk for schizophrenia and bipolar disorder. Psychiatr Genet [Internet]. 2013 Feb [cited 2019 Jul 17];23(1):20–8. Available from: http://www.ncbi.nlm.nih.gov/pubmed/23196875

44. Bierut LJ, Stitzel JA, Wang JC, Hinrichs AL, Grucza RA, Xuei X, et al. Variants in Nicotinic Receptors and Risk for Nicotine Dependence. Am J Psychiatry [Internet]. 2008 Sep [cited 2019 Jun 11];165(9):1163–71. Available from: http://www.ncbi.nlm.nih.gov/pubmed/18519524

45. Won H, de la Torre-Ubieta L, Stein JL, Parikshak NN, Huang J, Opland CK, et al. Chromosome conformation elucidates regulatory relationships in developing human brain. Nature [Internet]. 2016 Oct 19 [cited 2019 Jun 11];538(7626):523–7. Available from: http://www.ncbi.nlm.nih.gov/pubmed/27760116

46. Sumitomo A, Horike K, Hirai K, Butcher N, Boot E, Sakurai T, et al. A mouse model of 22q11.2 deletions: Molecular and behavioral signatures of Parkinson's disease and schizophrenia [Internet]. Vol. 4, Sci. Adv. 2018 [cited 2019 Jun 10]. Available from: https://www.ncbi.nlm.nih.gov/pmc/articles/PMC6093626/pdf/aar6637.pdf

47. Bassett AS, Chow EWC. Schizophrenia and 22q11.2 deletion syndrome. Curr Psychiatry Rep [Internet]. 2008 Apr [cited 2019 Jul 19];10(2):148–57. Available from: http://www.ncbi.nlm.nih.gov/pubmed/18474208

48. Karayiorgou M, Simon TJ, Gogos JA, Gogos' JA. 2q11.2 microdeletions: linking DNA structural variation to brain dysfunction and schizophrenia FURTHER INFORMATION. Nat Rev Neurosci [Internet]. 2010 [cited 2019 Jun 10];11(6):402–16. Available from: https://www.ncbi.nlm.nih.gov/pmc/articles/PMC2977984/pdf/nihms-218108.pdf

49. Moran P, Stokes J, Marr J, Bock G, Desbonnet L, Waddington J, et al. Gene × Environment Interactions in Schizophrenia: Evidence from Genetic Mouse Models. Neural Plast [Internet]. 2016 [cited 2019 Jul 19];2016:2173748. Available from: http://www.ncbi.nlm.nih.gov/pubmed/27725886

50. International Schizophrenia Consortium T, preparation M, analysis D, analysis subgroup G, analyses subgroup P, committee M, et al. Common polygenic variation contributes to risk of schizophrenia and bipolar disorder The International Schizophrenia Consortium*. Nature [Internet]. 2009 [cited 2019 Jun 10];460. Available from: http://zzz.bwh.harvard.edu/library/isc-2009.pdf

51. Schlachetzki JCM, Saliba SW, de Oliveira ACP. Studying neurodegenerative diseases in culture models. Rev Bras Psiquiatr [Internet]. 2013 [cited 2019 Jun 9];35(SUPPL.2):S92–100. Available from: http://www.scielo.br/scielo.php?script=sci_arttext&pid=S1516-44462013000600005&lng=en&tlng=en

52. Gaspard N, Bouschet T, Hourez R, Dimidschstein J, Naeije G, van den Ameele J, et al. An intrinsic mechanism of corticogenesis from embryonic stem cells. Nature [Internet]. 2008 Sep 17 [cited 2019 Jun 23];455(7211):351–7. Available from: http://www.nature.com/articles/nature07287

53. Hu B-Y, Du Z-W, Li X-J, Ayala M, Zhang S-C. Human oligodendrocytes from embryonic stem cells: conserved SHH signaling networks and divergent FGF effects. Development [Internet]. 2009 May [cited 2019 Jul 19];136(9):1443–52. Available from: http://www.ncbi.nlm.nih.gov/pubmed/19363151

54. Perrier AL, Tabar V, Barberi T, Rubio ME, Bruses J, Topf N, et al. Derivation of midbrain dopamine neurons from human embryonic stem cells. Proc Natl Acad Sci U S A [Internet]. 2004 Aug 24 [cited 2019 Jul 19];101(34):12543–8. Available from: http://www.ncbi.nlm.nih.gov/pubmed/15310843

55. Kawasaki H, Mizuseki K, Nishikawa S, Kaneko S, Kuwana Y, Nakanishi S, et al. Neurotechnique Induction of Midbrain Dopaminergic Neurons from ES Cells by Stromal Cell-Derived Inducing Activity [Internet]. Vol. 28, Neuron. 2000 [cited 2019 Jun 23]. Available from: https://www.cell.com/action/showPdf?pii=S0896-6273%2800%2900083-0

56. Winkler J, Sotiriadou I, Chen S, Hescheler J, Sachinidis A. The potential of embryonic stem cells combined with -omics technologies as model systems for toxicology. Curr Med Chem [Internet]. 2009 [cited 2019 Jul 19];16(36):4814–27. Available from: http://www.ncbi.nlm.nih.gov/pubmed/19929785

57. Volarevic V, Markovic BS, Gazdic M, Volarevic A, Jovicic N, Arsenijevic N, et al. Ethical and Safety Issues of Stem Cell-Based Therapy. Int J Med Sci [Internet]. 2018 [cited 2019 Jun 20];15(1):36–45. Available from: http://www.ncbi.nlm.nih.gov/pubmed/29333086

58. Daley GQ, Hyun I, Apperley JF, Barker RA, Benvenisty N, Bredenoord AL, et al. Setting Global Standards for Stem Cell Research and Clinical Translation: The 2016 ISSCR Guidelines. Stem Cell Reports [Internet]. 2016 Jun 14 [cited 2019 Jun 20];6(6):787–97. Available from: https://www.sciencedirect.com/science/article/pii/S2213671116300418#bbib4

59. Hochedlinger K, Jaenisch R. Monoclonal mice generated by nuclear transfer from mature B and T donor cells. Nature [Internet]. 2002 Feb 10 [cited 2019 Jun 20];415(6875):1035–8. Available from: http://www.nature.com/articles/nature718

60. Cowan CA, Atienza J, Melton DA, Eggan K. Nuclear reprogramming of somatic cells after fusion with human embryonic stem cells. Science [Internet]. 2005 Aug 26 [cited 2019 Jun 20];309(5739):1369–73. Available from: http://www.ncbi.nlm.nih.gov/pubmed/16123299

61. Takahashi K, Yamanaka S. Induction of Pluripotent Stem Cells from Mouse Embryonic and Adult Fibroblast Cultures by Defined Factors. Cell [Internet]. 2006 Aug 25 [cited 2019 Jun 9];126(4):663–76. Available from: http://www.ncbi.nlm.nih.gov/pubmed/16904174

62. Takahashi K, Tanabe K, Ohnuki M, Narita M, Ichisaka T, Tomoda K, et al. Induction of Pluripotent Stem Cells from Adult Human Fibroblasts by Defined Factors [Internet]. Vol. 131, Cell. 2007 [cited 2019 Jun 9]. p. 861–72. Available from: https://linkinghub.elsevier.com/retrieve/pii/S0092867407014717

63. Loh Y-H, Agarwal S, Park I-H, Urbach A, Huo H, Heffner GC, et al. Generation of induced pluripotent stem cells from human blood. Blood [Internet]. 2009 May 28 [cited 2019 Jul 19];113(22):5476–9. Available from: http://www.ncbi.nlm.nih.gov/pubmed/19299331

64. Bar-Nur O, Russ HA, Efrat S, Benvenisty N. Epigenetic Memory and Preferential Lineage-Specific Differentiation in Induced Pluripotent Stem Cells Derived from Human Pancreatic Islet Beta Cells. Cell Stem Cell [Internet]. 2011 Jul 8 [cited 2019 Jul 19];9(1):17–23. Available from: http://www.ncbi.nlm.nih.gov/pubmed/21726830

65. Li C, Zhou J, Shi G, Ma Y, Yang Y, Gu J, et al. Pluripotency can be rapidly and efficiently

induced in human amniotic fluid-derived cells. Hum Mol Genet [Internet]. 2009 Nov 15 [cited 2019 Jul 19];18(22):4340–9. Available from: http://www.ncbi.nlm.nih.gov/pubmed/19679563

66. Aoki T, Ohnishi H, Oda Y, Tadokoro M, Sasao M, Kato H, et al. Generation of induced pluripotent stem cells from human adipose-derived stem cells without c-MYC. Tissue Eng Part A [Internet]. 2010 Jul [cited 2019 Jul 19];16(7):2197–206. Available from: http://www.ncbi.nlm.nih.gov/pubmed/20146561

67. Ardhanareeswaran K, Mariani J, Coppola G, Abyzov A, Vaccarino FM. Human induced pluripotent stem cells for modelling neurodevelopmental disorders. Nat Rev Neurol [Internet]. 2017 May [cited 2019 Jul 19];13(5):265–78. Available from: http://www.ncbi.nlm.nih.gov/pubmed/28418023

68. Falk A, Heine VM, Harwood AJ, Sullivan PF, Peitz M, Brüstle O, et al. Modeling psychiatric disorders: From genomic findings to cellular phenotypes. Vol. 21, Molecular Psychiatry. Nature Publishing Group; 2016. p. 1167–79.

69. Schwartzentruber J, Foskolou S, Kilpinen H, Rodrigues J, Alasoo K, Knights AJ, et al. Molecular and functional variation in iPSC-derived sensory neurons. Nat Genet [Internet]. 2018 [cited 2019 Jul 19];50(1):54–61. Available from: http://www.ncbi.nlm.nih.gov/pubmed/29229984

70. Kanjhan R, Noakes PG, Bellingham MC. Emerging Roles of Filopodia and Dendritic Spines in Motoneuron Plasticity during Development and Disease. Neural Plast [Internet]. 2016 [cited 2019 Jul 14];2016:3423267. Available from: http://www.ncbi.nlm.nih.gov/pubmed/26843990

71. Cheng C, Fass DM, Folz-Donahue K, MacDonald ME, Haggarty SJ. Highly Expandable Human iPS Cell-Derived Neural Progenitor Cells (NPC) and Neurons for Central Nervous System Disease Modeling and High-Throughput Screening. Curr Protoc Hum Genet [Internet]. 2017 [cited 2019 Jul 19];92:21.8.1-21.8.21. Available from: http://www.ncbi.nlm.nih.gov/pubmed/28075486

72. N E, S K, K TT, M N, T Y, F A, et al. Response to comment on "Drug screening for ALS using patient-specific induced pluripotent stem cells." Science Translational Medicine [Internet]. 2013 [cited 2019 Jun 20];5(188):188lr2. Available from: www.ScienceTranslationalMedicine.org

73. Hanna J, Wernig M, Markoulaki S, Sun C-W, Meissner A, Cassady JP, et al. Treatment of Sickle Cell Anemia Mouse Model with iPS Cells Generated from Autologous Skin. Science

(80-) [Internet]. 2007 Dec 21 [cited 2019 Jul 19];318(5858):1920–3. Available from: http://www.sciencemag.org/cgi/doi/10.1126/science.1152092

74. Saha K, Jaenisch R. Technical Challenges in Using Human Induced Pluripotent Stem Cells to Model Disease [Internet]. Vol. 5, Cell Stem Cell. 2009 [cited 2019 Jul 18]. p. 584–95. Available from: https://www.ncbi.nlm.nih.gov/pmc/articles/PMC2921621/pdf/nihms165809.pdf

75. Lemonnier T, Blanchard S, Toli D, Roy E, Bigou S, Froissart R, et al. Modeling neuronal defects associated with a lysosomal disorder using patient-derived induced pluripotent stem cells. Hum Mol Genet [Internet]. 2011 [cited 2019 Jul 9];20(18):3653–66. Available from: https://academic.oup.com/hmg/article-abstract/20/18/3653/557448

76. Brennand KJ, Gage FH. Concise Review: The Promise of Human Induced Pluripotent Stem Cell-Based Studies of Schizophrenia. Stem Cells [Internet]. 2011 Dec [cited 2019 Jul 19];29(12):1915–22. Available from: http://www.ncbi.nlm.nih.gov/pubmed/22009633

77. Real R, Peter M, Trabalza A, Khan S, Smith MA, Dopp J, et al. In vivo modeling of human neuron dynamics and down syndrome. Science (80-) [Internet]. 2018 [cited 2019 Jun 24];362(6416). Available from: https://www.ncbi.nlm.nih.gov/pmc/articles/PMC6570619/pdf/EMS83312.pdf

78. Lui JH, Hansen D V., Kriegstein AR. Development and evolution of the human neocortex [Internet]. Vol. 146, Cell. 2011 [cited 2019 Jun 11]. p. 18–36. Available from: http://www.ncbi.nlm.nih.gov/pubmed/21729779

79. Doetsch F, García-Verdugo JM, Alvarez-Buylla A. Cellular composition and three-dimensional organization of the subventricular germinal zone in the adult mammalian brain. J Neurosci [Internet]. 1997 Jul 1 [cited 2019 Jul 18];17(13):5046–61. Available from: http://www.ncbi.nlm.nih.gov/pubmed/9185542

80. Oberheim NA, Takano T, Han X, He W, Lin JHC, Wang F, et al. Uniquely hominid features of adult human astrocytes. J Neurosci [Internet]. 2009 Mar 11 [cited 2019 Jul 18];29(10):3276–87. Available from: http://www.ncbi.nlm.nih.gov/pubmed/19279265

81. Zhou J, Su P, Li D, Tsang S, Duan E, Wang F. High-efficiency induction of neural conversion in human ESCs and human induced pluripotent stem cells with a single chemical inhibitor of transforming growth factor beta superfamily receptors. Stem Cells [Internet]. 2010 Oct [cited 2019 Jul 1];28(10):1741–50. Available from: http://www.ncbi.nlm.nih.gov/pubmed/20734356

82. Chambers SM, Fasano CA, Papapetrou EP, Tomishima M, Sadelain M, Studer L, et al.

Highly efficient neural conversion of human ES and iPS cells by dual inhibition of SMAD signaling HHS Public Access Author manuscript. Nat Biotechnol [Internet]. 2009 [cited 2019 Jul 1];27(3):275–80. Available from: http://www.nature.com/authors/editorial_policies/license.html#terms

83. Ye L, Haroon MA, Salinas A, Paukert M. Comparison of GCaMP3 and GCaMP6f for studying astrocyte Ca2+ dynamics in the awake mouse brain. PLoS One [Internet]. 2017 [cited 2019 Jun 13];12(7). Available from: https://doi.org/10.1371/journal.pone.0181113

84. Weiss S, Dunne C, Hewson J, Wohl C, Wheatley M, Peterson AC, et al. Multipotent CNS Stem Cells Are Present in the Adult Mammalian Spinal Cord and Ventricular Neuroaxis [Internet]. 1996 [cited 2019 Jul 1]. Available from: http://www.jneurosci.org/content/jneuro/16/23/7599.full.pdf

85. Kuhn HG, Winkler J, Kempermann G, Thal LJ, Gage FH. Epidermal Growth Factor and Fibroblast Growth Factor-2 Have Different Effects on Neural Progenitors in the Adult Rat Brain. J Neurosci [Internet]. 1997 Aug 1 [cited 2019 Jul 1];17(15):5820–9. Available from: http://www.ncbi.nlm.nih.gov/pubmed/9221780

86. Fainstein N, Ben-Hur T. Brain Region-Dependent Rejection of Neural Precursor Cell Transplants. Front Mol Neurosci [Internet]. 2018 [cited 2019 Jul 11];11:136. Available from: http://www.ncbi.nlm.nih.gov/pubmed/29760649

87. Espuny-Camacho I, Michelsen KA, Gall D, Linaro D, Hasche A, Bonnefont J, et al. Pyramidal Neurons Derived from Human Pluripotent Stem Cells Integrate Efficiently into Mouse Brain Circuits In Vivo. Neuron. 2013 Feb 6;77(3):440–56.

88. D'Alessio R, Koukouli F, Blanchard S, Catteau J, Raïs C, Lemonnier T, et al. Long-term development of human iPSC-derived pyramidal neurons quantified after transplantation into the neonatal mouse cortex. 2019.

89. Lee KFH, Soares C, Bé¨ıque J-CB. Examining Form and Function of Dendritic Spines. Neural Plast [Internet]. 2012 [cited 2019 Jun 21];2012. Available from: https://www.ncbi.nlm.nih.gov/pmc/articles/PMC3345238/pdf/NP2012-704103.pdf

90. Stathakis DG, Hoover KB, You Z, Bryant PJ. Human Postsynaptic Density-95 (PSD95): Location of the Gene (DLG4) and Possible Function in Nonneural as Well as in Neural Tissues. Genomics [Internet]. 1997 Aug 15 [cited 2019 Jun 11];44(1):71–82. Available from: https://www.sciencedirect.com/science/article/pii/S0888754397948485?via%3Dihub

91. Romorini S, Piccoli G, Jiang M, Grossano P, Tonna N, Passafaro M, et al. A functional role

of postsynaptic density-95-guanylate kinase-associated protein complex in regulating Shank assembly and stability to synapses. J Neurosci [Internet]. 2004 Oct 20 [cited 2019 Jun 11];24(42):9391–404. Available from: http://www.ncbi.nlm.nih.gov/pubmed/15496675

92. Tanapat P. Neuronal Cell Markers. Mater Methods [Internet]. 2013 Jun 5 [cited 2019 Jul 3];3. Available from: http://www.labome.com/method/Neuronal-Cell-Markers.html

93. Mullen RJ, Buck CR, Smith AM. NeuN, a neuronal specific nuclear protein in vertebrates. Development [Internet]. 1992 Sep [cited 2019 Jul 11];116(1):201–11. Available from: http://www.ncbi.nlm.nih.gov/pubmed/1483388

94. Lee MK, Tuttle JB, Rebhun LI, Cleveland DW, Frankfurter A. The expression and posttranslational modification of a neuron-specific ?-tubulin isotype during chick embryogenesis. Cell Motil Cytoskeleton [Internet]. 1990 [cited 2019 Jul 11];17(2):118–32. Available from: http://www.ncbi.nlm.nih.gov/pubmed/2257630

95. Avilion AA, Nicolis SK, Pevny LH, Perez L, Vivian N, Lovell-Badge R. Multipotent cell lineages in early mouse development depend on SOX2 function. Genes Dev [Internet]. 2003 Jan 1 [cited 2019 Jun 9];17(1):126–40. Available from: http://www.ncbi.nlm.nih.gov/pubmed/12514105

96. Ellis P, Fagan BM, Magness ST, Hutton S, Taranova O, Hayashi S, et al. SOX2, a Persistent Marker for Multipotential Neural Stem Cells Derived from Embryonic Stem Cells, the Embryo or the Adult. Dev Neurosci [Internet]. 2004 [cited 2019 Jun 9];26(2–4):148–65. Available from: http://www.ncbi.nlm.nih.gov/pubmed/15711057

97. Farhy-Tselnicker I, Allen NJ. Astrocytes, neurons, synapses: a tripartite view on cortical circuit development. Neural Dev [Internet]. 2018 Dec 1 [cited 2019 Jul 12];13(1):7. Available from: https://neuraldevelopment.biomedcentral.com/articles/10.1186/s13064-018-0104-y

98. Barres BA. A new role for glia: Generation of neurons! Cell [Internet]. 1999 [cited 2019 Jun 11];97(6):667–70. Available from: https://www.cell.com/cell/pdf/S0092-8674(00)80777-1.pdf

99. Graham V, Khudyakov J, Ellis P, Pevny L. SOX2 Functions to Maintain Neural Progenitor Identity. Neuron [Internet]. 2003 Aug [cited 2019 Jun 11];39(5):749–65. Available from: https://linkinghub.elsevier.com/retrieve/pii/S0896627303004975

100. Baumann N, Pham-Dinh D. Biology of Oligodendrocyte and Myelin in the Mammalian Central Nervous System [Internet]. 2001 [cited 2019 Jun 27]. Available from: http://physrev.physiology.org

101. Lu QR, Sun T, Zhu Z, Ma N, Garcia M, Stiles CD, et al. Common Developmental Requirement for Olig Function Indicates a Motor Neuron/Oligodendrocyte Connection. Cell [Internet]. 2002 Apr 5 [cited 2019 Jul 11];109(1):75–86. Available from: https://www.sciencedirect.com/science/article/pii/S0092867402006785

102. Bergom C, Paddock C, Gao C, Holyst T, Newman DK, Newman PJ. An alternatively spliced isoform of PECAM-1 is expressed at high levels in human and murine tissues, and suggests a novel role for the C-terminus of PECAM-1 in cytoprotective signaling. J Cell Sci [Internet]. 2008 [cited 2019 Jun 24];121(8):1235–42. Available from: https://www.ncbi.nlm.nih.gov/pmc/articles/PMC2567807/pdf/nihms71027.pdf

103. De Paola V, Holtmaat A, Knott G, Song S, Wilbrecht L, Caroni P, et al. Cell Type-Specific Structural Plasticity of Axonal Branches and Boutons in the Adult Neocortex. Neuron [Internet]. 2006 Mar 16 [cited 2019 Jul 16];49(6):861–75. Available from: http://www.ncbi.nlm.nih.gov/pubmed/16543134

104. El-Husseini AE, Schnell E, Chetkovich DM, Nicoll RA, Bredt DS. PSD-95 involvement in maturation of excitatory synapses. Science [Internet]. 2000 Nov 17 [cited 2019 Jul 15];290(5495):1364–8. Available from: http://www.ncbi.nlm.nih.gov/pubmed/11082065

105. McDougall S, Vargas Riad W, Silva-Gotay A, Tavares ER, Harpalani D, Li G-L, et al. Myelination of Axons Corresponds with Faster Transmission Speed in the Prefrontal Cortex of Developing Male Rats. eNeuro [Internet]. 2018 [cited 2019 Jul 15];5(4). Available from: http://www.ncbi.nlm.nih.gov/pubmed/30225359

106. Kim KK, Adelstein RS, Kawamoto S. Identification of neuronal nuclei (NeuN) as Fox-3, a new member of the Fox-1 gene family of splicing factors. J Biol Chem. 2009 Nov 6;284(45):31052–61.

107. Gusel'nikova V V, Korzhevskiy DE. NeuN As a Neuronal Nuclear Antigen and Neuron Differentiation Marker. Acta Naturae [Internet]. 2015 [cited 2019 Jul 15];7(2):42–7. Available from: http://www.ncbi.nlm.nih.gov/pubmed/26085943

108. Pang ZP, Yang N, Vierbuchen T, Ostermeier A, Fuentes DR, Yang TQ, et al. Induction of human neuronal cells by defined transcription factors. Nature [Internet]. 2011 Aug 26 [cited 2019 Jul 16];476(7359):220–3. Available from: http://www.ncbi.nlm.nih.gov/pubmed/21617644

109. Von Bohlen Und Halbach O. Immunohistological markers for staging neurogenesis in adult hippocampus [Internet]. Vol. 329, Cell and Tissue Research. 2007 [cited 2019 Jul 16]. p. 409–20. Available from: https://link.springer.com/content/pdf/10.1007%2Fs00441-007-

0432-4.pdf

110. Cahoy JD, Emery B, Kaushal A, Foo LC, Zamanian JL, Christopherson KS, et al. A Transcriptome Database for Astrocytes, Neurons, and Oligodendrocytes: A New Resource for Understanding Brain Development and Function. 2008 [cited 2019 Jun 27]; Available from: www.jneurosci.org

111. Sofroniew M V. Astrogliosis. Cold Spring Harb Perspect Biol [Internet]. 2014 Nov 7 [cited 2019 Jun 30];7(2):a020420. Available from: http://www.ncbi.nlm.nih.gov/pubmed/25380660

112. Cicchetti F, Barker RA. The glial response to intracerebrally delivered therapies for neurodegenerative disorders: is this a critical issue? Front Pharmacol [Internet]. 2014 Jul 10 [cited 2019 Jul 13];5:139. Available from: http://journal.frontiersin.org/article/10.3389/fphar.2014.00139/abstract

113. Nowakowski TJ, Pollen AA, Sandoval-Espinosa C, Kriegstein AR. Transformation of the Radial Glia Scaffold Demarcates Two Stages of Human Cerebral Cortex Development. Neuron [Internet]. 2016 [cited 2019 Jun 27];91(6):1219–27. Available from: https://www.ncbi.nlm.nih.gov/pmc/articles/PMC5087333/pdf/nihms-815478.pdf

114. Valério-Gomes B, Guimarães DM, Szczupak D, Lent R. The Absolute Number of Oligodendrocytes in the Adult Mouse Brain. Front Neuroanat [Internet]. 2018 Oct 30 [cited 2019 Jul 14];12:90. Available from: https://www.frontiersin.org/article/10.3389/fnana.2018.00090/full

115. Dimou L, Gallo V. NG2-glia and their functions in the central nervous system [Internet]. Vol. 63, GLIA. 2015 [cited 2019 Jul 14]. p. 1429–51. Available from: https://www.ncbi.nlm.nih.gov/pmc/articles/PMC4470768/pdf/nihms688943.pdf

116. Minocha S, Valloton D, Brunet I, Eichmann A, Hornung J-P, Lebrand C. NG2 glia are required for vessel network formation during embryonic development. Elife [Internet]. 2015 Dec 10 [cited 2019 Jul 14];4. Available from: https://elifesciences.org/articles/09102

117. Patterson M, Chan DN, Ha I, Case D, Cui Y, Van Handel B, et al. Defining the nature of human pluripotent stem cell progeny. Cell Res [Internet]. 2012 Jan [cited 2019 Jul 15];22(1):178–93. Available from: http://www.ncbi.nlm.nih.gov/pubmed/21844894

8. Appendix

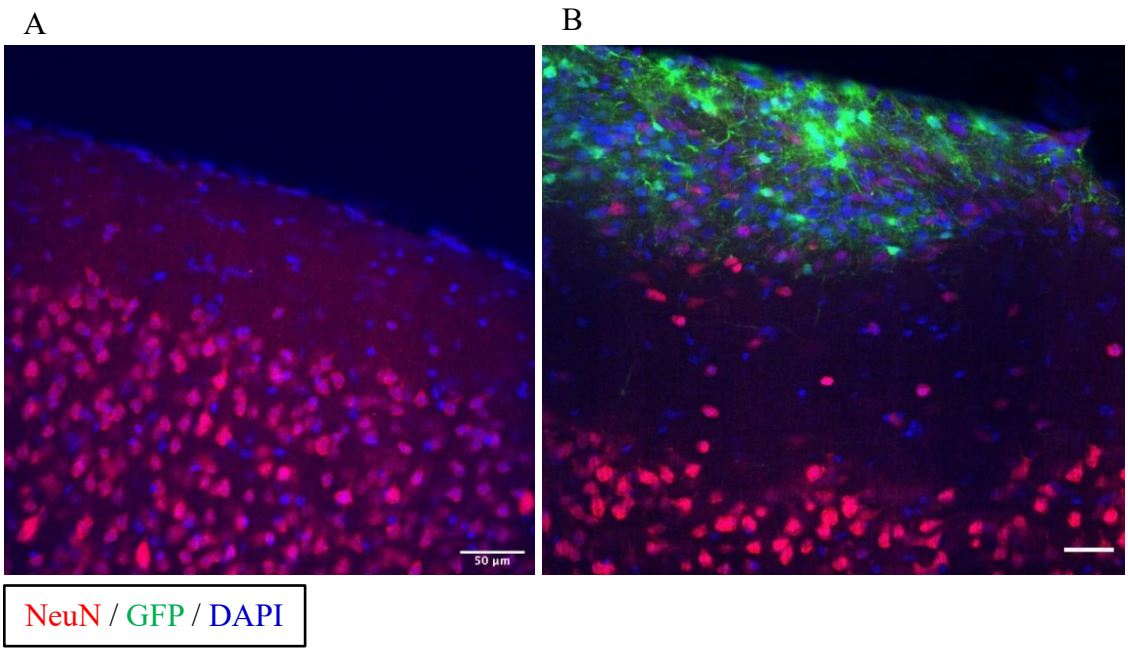

Figure 26 - Fluorescent microscope images of the NeuN and GFP staining. (A) Non-grafted brain where the NeuN distribution in the cortex is very well organized. (B) Brain that received a graft and where a less NeuN is less stratified, at 5 mpi. NeuN is in red, GFP in green and nuclei are counterstained with DAPI, in blue. Scale bars: 50 µm

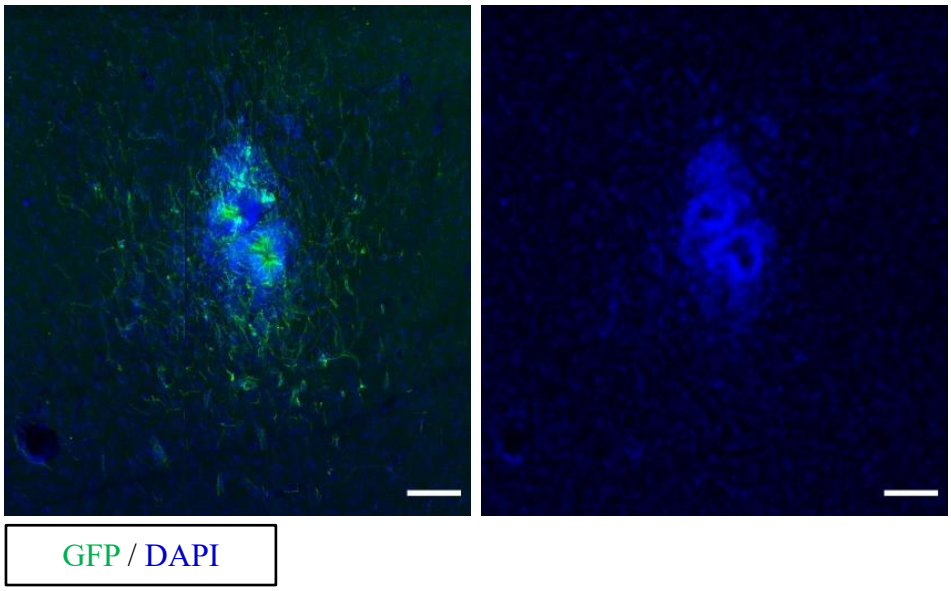

Figure 27 - Fluorescent microscope image of the injection site, at 1 mpi. A cluster of human cells that did not migrate to the cortex is visible and, in the centre, several nuclei assemble in round shapes, resembling neural rosettes detected *in vitro*. Scale bars:100 µm

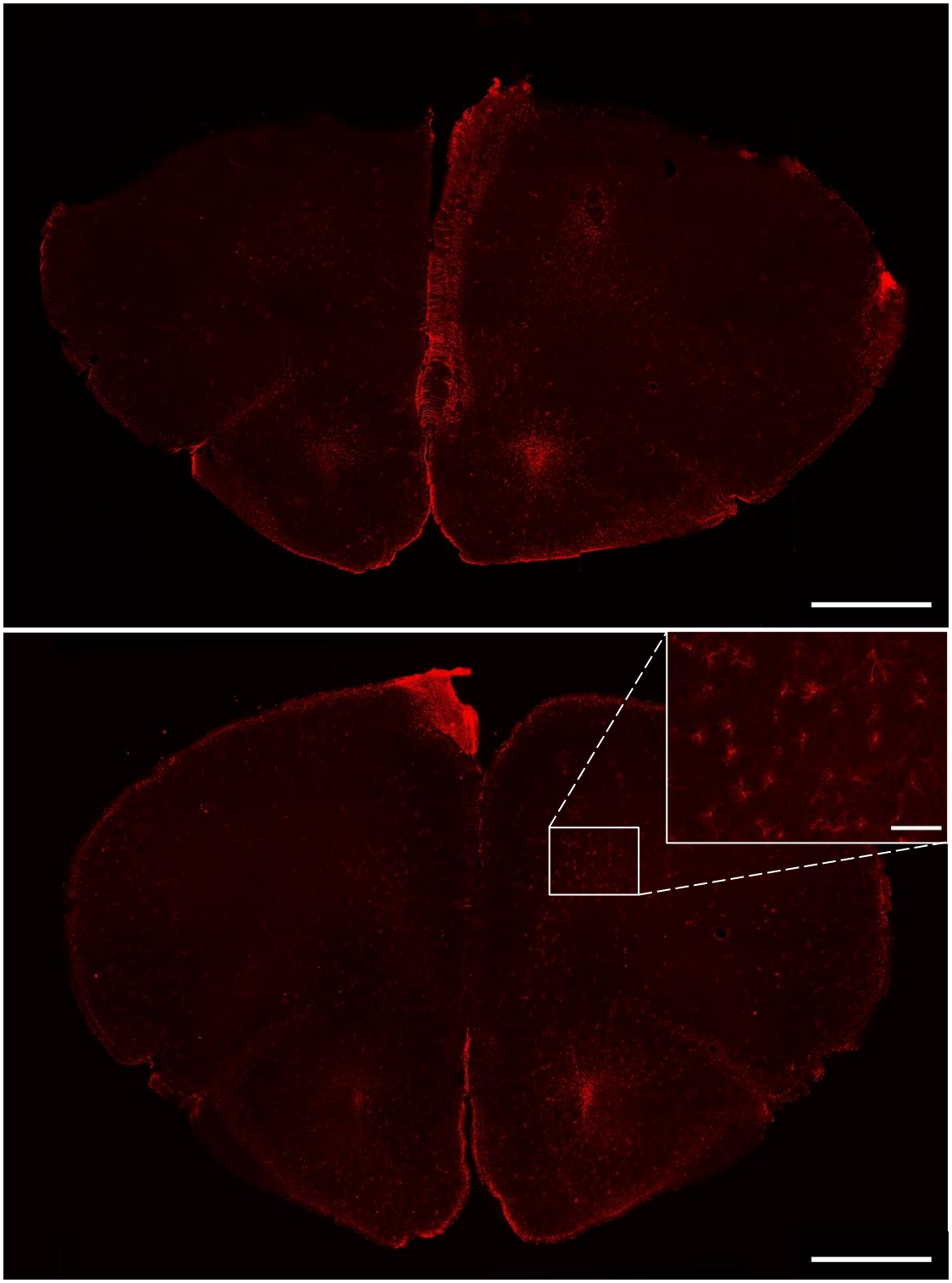

GFAP

Figure 28 – Representative images of entire slices stained with GFAP at 1 mpi (upper image) and 4 mpi (lower image). The graft location is evidenced by a very strong signal. A zoomed in section of the lower image is highlighted to demonstrate the existence of star-shape astrocytes in the mouse brain, as predicted. Scale bars: 1000 µm

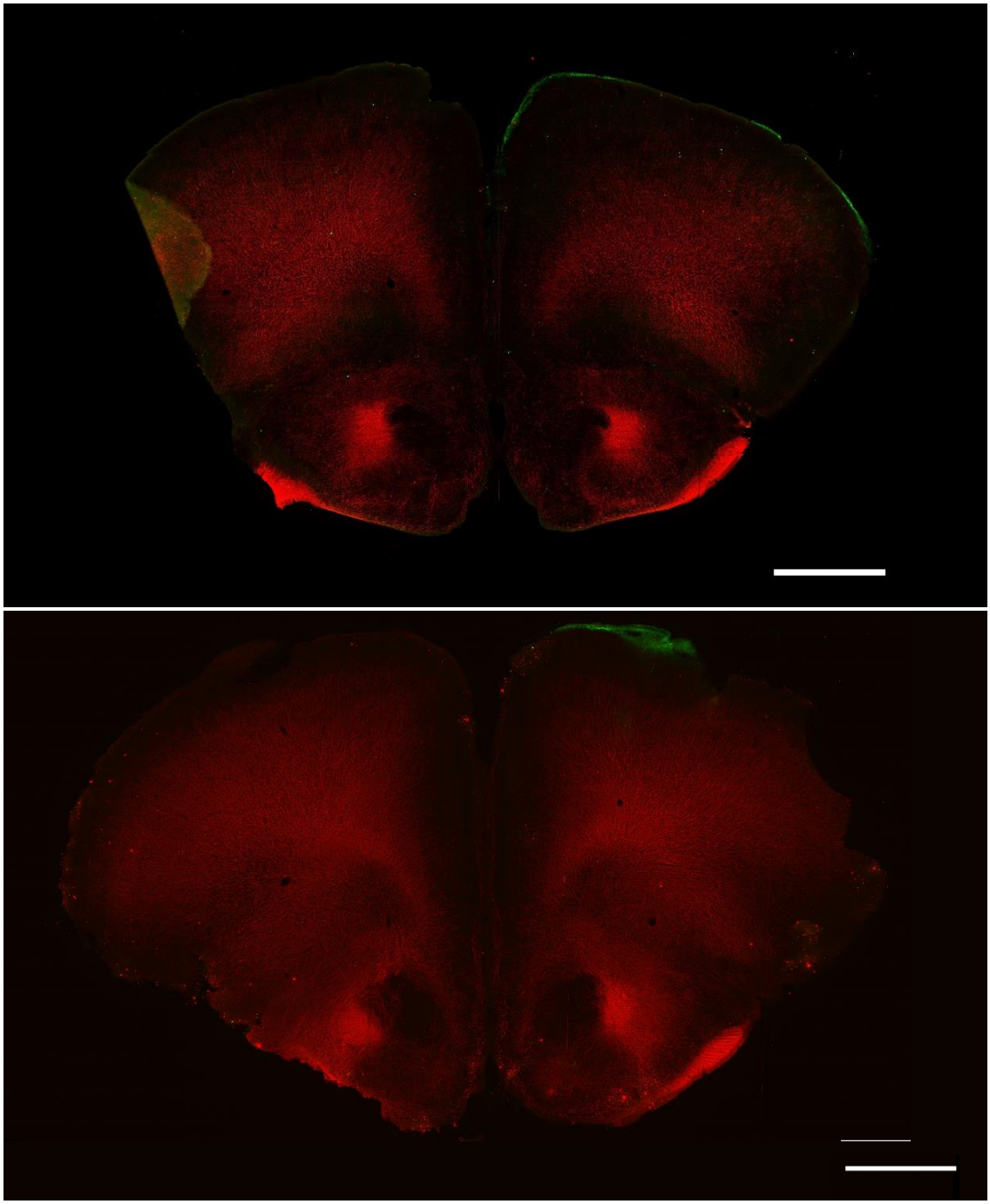

MBP / GFP

Figure 29 - Representative images of entire slices stained with MBP and GFP at 1 mpi (upper image) and 3 mpi (lower image). The MBP is similarly distributed across the slice in both timepoints. The graft region corresponds to a decreased MBP signal, suggested by the bright green staining that never colocalizes with MBP. Scale bars: 1000 µm